Dissertation

submitted to the

Combined Faculties for the Natural Sciences and for Mathematics

of the Ruperto-Carola University of Heidelberg, Germany

for the degree of

Doctor of Natural Sciences

Put forward by

Diplom-Physicist: Stefanie Elisabeth Karolina Kirschbaum-Harriman

Born in: Gruenstadt, Germany

Oral examination: 3rd of February 2016

Investigating Electrochemiluminescence (ECL) as highly sensitive and effective signaling means for microfluidic biosensors

Referees: Prof. Dr. Joachim Spatz

Prof. Dr. Michael Hausmann

Abstract

The conception and realization of microfluidic Total Analysis Systems (microTAS) has revolutionized the analytical process by integrating the whole breadth of analytical techniques into miniaturized systems. Paramount for efficient and competitive microTAS are integrated detection strategies, which lead to low limits of detection while reducing the sample volume. The concept of electrochemiluminescence (ECL) has been especially intriguing ever since the introduction of a version based on $Ru(bpy)_3^{2+}$ by Alan Bard in 1972[1], due to its immense sensitivity, non-existent auto-luminescent background signal, and simplicity in experimental design. Therefore, integrating ECL detection into microTAS is a logical consequence to achieve simple, yet highly sensitive sensors.

ECL follows complex electron transfer pathways, and its efficiency can be enhanced, but also hindered, by numerous factors. Our studies identified the novel combination of the coreactant N-butyldiethanolamine (NBEA) with the surfactant Zonyl FSN as an optimal signal enhancer for $Ru(bpy)_3^{2+}$-based ECL. This combination of coreactant and surfactant led to a limit of detection (LOD) for $Ru(bpy)_3^{2+}$ of 2.2 nM, compared to 0.59 µM for the commonly used Tripropylamine/Triton X-100 system, and a 50-fold increase in sensitivity. Investigations under different buffer conditions revealed that the ECL signal was significantly influenced by buffer composition and pH values. Furthermore it was possible to generate an ECL signal at a potential well below 1.2 V vs. Ag/AgCl, the common potential for $Ru(bpy)_3^{2+}$-based ECL. The low oxidation potential (LOP) signal was significantly increased under the use of the coreactant NBEA with Tris buffer at pH 8.5, and was about three times higher than for the standard coreactant, TPA, in phosphate-based buffer at pH 7. Such low potential ECL signals are desirable for electrode lifetime enhancement and prevention of possible DNA damage in bioassays.

However, to truly extend a sensor's limit of detection, one must go beyond a mere one-to-one labeling approach, especially when dealing with DNA, which, by its nature, is mostly present at low concentrations in real-life samples. Liposomes, molecules capable of encapsulating large quantities of analyte and of being DNA-specific, offer a convenient way of enhancing detection capabilities. Therefore, $Ru(bpy)_3^{2+}$encapsulating liposomes were successfully synthesized and linked to *Cryptosporidium parvum* (*C. parvum*) DNA. ECL detection of the DNA was achieved inside a microfluidic chip with a microfabricated three electrode system. After identification of the appropriate assay and flow parameters, it was possible to achieve on-chip ECL detection in less than ten minutes, while the microfluidic chip was also capable of fluorescent and electrochemical detection.

The study not only presents a novel ECL-based microfluidic biosensor, but functioning strategies that are urgently required to increase its usability and sensitivity.

Die Konzeptionierung und Realisierung von microfluidic Total Analysis Systems (microTAS) hat durch die Integrierung analytischer Techniken in miniaturisierte Systeme entscheident zur Revolutionierung von analytischen Prozessen beigetragen. Besonders wichtig sind hierbei Detektionsstrategien, die hohe Sensitivitaeten bei geringen Probekonzentrationen erlauben. Elektrochemilumineszenz (ECL) ist hierbei besonders interessant, durch den Wegfall eines Hintergrundsignals, seiner hohen Sensitivitaet und vereinfachtem experimentellem Design. Es ist somit eine logische Konsequenz ECL in microTAS zu integrieren um einfache und gleichzeitig sensitive Sensoren zu erhalten.

ECL durchlaeuft komplexe Elektronentransferreaktionen, und seine Effizienz kann durch viele Faktoren positiv, aber auch negativ beeinflusst werden. In der vorgelegten Studie wurden N-butyldiethanolamine (NBEA) mit dem Tensid Zonyl FSN als optimale Signalverstaerker fuer $Ru(bpy)_3^{2+}$-basierte ECL identifiziert und fuehrten zu einem $Ru(bpy)_3^{2+}$ Detektionslimit von 2.2 nM, im Vergleich zu nur 0.59 µM fuer das meist verwendete System aus Tripropylamine und Triton X-100, und gleichzeitig zu einer 50 mal hoeheren Sensitivitaet. Pufferbedingungen und pH zeigten einen starken Einfluss auf das ECL System mit der Moeglichkeit eines low oxidation potential (LOP) ECL Signals unter der Verwendung des Coreaktanten NBEA mit Tris Puffer bei pH 8.5, welches zu einem drei mal so starken ECL Signal fuehrt als der Standard Coreaktant TPA in phoshpathaltigem Puffer bei pH 7. Die Verwendung von LOP ECL spielt besonders eine Roller bei der Verlaengerung der Verwendungsdauer der Elektroden und der Verhinderung von moeglichen DNA Stoerungen durch zu hohe Spannungen.

Um das Detektionslimit noch weiter zu verbessern, ist es essentiell mehrere Signaltraeger mit der Probe zu koppeln, besonders fuer DNA, die generell in natuerlichen Proben in niedrigen Konzentrationen vorliegt. Liposome, die eine grosse Anzahl an Molekuelen einschliessen koennen und sich spezifisch an DNA binden lassen, sind predestiniert fuer diesen Zweck, weshalb $Ru(bpy)_3^{2+}$ einschliessende Liposome erfolgreich hergestellt wurden, die an *Cryptosporidium parvum* (*C. parvum*) DNA koppeln. Die DNA wurde per ECL in einem mikrofluidischen Chip mit integriertem drei-Elektroden-System detektiert. Nach der Identifizierung der geeigneten experimentellen- und Fliessparametern, war ECL Detektion im Chip in weniger als zehn Minuten moeglich, wobei der Chip auch fuer Fluoreszenz und EC Detektion nutzbar ist.

Die vorliegende Studie praesentiert nicht nur einen neuartige ECL-basierten mikrofluidischen Biosensor, sondern auch funktionierende Strategien, um dessen Brauchbarkeit und Sensitivitaet zu erhoehen.

Table of Contents

Aims

Microfluidic devices, with their advantages of fast response and low sample consumption, are continuously being integrated into analytical applications. However, herein also lies one of the biggest hurdles one needs to overcome in the development of a sensitive chip; the low analyte concentration. For example, DNA, due to its generally low representation in real-life samples, requires detectors with low limits of detection. Strategies addressing the problem of reduced signal intensity are therefore essential to allow for comparability to bench-top devices.

Electrochemiluminescence (ECL), a process in which molecules emit photons upon excitation via an applied voltage, offers a strong tool to reach high sensitivity within a system. ECL of $Ru(bpy)_3^{2+}$ is a complex process, and not entirely understood up to this point. It is known, however, that certain environmental conditions can enhance the signal intensity of $Ru(bpy)_3^{2+}$-based ECL. Most often, a so-called coreactant is present in solution, participating in the electron transfer reactions and facilitating the formation of the photon-emitting state of $Ru(bpy)_3^{2+}$. Tripropylamine (TPA) is the most commonly-employed coreactant in the literature, though other coreactants, namely N-butyldiethanolamine (NBEA) and 2-(dibutylamino)ethanol (DBAE), have been shown to enhance the ECL signal even further than TPA. In addition, a surfactant, almost exclusively Triton X-100, is sometimes employed for the same purpose: signal enhancement. Alternative surfactants have been investigated as well, and Zonyl FSN has been the most outstanding one compared to Triton X-100. It is believed that the electrode surface is rendered more hydrophobic by the surfactant, allowing the hydrophobic TPA to be enriched in close proximity to the electrode, and facilitating the presence of more $Ru(bpy)_3^{2+}$ molecules in the photon-emitting excited state.

Even though it has been demonstrated that DBAE and NBEA increase the ECL signal, no publication shows the two coreactants in combination with Triton X-100 or Zonyl FSN for $Ru(bpy)_3^{2+}$. Also, a comparative study is missing. We therefore investigated the effects of both surfactants, Triton X-100 and Zonyl FSN, in combination with the three coreactants, TPA, DBAE and N-Butyldiethanolamine, on $Ru(bpy)_3^{2+}$ ECL, with the intent to identify conditions under which the ECL signal can be even further increased, compared to the already investigated cases.

Another goal of this study was the fabrication of a transparent microfluidic device with integrated three-electrode configuration to achieve on-chip ECL detection of DNA sequences. In this study, *Cryptosporidium parvum* (*C. parvum*), a waterborne pathogen responsible for disease outbreaks worldwide, was chosen as model analyte. In addition to detection via ECL, we also aim for a chip capable of electrochemical (EC) and fluorescent detection, to increase the capabilities of the device and to develop a system in which all three methods can be compared with each other under equivalent conditions.

Relying on a sensitive detection technique is only one way to ensure high sensitivity. Another approach is an increase in signaling molecules. In the case of DNA, it is common to link the DNA to a labeling molecule, e.g. a fluorescent marker, or to $Ru(bpy)_3^{2+}$, the most common ECL molecule. Under the best conditions, each DNA molecule would be linked to one marker molecule. If, however, the DNA is linked to a molecule capable of accumulating multiple signaling molecules, the signal can be increased, and lower limits of detection are attainable. Liposomes can be employed for such purposes. They form a vesicle of a bilipid layer in which other molecules can be encapsulated and subsequently released when needed. Their surface can, furthermore, be modified to achieve specific binding to target molecules, e.g. DNA, proteins, and antibodies.

Part of the study was, therefore, the synthesis of $Ru(bpy)_3^{2+}$-encapsulating liposomes and their integration into a DNA hybridization assay. Subsequently, the development of an assay protocol is required which enables the detection of a target DNA linked to a liposome via release of $Ru(bpy)_3^{2+}$ molecules trapped inside the liposome.

The aim of this research was the identification of signal enhancing strategies for ECL to make an incorporation into a microfluidic system lucrative, as well as the investigation of biological parameters for a working assay to achieve ECL detection on chip.

2. Introduction

2.1 Electrochemiluminescence (ECL)

2.1.1 Mechanism of Electrochemiluminescence (ECL)

Electrochemiluminescence (ECL) is an electrochemical process in which molecules undergo electron-transfer reactions at an electrode surfaces to form an excited, photon emitting state (see Fig. 1). Thus, the emitted light is detected upon ECL reaction at the introduction of a required voltage. Highly sensitive photon detection is possible, due to a number of existing high performance detectors and ongoing development of more sensitive and smaller sensor systems. This has led to the development of light emission reactions into highly sensitive analytical methods and tools[2]. While fluorescence remains the predominant light-emission-based detection method, ECL offers great advantages over fluorescence, which are due to the mechanism by which the excited state is generated. While fluorescence requires an external light source, none is needed for ECL. Light scattering, and thus, importantly, the background signal, is reduced. Thus the virtually background-free detection of ECL can reach higher signal-to-noise ratios and lower limits of detection. Besides, ECL is a highly localized and time-triggered detection method, since ECL signal generating reactions will only take place at the electrode for the duration of an applied potential.

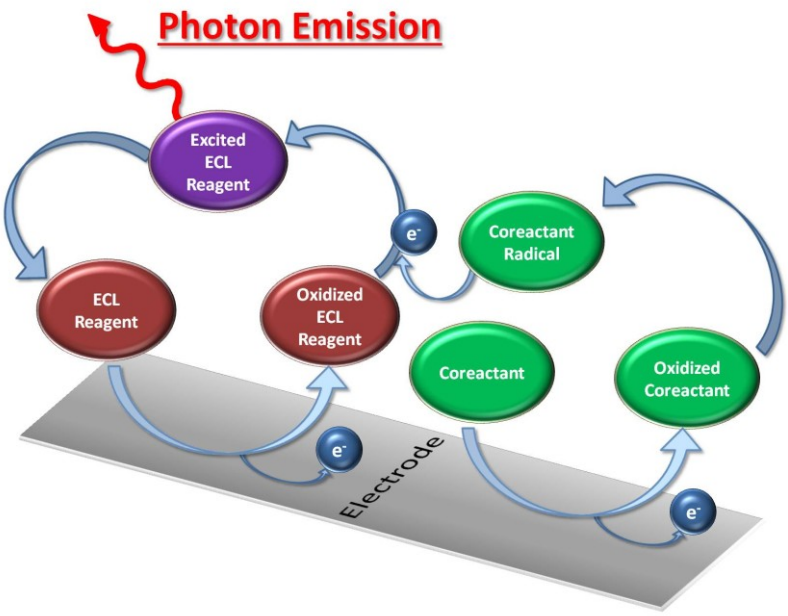

Fig. 1 ECL Process
A ECL reagent (e.g. $Ru(bpy)_3^{2+}$, luminol, QD) is being oxidized at an electrode. The oxidized species can undergo transfer into an exited, photon emitting state. A coreactant can participate in and facilitate the electron transfer processes into the ECL reagent's excited state and allow for a constant applied potential.

Throughout literature, the most common ECL reagents are $Ru(bpy)_3^{2+}$ and luminol, though many others are known, and more complete lists can be found, for example in reviews by Richter[3] and Miao[4]. In recent years, quantum dots (QDs) have also been studied as ECL

reagents[5]. ECL of $Ru(bpy)_3^{2+}$ can be generated through an annihilation process, requiring only $Ru(bpy)_3^{2+}$ in an electrolyte solution [3, 4, 6]. More common, however, a coreactant, such as Tripropylamine (TPA), is present during the ECL process, facilitating the generation of the light-emitting excited state of $Ru(bpy)_3^{2+}$ and allowing for a constantly applied voltage. $Ru(bpy)_3^{2+}$ coreactant ECL can occur in aqueous solution, making it usable for a large variety of biological and medical applications and diagnostics.

ECL's main characteristics and advantages are its utility for biological assays; its high sensitivity and specificity; and its minimal hardware requirements (i.e. electrodes, voltage source and light sensor, all of which can be miniaturized). This makes it an ideal analytical detection method for integration into microfluidic systems. Microfluidic Total Analysis Systems (microTAS) integrate complex sample processing steps specific to the application, such as sample incubation, mixing and detection, on a micrometer scale with small sample volumes. In recent decades, microTAS have been increasingly used for biological and clinical research and applications[7–12]. However, most microscale ECL systems are not microTAS, but microfluidic systems with integrated ECL detection.

2.1.2 Strategies towards ECL Enhancement

ECL as a detection method has the particular advantage of being a no-background technique, resulting in high sensitivity levels and high time and space resolution of the signal. To increase the limit of detection for ECL systems means to increase the number of photons emitted from the ECL system during the assay time. Since only the excited state of the ECL reagent is emitting the photons, two general signal enhancement approaches can be taken: (1) to increase the number of ECL molecules in the excited state during detection (through chemical environment, electrode modification or ECL reagent alternatives), or (2) to increase the number of ECL molecules capable of reaching the excited state (through multiplication effects in solution and on the electrode surface) (Fig. 2). The first can be accomplished by employing new ECL reagents with higher quantum yields or modifications of the chemical environment, or electrodes facilitating the ECL reagent oxidation. The second one can be achieved by an accumulation of ECL reagents via another molecule bearing multiple binding sites. The latter will act as linker between the analyte and the now-multiplied ECL molecules. Both strategies have shown great potential throughout the literature to increase the sensitivity of ECL detection.

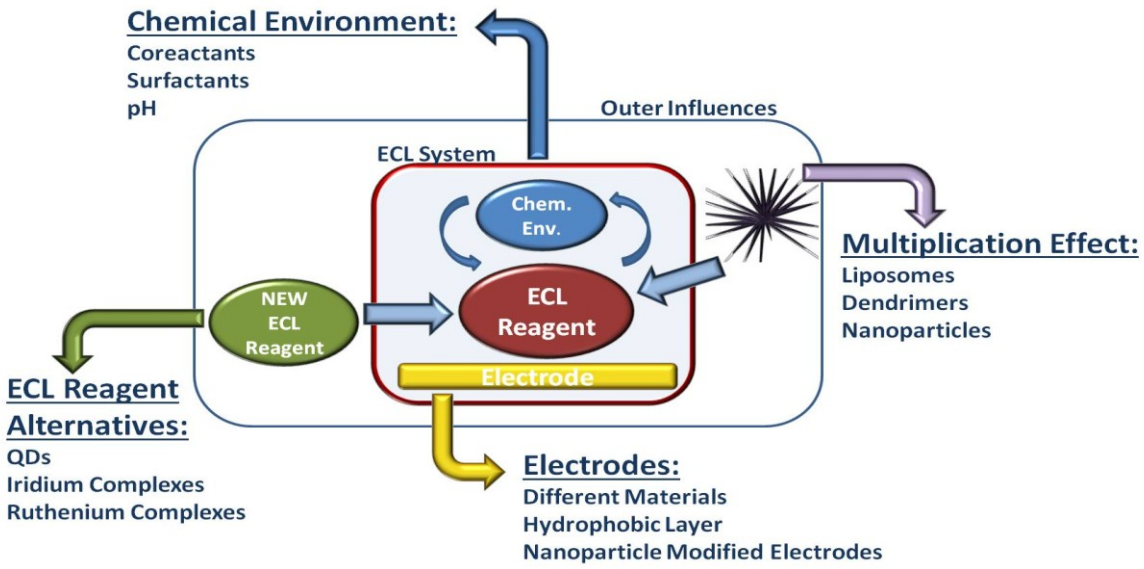

Fig. 2 Signal Enhancement Strategies for ECL
The ECL signal can be enhanced through multiple approaches, mainly falling into one of the following categories: manipulation of the ECL system's chemical environment; changes in the electrodes; introduction of a new ECL reagent; or using a molecule capable of binding multiple ECL molecules and thereby creating a multiplication effect.

ECL Signal Enhancement: Chemical Environment for $Ru(bpy)_3^{2+}$

Increasing the number of emitted photons for the $Ru(bpy)_3^{2+}$ complex means either increasing the number of molecules reaching the excited state, or the probability for a single molecule to reach the excited state. Adding a coreactant to the $Ru(bpy)_3^{2+}$ complex-containing solution is a well-known strategy to increase the complex's ECL signal. The classical coreactant used is Tripropylamine (TPA). But others have been investigated and found to lead to even higher ECL signals than TPA. A prime example is DBAE[13]. Han et al. investigated multiple coreactants such as monoamines, e.g. 2-(dibutylamino)ethanol and N-butyldiethanolamine and diamines including N,N,N',N'-tetrakis-(2-hydroxyethyl)-ethylenediamine and N,N,N',N'-tetrakis-(2-hydroxypropyl)ethlenediamine[14]. The monoamines led to higher ECL signals than the diamines with N-Butyldiethanolamine, leading to the highest so far published signal increase for $Ru(bpy)_3^{2+}$ from the compared systems and also in comparison with the already published system of TPA and DBAE. DBAE has found increasing use in ECL applications[15–35]. It is used as coreactant, not only for $Ru(bpy)_3^{2+}$ but also for its derivatives or for quantum dots, partly applied in quenching techniques. To our knowledge,

however, only the publication by Han employed N-butyldiethanolamine, which is even more promising than DBAE in terms of detected $Ru(bpy)_3^{2+}$ ECL signal.

Surfactants are known to increase the ECL signal for $Ru(bpy)_3^{2+}$ with TPA, as show by Workman and Richter[36]. The authors showed an 8-fold increase in ECL efficiency in the presence of Triton X-100. It is assumed that the surfactant renders gold and platinum electrode surfaces more hydrophobic, allowing more TPA molecules to reach the electrode surfaces to be oxidized (Fig. 3). Through the larger number of oxidized TPA molecules, more reacting $Ru(bpy)_3^{2+}$ can reach the excited state and emit a photon. The most commonly used surfactant is Triton X-100. In 2004, Li et al. introduced Zonyl FSN, a nonionic fluorosurfactant, as an alternate surfactant capable of ECL signal increase with a higher yield than Triton X-100[37]. Their publication shows an about fifty-fold increase in ECL signal by using Zonyl FSN instead of Triton X-100 for a $Ru(bpy)_3^{2+}$/TPA system on gold

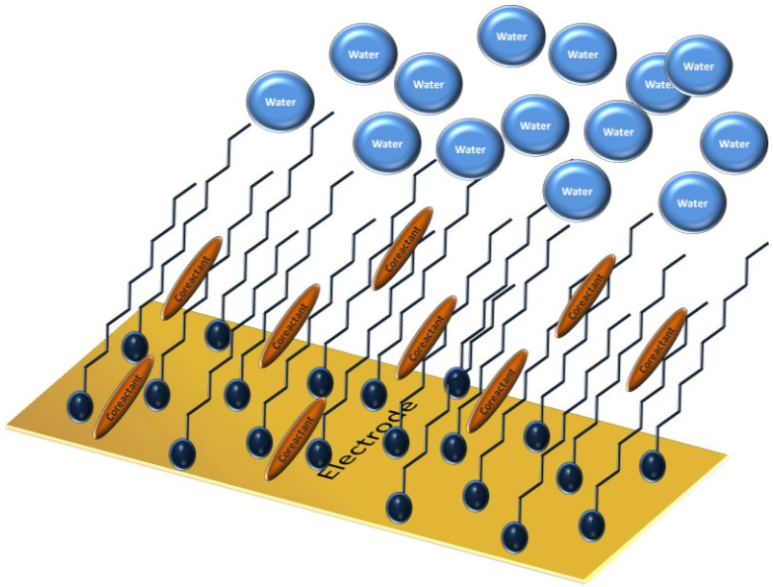

Fig. 3 Surfactant arrangement on a gold electrode and its hydrophobic effect. Through rendering the surface more hydrophobic but the alignment of surfactant (blue) the coreactant (shown in orange) can reach the electrode easier and more coreactant molecules undergo electron transfer.

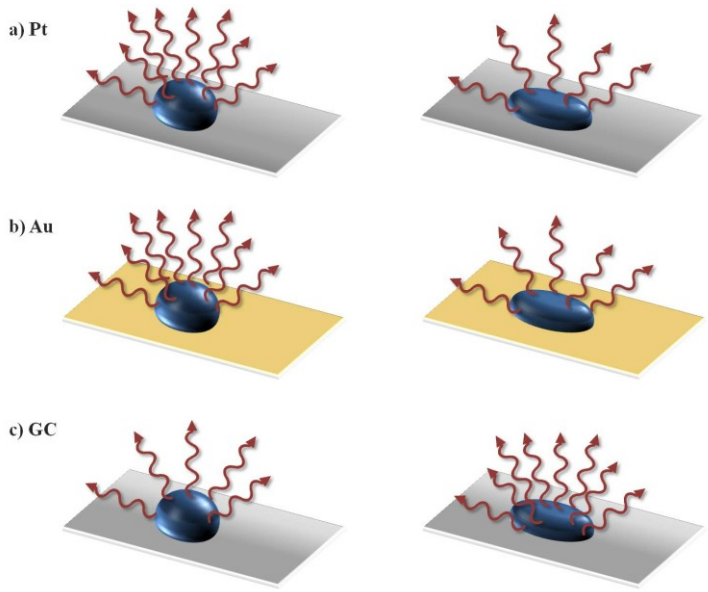

Fig. 4 Proposed influence of surface hydrophobicity on ECL signal for different electrode materials
For Au and Pt electrodes (a and b) the ECL signal of $Ru(bpy)_3^{2+}$ with TPA is increased on hydrophobic surfaces, whereas the opposite effect is observed on glassy carbon electrodes (c).

electrodes. Furthermore, they found a low oxidation potential, attributed to TPA oxidation below 1 V.

Whereas the ECL signal of the $Ru(bpy)_3^{2+}$/TPA system on gold and platinum electrodes can be enhanced by the addition of Triton X-100, this is not the case for glassy carbon electrodes (GC) [38], leading to the conclusion, as shown in other publications, that coreactant-based ECL is highly dependent on the electrode material[37, 39–41] (Fig. 4).

The increase in hydrophobicity that leads to the significantly increased ECL signal on gold and platinum can be observed by adding the surfactant to the buffer solution, but also by directly rendering the surface hydrophobic. Bard and colleagues showed that hydrophobic thiolated gold and platinum electrodes facilitated TPA oxidation and therewith enhanced the ECL signal of the $Ru(bpy)_3^{2+}$/TPA system[38].

ECL Signal Enhancement: Novel ECL Reagent Research

In the search for novel ECL reagents with higher ECL intensity or different ECL properties, e.g. emission wavelength, a variety of alternatives to $Ru(bpy)_3^{2+}$ have been investigated, such as metal–saline complexes[42], which showed ECL activity in acetonitrile solutions, though with lower intensity than $Ru(bpy)_3^{2+}$. An interesting finding was reached by Zhou et al. during their study of $Ru(bpy)_3^{2+}$ and several of its derivatives: one of the most efficient luminophores under photoexcitation, the ethoxycarbonyl-substituted derivative, $[Ru(bpy\text{-}COOEt)_3]^{2+}$, did not display an intense ECL signal, but, on the other hand, luminophores with lower photoluminescence quantum yields showed higher ECL intensity[43]. This shows that no direct conclusion can be drawn from spectroscopic data to an ECL emission yield. In search of blue-emitting ECL reagents, thienyltriazoles were investigated[44]. The blue emission would be advantageous to broaden the detection range of ECL reagents, especially for multianalyte detection strategies. Superradiant organic dye J-aggregates were investigated for their ECL properties with DBAE, as coreactant immobilized on glassy carbon electrodes[45], and also on pyrolyzed photoresist film (PPF)-based carbon optically transparent carbonelectrodes (COTEs)[25]. These papers demonstrated a proof of principle for this new class of ECL molecules, but a comparison with conventional ECL systems would need to be done to reveal the extent of actual signal enhancement. Iridium complexes and their ECL characteristics have been studied as well[46]: for example, water soluble cyclometalated iridium(III) complexes with disulfonated bathophenanthroline undergo ECL

processes, but their intensity has been found to be less than for the $Ru(bpy)_3^{2+}$/TPA reference system[47]. By investigating ruthenium polypyridyl complexes containing 5-aryltetrazolate ligands[48], it was even found that one complex, $Ru(4\text{-}TBN)Ru^{2+}$, displays a higher ECL efficiency than $Ru(bpy)_3^{2+}$.

Quantum dots are semiconductor nanocrystals that are tunable in size and physical characteristics, and are capable of ECL, as first shown by Bard's group in 2002[49] and shortly thereafter[50, 51]. ECL of QDs can be coreactant-assisted or not, with H_2O_2, $K_2S_2O_8$, TPA and DBAE being some of the most common coreactants. In addition to direct quantitative analytical methods, which rely on ECL signal increase with increased analyte concentration, the use of quenching reagents and effects is common in QD ECL applications. Quenching can occur through either the analyte itself, interactions with the coreactant, or interactions with the ECL pathway products, and has been used in a variety of assays[52–59].

Bioanalytical applications using QD ECL are most often found in immunoassays[55, 60–66], but have also been published, for example, for aptasensor development[67, 68], detection of DNA[69, 70], cancer cells[69, 71, 72], ATP[67, 73] or Dopamine[74]. Research, however, is not limited to analytical applications for medical or biological assays. Research about new ECL QDs[56, 72, 75], Near-infrared ECL[76–79] or sensing techniques[57, 80] for example, is being conducted. Use of QD films[81, 82], QD-on-electrode systems with ITO electrodes[74, 82], bipolar electrodes carbon nanotube modified glass carbon electrodes [83] and their characterization has been shown as well.

Comparing the ECL efficiency of QDs with the classical $Ru(bpy)_3^{2+}$ system is not carefully done in literature, making thus a direct comparison statement here difficult. The advantages of QDs lie in their tunability and in areas such as Near-infrared ECL, which cannot be done with $Ru(bpy)_3^{2+}$ due to the emitted wavelength. Also, QDs display a better capability for applications on ITO electrodes. However, their disadvantages are related to their synthesis, which is performed in organic solvents and caps of hydrophobic ligands, which requires a surface functionalization prior to biosensing applications, making the preparation more expensive and time-consuming than the commercially cheaply available $Ru(bpy)_3^{2+}$. A fair comparison of QDs and organic ECL reagents is needed though.

2.1.3 Low Oxidation Potential ECL

The voltage required to initiate $Ru(bpy)_3^{2+}$ ECL is typically 1.2 V vs. Ag/AgCl reference electrodes: a high voltage, close to the potential of water electrolysis which is -1.23 V at 25°C at pH 0. This can cause bubbling of the solution. And while disc or macro electrodes are stable against such high potentials, can it become a challenge for thin microfabricated electrodes, especially when combined with a high currents and gas formation in solution. Electrode damage, for example due to electrode fouling and detachment of the electrode from its substrate, can occur. Furthermore, it might interfere with DNA stability, as oligonucleotide sequences could get damaged at +1.0 V vs. SCE[84, 85].

An approach to overcome this issue could be the use of low oxidation potential (LOP) ECL. However, LOP ECL has not been applied to microfluidic systems yet. It is only on a few occasions that LOP ECL is even described in greater detail in the literature.

The existence of a LOP ECL signal for $Ru(bpy)_3^{2+}$ with TPA and the nonionic fluorosurfactant Zonyl FSN was demonstrated by Li et al. in 2004[37]. The explanation for the low oxidation potential at gold and platinum electrodes was based on the hydrophobic condition on the electrode surface and, most importantly, the inhibiting effect on oxide layer growth on the electrodes, facilitating the direct oxidation of TPA. The same group published a second paper characterizing the LOP of the $Ru(bpy)_3^{2+}$/TPA system in greater detail on gold electrodes in the presence of Zonyl FSN-100[39]. In the search for coreactants leading to a higher LOP ECL signal, multiple tertiary amine coreactants for $Ru(bpy)_3^{2+}$ were compared to the most common coreactant, TPA, in terms of their LOP ECL capability[86]. Tri-n-ethylamine (TEtA), TPA, and tri-n-butylamine (TBuA) were investigated at a Zonyl-FSO-100-modified gold electrode. Changes to the electrode hydrophobicity showed that more hydrophobic surfaces increased the LOP ECL signal.

LOP ECL is also possible without the addition of actual surfactants. Jiang et al.[87] showed the existence of a LOP for the $Ru(bpy)_3^{2+}$/TPA ECL system at gold electrodes while introducing pyridine and its analogues, quinoline and 4,4'-dipyridine, to the system. The proposed assumption was that pyridine and its analogues in fact acted as surfactants, and therefore facilitated direct TPA oxidation.

LOP ECL, however, is not limited to the $Ru(bpy)_3^{2+}$/TPA system. For ECL quantum dot (QD) applications, Zou et al.[88] showed that, at low oxidation potentials on glass carbon electrodes, anodic near-infrared (NIR) ECL from CdTe QDs could be achieved. Furthermore,

a strategy for greatly enhanced band-gap NIR ECL at low oxidation potential with the dual-stabilizer-capped CdTe QDs was presented. The CdTe QDs were used as ECL emitters, while TPA was employed as coreactant, leading to two distinct ECL processes at 0.63 and 0.88 V. The two identified ECL potentials are much lower than for other reported NIR-emitting QDs[75, 89] and visible-emitting QDs[90, 91].

The ECL signal produced at the low oxidation potential can furthermore be used to measure quenching, as the quenching effects on the ECL pathway of $Ru(bpy)_3^{2+}$ with TPA can be more significantly and sensitively observed under LOP ECL conditions. This phenomenon and detection approach was, for example, shown for detection of oxygen[92], uric acid[93] and phenolic compounds[94].

2.1.4 Alternative Detection Methods: Fluorescence and Electrochemical

Fluorescence

Fluorescence is a form of luminescence, just as ECL. However in the case of fluorescence, light is emitted upon excitation of the fluorescent substance with absorbed light or other electromagnetic radiation. In particular, an orbital electron of the fluorophore is brought to an excited singlet state upon energy transfer from the external radiation. A photon is then emitted when the excited electron falls back to the ground state. The energy of the emitted photon is usually less than the energy of the excitation photon and can be given by the Planck–Einstein relation:

$$E = h\nu \qquad (1)$$

E = Energy of the photon

h = Planck constant, $h \approx 6.6\times10^{-34}\ J\cdot s$

ν = frequency of the photon

Meaning that, when the emitted photon has less energy, its wavelength is red-shifted, since the frequency ν is correlated to the wavelength λ and the speed of light c by:

$$\nu = \frac{c}{\lambda} \qquad (2)$$

This phenomenon is called the Stokes shift. The reason for the shorter wavelength and corresponding lower energy of the emitted photon can be, for example, a non-radiative relaxation, but can also be caused while interacting with a quencher, a molecule to which the energy is transferred, but where the relaxation to the ground state is not accompanied by photon emission.

Fluorescence detection is common and frequently incorporated into biological and clinical applications on the macro as well as micro scale. Fluorescence benefits from a wide variety of fluorophores that cover the whole visible range while displaying high quantum yields. The quantum yield (Φ) refers to the ratio between of emitted photons to absorbed photons and gives a measure for the efficiency of the fluorescence process of the fluorophore:

$$\Phi = \frac{number\ of\ emitted\ photons}{number\ of\ absorbed\ photons} \qquad (3)$$

The widespread use of fluorescence in cell and molecular biology assays is furthermore based on the introduction of florescent proteins, which can be directly integrated into, for example, cellular structures, where they function as reporter molecules.

This choice of different fluorescent markers is definitely an advantage of fluorescence upon ECL detection. Even though numerous ECL reagents are known[3], only two of them are usually used for commercial applications: luminol and $Ru(bpy)_3^{2+}$. Another limiting factor for ECL, compared to other luminescence techniques, is the typically lower efficiency of ECL[95]. The main reason is the suboptimal stability of the electrogenerated species that undergo transfer into the excited, photon emitting, state of the ECL molecule[95]. But the efficiency can be enhanced, e.g. by the use of a coreactant, which makes research to obtain better ECL conditions in terms of higher photon yields so essential.

ECL has many ather advantages over fluorescence which make it ideal for incorporation into microfluidic devices. From a detection standpoint, is it easier to reach lower limits of detection with ECL than with fluorescence. This is due to the requirements for both techniques. While fluorescence requires a light source, light scattering and autofluorescence can cause high background levels, and it is a common to invest in strategies to lower the background level to increase the signal to noise ratio. ECL is not faced with this problem, as light is only emitted upon introduction of the right voltage. This correlates with higher specificity, since usually only one ECL species is present. How much lower the limits of

detection (LOD) can be is shown by a comparison published by Yuan et al. in 2014[96]. They compared the sensitivity of their ECL aptasensor with published values of other sensors for the same model analyte but different detection technique. The publications showed the LOD reached with fluorescence at 2.48 nM[97] and 0.05 nM[98], with CL at 74.4 pM[99] but as low as 10 fM with ECL.

Another important advantage ECL has over fluorescence for microfuidic sensors is the ease in miniaturization of the hardware requirements. Basically, the only requirements are a voltage source and a light detector. The voltage source can be as easy and cheap as a battery.

Considering all factors, ECL is a promising alternative to fluorescence and for incorporation into microfludic sensors. The biggest challenge ECL needs to overcome is identifying conditions under which higher signals can be achieved.

Electrochemistry

Electrochemistry deals with the interconversion of chemical and electrical energy, and the relation of electricity to chemical changes in a substance. Electron transfers can occur at an electrode interacting with electrolytes and can be measured. In electrochemical (EC) detection, as it is used in sensor applications, usually the analyte itself is a molecule that can undergo detectable electron transfer reactions at an electrode, or the analyte is linked to a molecule that does. Often, either a constant potential or a swept potential is applied to the system, and the current, resulting from the electrons that are transferred from and to the electrodes, is measured. Cyclic voltammetry (CV) is an example of a sweep voltammetry technique. A potential is applied and swept from a starting value to an end value and back, so that a "circle" in potential is introduced to the system. This technique can help identify, for example, the oxidation and reduction potentials of the analyte.

As for ECL, the mechanism relies on chemical changes of the molecule while interacting with electric energy introduced at an electrode. However, while photons are detected by ECL, electrons are detected by EC. The advantage is, that EC is a highly sensitive technique. The disadvantage is the high background caused by other reagents in solution. Usually, not just one EC capable species is present in solution, but, especially in biological applications, ions from buffers and the analyte itself. So multiple molecules will participate in electron transfer

reactions and increase the signal, even if not from the molecule of interest. ECL, therefore, can bring an increase in sensitivity and specificity compared to EC detection.

2.2 Microfluidic Devices

2.2.1 Microfluidics

Microfluidics refers to the science of describing and dealing with the behavior of fluids at small volumes, typically in the range of microliters and lower, and the manufacturing, design and manipulation of the devices containing the liquid in channels ranging from millimeters to micrometers in their dimensions. Microfluidics presents itself as a separate research field, as different effects than on the macro scale can become dominant. The larger ratio of surface area to volume, and corresponding increase in surface tension and fluid resistance, plays an important role. One further factor to consider is the fluid flow itself, and how this affects mixing if multiple liquids are injected into one device. The flow at such small scales becomes laminar instead of turbulent. This can be quantified by the Reynolds number (Re), given by the ratio of inertial forces (ρvL) to viscous forces (μ).

$$Re = \frac{inertial\ forces}{viscous\ forces} = \frac{\rho v\ dv/dx}{\mu\ d^2v/dx^2} \qquad (4)$$

$$= \frac{\rho v\ v/L}{\mu\ v/L^2}$$

$$= \frac{\rho v L}{\mu}$$

Re = Reynolds Number (non-dimensional)

ρ = density (kg/m^3)

v = velocity based on the actual cross section area of the channel (m/s)

μ = dynamic viscosity (Ns/m^2)

L = characteristic length (m)

With the kinematic viscosity ν giving the ration between the dynamic viscosity μ to the density of the fluid ρ:

$$\nu = \frac{\mu}{\rho} \qquad (5)$$

The Reynolds Number Re can be given by:

$$Re = \frac{vL}{\nu} \qquad (6)$$

v = kinematic viscosity (m^2/s)

For laminar flow, the value of Re is below 2300. When Re is above 4000, the flow is turbulent, while in between 2300 and 4000, both laminar and turbulent flow are possible, which is referred to as transition flow. However, Re depends on the channel geometry. Practical implications are, for example, the mixing of two liquids. At low Re values, where the flow is laminar flow, the mixing is caused mainly by diffusion.

When designing microfluidic channels, the parameters resulting in the chips' performance are important. For example, the sample volume needs to be adequate to the volume the channels can process, in order to not dilute the analyte or extend the analysis time. Smaller sample volumes than used in bench-top devices correlate with smaller analyte amounts, if no other measures are taken to enhance the amount of analyte or signaling molecules. In general the relationship between analyte concentration (c) and sample volume (V) can be given by[100]:

$$V = \frac{1}{\eta_s N_A c} \qquad (7)$$

N_A = Avogadro's number

η_s = sensor efficiency,

V = sample volume

c = analyte concentration

2.2.2 Definition and Advantages of Microfluidic Devices and microfluidic Total Analysis Systems

Microfluidic Total Analysis Systems (μTAS), or sometimes called lab-on-a-chip (LOC), are devices that perform a whole laboratory process, conventionally conducted with bench top tools, starting from sample preparation and treatment to detection, on a nm to cm scale. μTAS are usually based on microfluidic processes, to achieve goals such as sample transport. However, so called microfluidic chips should not be confused with μTAS. μTAS refer only to devices in which all required sequences of an assay are executed on the chip itself, while microfluidic devices commonly transfer only parts of an assay to its small scale, e.g. mixing or detection.

The advantages of both μTAS and microfluidic chips are numerous, and can be perhaps summed up in three words: faster, smaller, cheaper. Obviously, due to the sheer dimensions of microscale systems, only a small sample volume, in the nL to mL range, is required. This is essential in applications where low sample quantities are available for processing or are desirable to minimize costs, as for example the case in DNA related applications or blood analysis. The costs are not only minimized due to the lower use of expensive analytes, but also due to the relatively cheap manufacturing costs for microfluidic systems based on the chip material. The commonly used substrates such as Polydimethylsiloxane (PDMS), Poly(methyl methacrylate) (PMMA), glass, and even paper, are relatively cheap in production and manipulation costs compared to the requirements for bench top devices.

The μTAS and microfluidic dimensions also correlate to faster analysis times and the ability for high throughput analysis, as multiple analytical steps can be run simultaneously on one device. The small size correlates with a larger surface area to volume ratio, enabling diffusion processes, whole sample heating or cooling, and more processing on a shorter time scale, while using less energy than large scale systems. Faster results and lowered costs are, of course, desirable for every application, especially for health-related tests in hospitals or in the field. In fact, chips are ideal for in-field applications: they are small, portable, and aim for ease of use, so that even untrained personnel can operate the device.

Its disadvantages hinder a wide-spread replacement of existing technology with μTAS. One barrier is the cost and time-consuming development of a novel device. Even though the finished products are generally faster and cheaper per analysis, the development itself requires

more labor-intensive steps. Part of this is caused by physical and chemical effects on µm scales, which do not allow for a simple down-scaling of existing protocols.

Maybe the biggest problem with microfluidic devices is based on one of its greatest advantages, the small sample volume. The reduced analyte concentration leads, obviously, to a lower signal, and possibly higher signal-to-noise ratio based on the device itself. It is therefore unrealistic to expect microfluidic device to approach limits of detection (LOD) and sensitivities of established bench top devices.

Microfluidic applications are wide spread throughout scientific applications, ranging from in-field applications such as the detection of pathogens or heavy metals in water, over clinical use for the analysis of blood samples, to lab applications such as PCR and immunoassays.

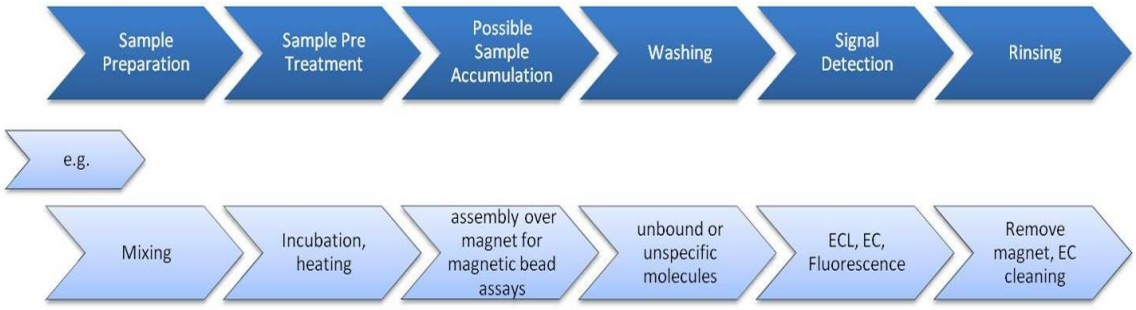

Fig. 5 Principal of a microTotal Analysis System (microTAS) with all steps integrated on chip

2.2.3 Microfluidic ECL Systems

ECL shows great potential for miniaturization, due to its few hardware requirements. Since no external light source is required for light emission, but only a power source, miniaturization can be done with batteries[101, 102], or even phones[103], and thus easily be integrated into a microTAS (Fig. 5). The electrodes can be fabricated on microscale levels with various simple techniques, while light sensors can be integrated into the device via small PIN photodiodes. This, combined with research in microfluidic development, allows for microscale, high sensitivity, analytical ECL-devices. In literature, most microanalytical devices employing ECL are not microTAS, but focus on the detection aspects rather than the sample preparation components of a microTAS.

The most common ECL reagent is $Ru(bpy)_3^{2+}$ [101, 103–110] with or without TPA as coreactant. But other systems, like luminol[111–114], carbon nanodots[101] or carbon nanocrystals[106] have also been used. In order to realize ECL in microfluidic systems, different strategies and methods have to be chosen depending on substrate material, channel design, and electrode fabrication and material. The electrodes are most often either produced by evaporation of the metal onto the substrate with additional lithography, printed circuit board (PCB) technology[113, 114] or by using screen printed electrodes (SPE),[101, 102, 104–107, 111, 115] with the most common electrode materials being gold, and recently also ITO electrodes. Screen printed electrodes (SPE) are often used in microfluidic paper-based analytical devices, μPADs, which have been investigated for analytical purposes over the last few years since the first proof of concept demonstration by Whitesides and his group in 2007[116]. Combining paper based microfluidic systems with ECL detection is a relatively young, but promising, research field[117] and has been demonstrated by several groups[101–105, 107, 112, 118, 119]. The publications about ECL microfluidic devices mostly deal with the fabrication and characterization of the device itself[103, 109, 111, 113, 120–122] or for its use in biosensing, mainly immunosensor applications[101, 102, 105, 107, 110, 112, 123].

Currently, it is impossible to find a quantitative comparison between ECL and other detection technologies in microfluidic systems (as is possible in bench-top assays), i.e. where the same assay has been optimized for ECL and also fluorescence, electrochemical or other detection principles. Comparisons, if any, are typically done through literature citations. However, all ECL-microfluidic publications present highly sensitive detection approaches that demonstrate LODs at the lowest concentration ranges shown thus far. Therefore, ECL- integrated microfluidic devices show great potential as analytical tools with increased sensitivity.

Another microfluidic application of ECL is found in the field of capillary electrophoresis (CE) and the use of Bipolar Electrodes. CE is an analytical separation technique. Ions are separated by CE according to their ionic mobility under the influence of an electric field. Microchip CE is an attractive variation of CE, due to its high performance, short analysis time, smaller sample volume, portability and disposability[124].

One major challenge in microchip CE development is the detector module. UV absorption, commonly used for CE, lacks sensitivity on the microscale format, due to the short path length available for the optical measurement. Laser-induced fluorescence is likely still the

most commonly used detection method, which is also commercially available. Still, for most analytes, the fluorescence efficiency is not sufficient. ECL CE, though not commonly applied yet, could provide the necessary sensitivity, and has already shown appropriately low limits of detection for many tested analytes[124]. For example, it was shown that limits of detection could be reached in the sub-nM level for proteins labeled with $Ru(phen)_3^{2+}$ with TPA as coreactant, in a CE-ECL system with less than 0.5 μL dead volume of the microfluidic ECL detection cell[125]. Also for ECL CE, alternative ECL reagents are tested, e.g. using 2-(2-aminoethyl)-1-methylpyrrolidine (AEMP) as a different ECL label than $Ru(bpy)_3^{2+}$ with TPA or proline as coreactant, with a limit of detection of 2.7 μM and a signal-to-noise ratio of 3[126]. As in other ECL research, ITO electrodes have been incorporated into CE-ECL systems[124]. Thus, for CE, the use of ECL will open the door for applications with more difficult and low-concentration analytes, and render the separation technology even more powerful.

The term bipolar electrode (BPE) describes an electronic conductor which is in contact with an ionically conductive phase to which an electric field is applied, and causes, at sufficient intensity, faradaic reactions at the bipolar electrode[127]. In other words, the electrode itself is not directly in contact with the current supply, and a simple power supply, like a battery, is sufficient for experimental use. This leads to the main advantage of BPE, i.e. their potential is easy to control. This can be especially helpful in microfluidic systems, where the working electrode potential can be harder to control than with a conventional three electrode system, due to the high electric field and solution resistance[127]. Publications for BPE ECL microfluidic devices deal, in general, more with the characterization and fabrication of the device itself[120–122, 128–133], with and without demonstration[128, 131, 133] of model analytes[120–122, 132], than for its use in biosensing applications[134, 135].

For all microfluidic ECL devices, regardless of their substrate, electrode configuration, or model analyte (Table 1), the main advantage over the more common fluorescent detection approaches is the lower limit of detection that can be reached. The lack of background signal generally leads to a higher signal-to-noise ratio. Furthermore, the challenge of even better LODs combined with device miniaturization is easier to overcome than for fluorescence or EC detection. All of this makes ECL not only a valuable existing tool, but an analytical method that will become more integrated into the rising field of microfluidics for biological and clinical applications with the need for sensitive detection in small sample volumes.

Table 1: Analytes detected via ECL or microfluidic ECL.

Groups of molecules (left column) specific analytes (right column); bolded are those analytes that were detected in a microfluidic ECL device.

Main Groups of Analytes	***Specific Analyte***
Coreactants	**DBAE**[103, 104]
	l-proline[103]
	NADH[104]
	TPA[132]
	nicotine[136]
	Hydrogen Peroxide[132] [137] [80]
Cancer Research	**Tumor Markers**[105] [102] [101] [59]
	carcinoma antigen 125[112] [138] [66]
	carcinoembryonic antigens[107] [123] [60] [61] [139]
	Cancer Cells[71] [69] [72]
	tumor necrosis factor-alpha (TNF-R)[65]
Protein	cardiac troponin I [140]
	human C-reactive protein (CRP)[141] [142] [63]
	α-fetoprotein (AFP)[143] [123]
	interleukin-6[110]
	Thrombin [56] [68]
	folate receptors [134]
	human prealbumin (PAB)[55]
Amino Acids [108]	**l-proline, l-lysine, l-leucine, l-valine, and l-histidine** [109]
	Proline[124]
	Leucine[144]
Ions	**Lead Ions**[106]
	Mercury Ions[106] [145]
	$Fe(CN)_6^{3-}$ [133]
	cupric cation[53] [76]
Antigens	Legionella antigen[146]

	Prostate specific antigen (PSA)[110, 123] [147]
Antibodies	Immunoglobulin G (IgG)[148] [78]
	Rabit IgG[62]
DNA[142] [70] [69][149]	mutant K-ras gene[52]
Small Molecules	Drugs (Methimazole[83], Gossypol[54])
	Dopamine[132] [150] [74] [30]
	phenylethanolamine A (PA)[64]
	ATP[118] [67] [73]
Viruses	astrovirus[151]

2.3 *Cryptosporidium parvum*

Cryptosporidium parvum (*C. parvum*) is a waterborne pathogen that causes the intestine-affecting disease cryptosporidiosis. *C. parvum* spreads mostly through contact with contaminated water. Between 2004 and 2010, 60.3% of worldwide waterborne protozoan outbreak was due to *C. parvum*. This infection is often lethal to immunodeficient patients suffering from other diseases, such as AIDS, very present in resource limited countries. But children and elderly patients are also at a higher risk of a *C. parvum* infection. Outbreaks occur more frequently in areas with insufficient water treatment, but even happen in western countries as well. It is, in fact, considered one of the most threatening waterborne pathogenic organisms in developed countries. One of the biggest outbreaks, for example, happened 1993 in Milwaukee, WI in the United States, when 403,000 people were infected[152]. In this particular case, two water treatment plants serving the city had been contaminated, leading to the spread of the disease.

C. parvum is also being investigated for its possible carcinogenic effects[153]. It was shown that infected SCID mice are at higher risk of gastro-intestinal or biliary cancer, though it is not certain if this is the case for humans, as well[154–156]. One study on patients, however, showed a high frequency of cryptosporidiosis in patients with colorectal cancer[153, 157].

The prevention of infectious outbreaks is challenged by the resistance of *C. parvum* towards most commonly used water treatment methods, such as chlorination, and by its high infectiousness. Even though the actual number of oocysts found in contaminated water is often very low, the risk is not lessened by this fact, as a volunteer study showed that as few as 30 oocysts could cause illness in some people[158].

Due to the severe consequences of infection, is it important to develop novel systems that offer sensitive results on a fast time scale. Also, due to its prevalence in developing countries, is it important to have portable sensors that are easy to use, even by untrained personnel, and cheap in fabrication cost; an ideal application for microfluidic chips.

2.4 Liposomes

Liposomes are artificial bilipid structures, forming nano/microvessels that encapsulate molecules and/or are tagged on their surface with molecules [147, 159–163] (Fig. 6).

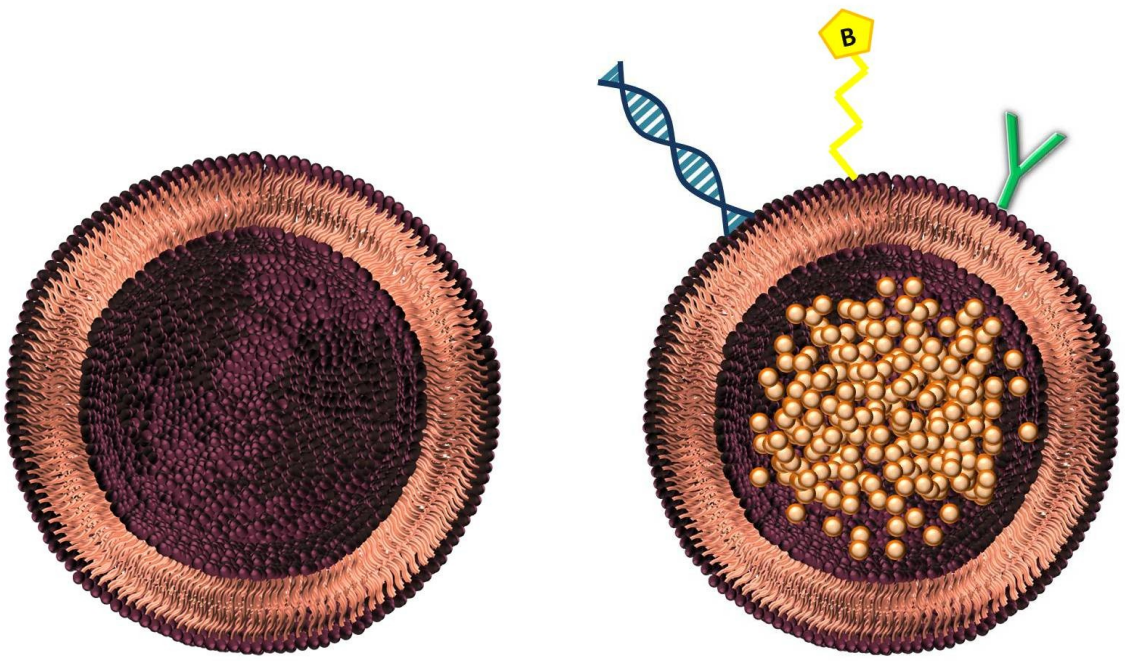

Fig. 6 Liposome Schematic
Left Figure: Liposomal structure cross section. The lipid bilayer forms a hollow vesicle.
Right Figure: Inside the lipid bilayer molecules, e.g. ECL reagents (orange) can be encapsulated in large quantities. The surface of the liposome can be modified, e.g. biotin (yellow), DNA tags (blue) or antibodies (green).

In most bioanalytical ECL applications employing liposomes, the ECL-active species is encapsulated inside the liposome. The liposome specifically binds to the analyte, either directly or through linker molecules.

To sense the encapsulant, a detergent is introduced to the system, leading to the lysis of the bilipid membrane and the release of ECL reagent into solution. A large number of molecules can be encapsulated inside a liposome (10^5-10^6 molecules per liposome), as has been shown for fluorescence (e.g. SRB[164–170], carboxyfluorescein[171]) and electrochemical (e.g.

potassium ferro/ferrihexacyanide[172]) markers. Improvements in limits of detection have been shown to be around 3 orders of magnitude[168]. Still, this strategy has not really been exploited for ECL detection yet. For example, liposomes were successfully synthesized with $Ru(bpy)_3^{2+}$ [141, 143, 146], luminol[173–176] (encapsulating either luminol itself or the co-reactant hydrogen peroxide), or [bis(2,2′-bipyridine)-4,4′-dicarboxybipyridine ruthenium-di(N-succinimidylester) bis(hexafluorophosphate)][177], with immunosensing[141, 143, 146, 178] being the most common application. However, in the case of the luminol studies, these were only employed for electrochemical detection, not for ECL signal generation. Still, the general proof of principle was demonstrated, leading to an LOD of 18 nM for the oligonucleotide strand, and a signal-to-noise ratio of almost 12 fold[173].

Liposomes provide an additional strategy for enhancing the ECL signal by simply increasing the number of $Ru(bpy)_3^{2+}$ able to undergo an ECL reaction. This multiplication of ECL molecules can be achieved not only through liposomes, but also by dendrimers or attachment to nanoparticles; here, mainly gold nanoparticles have been described[55, 179, 180].

Dendrimers are highly branched molecules that consist of a central core, a dendritic structure, and functional groups on the surface[181, 182]. Other molecules can be linked to the many available binding sites on dendrimers, making them ideal for applications such as labeling in bioassays or drug delivery in medical and therapeutic applications[183, 184]. By binding multiple ECL molecules to one dendrimer, which also binds specifically to the analyte molecule, a signal enhancement is achieved, due to the multiple ECL molecules involved. For example, in the case of a 5^{th} generation dendrimer, 128 ECL molecules can theoretically be bound to the dendritic structure. In addition, dendrimers were also used for surface modification, thus enhancing an ECL reaction. Namely, it was shown that a glassy carbon electrode functionalized with a poly(amidoamine) dendrimer with titanate nanotubes displays a higher ECL intensity for luminol than an unmodified glassy carbon electrode[137]. The same principle proved vital in an ECL assay on ITO electrodes, using $Ru(bpy)_3^{2+}$ with TPA as coreactant, which usually displays a low ECL intensity on ITOs, due to their slow kinetics of the electron-transfer process[136]. The described assay uses ITO surfaces modified with amine-terminated dendrimers encapsulating Pt and Au nanoparticles. This system led to an ECL signal increase of about 213-fold, in comparison to a bare ITO electrode, while only losing about 2 % of transparency over the whole visible region.

In addition to $Ru(bpy)_3^{2+}$ modified dendrimers[185] also $Ir(ppy)_3$[46], various polypyridyl Ru(II) complexes[145, 186], CdSe-ZnSquantum dots[71, 73], CdS-PAMAM/GNPs film[150]

and $[Ru(bpy)_2(PICH)_2]^{2+}$ [148] have been used for ECL detection, with similar signal enhancement achievements to those described above. Thus, while these bulky detection complexes do interfere with the kinetics of binding reactions, and likely suffer from stearic hindrance, the multiplication of ECL signal in one complex has proven to be a successful strategy on numerous occasions.

Liposomes offer the simple benefit of a higher signal multiplication capability compared to dendrimers. While a 5^{th} generation dendrimer can bind a theoretical maximum of 128 ECL molecules, an increase in magnitude up to 10^5-10^6 molecules can be achieved per liposome.

3. Material and Methods

3.1. Reagents

Tris(2,2′-bipyridyl)dichlororuthenium(II) hexahydrate, Tripropylamine, N-Butyldiethanolamine, 2-(Dibutylamino)ethanol, Triton™ X-100 and Zonyl® FSN fluorosurfactant were purchased from Sigma Aldrich. Potassium Phosphate Dibasic, Potassium Phosphate Monobasic and Tris were purchased from Fisher. Potassium phosphate monobasic was purchased from EMD and Potassium phosphate dibasic from Fisher. N-Hydroxysuccinimide (NHS) was purchased from Acros, Cystamine dihydrochloride from MP Biomedical, 2-(N-Morpholino)ethanesulfonic acid (MES) from OmniPur. Gold etchant trifluoroacetic acid (TFA) was used from Transene and Microposit S1813 Photo Resist and developer MF-321 was used from Shipley.

DPPC (1,2-dipalmitoyl-sn-glycero-3-phosphocholine) and DPPG (1,2-dipalmitoyl-sn-glycero-3-phospho-(1'-rac-glycerol)) were purchased from Avanti and Cholesterol from Calbiochem. The DNA sequences were ordered from Thermo Fisher Scientific. Dynabeads MyOne T1(magnetic beads with treptavidin) were ordered from Invitrogen.

Potassium Ferricyanide was purchased from EMD, Potassium Ferrocyanide from Mallinckrodt and Sulforhodamine B (Sulforhodamin B sodium salt) from Sigma. HEPES was purchased from Ambesco and Sodium Azide from Mallinckrodt Chemicals.

3.2. Procedures

3.2.1 Microelectrode Fabrication

Poly(methyl methacrylate) (PMMA) was placed under UV/ozon exposure (UV oven, Jelight Company Inc., UVO-Cleaner, Model#144AX) for 8 minutes before covering the surface with a stoichiometric solution of 0.3 M EDC and NHS in 50 mM MES solution at pH 6.0 for 30 minutes. Afterwards, the PMMA was rinsed with water, dried with nitrogen and covered with 0.3 M cysteamine solution in 50 mM sodium carbonate buffer at pH 9.0 by placing the solution in between two PMMA pieces and leaving them for three hours in humidified containers, then rinsed with water and dried with nitrogen. Gold evaporation with a thickness of 200 nm deposited gold was achieved using a CHA Mark50 evaporator at a deposition rate of 0.1 nm s^{-1}. S1813 photoresist was spun onto the evaporated gold surface for 30 s at 3000

rpm, with a ramp speed of 500 rpm s^{-1} and baked afterwards for 90 s at 90 °C. UV exposure (ABM Contact Aligner) with a mask was done for 12 s before washing the chip with developer MF-321 and gold etchant to reveal working, counter and reference electrodes. The RE was fabricated according to three different methods: electroplating, electroless plating and silver evaporation. For the first two, the RE consisted of gold, and was fabricated in the first step at the same time and in the same manner as the WE and CE. For electroplating, 30 µl of a 10 mM $Ag(NH_3)_2OH$ solution was pipetted onto the gold RE. A platinum wire and an Ag/AgCl electrode were used as external CE and RE, respectively. To electroplate the gold with silver, cyclic voltammetry steps were conducted from 300 mV to 500 mV at a scan rate of 50 mV/s. In electroless plating, no electrodes are required. A 0.1 M silver ammonia solution was prepared, to which drops of 10% NaOH were added for precipitation. By adding 26% NH_4OH and using an automated shaker, the precipitate completely redissolved again. Another solution of 0.5 M dextrose was prepared, 0.5 M dextrose and 0.1 M silver ammonia were mixed in a ratio of 1:5, and the gold surface was covered with the solution. After waiting several minutes and washing, the gold was covered with silver. With silver evaporation, an additional evaporation step was required with silver after the evaporation of PMMA with gold. The PMMA slide was half-covered with aluminum foil for both evaporations, resulting in a slide half covered with gold and silver (without gold underneath). In the first electrode design, the WE, CE and RE dimensions were 100 mm × 600 mm, 1200 mm × 600 mm and 100 mm × 300 mm, respectively. In the newer design, used for EC and ECL detection of *C. parvum* and the investigation of the influence of chemical environment, the working electrode dimensions were 300 µm x 5000 µm, and the counter electrode (CE) was 5000 µm x 5000 µm in size, with a distance of 300 µm between both electrodes.

3.2.2 Hot Embossing, Bonding and Chip Preparation

A copper mask with the microfluidic design was used as stamp for the PMMA. The PMMA piece itself (about 4 by 5 cm^2 and 2 mm thick) was placed on a blank sheet of copper on the hot press (Carver Laminating Hot Press, Fred S. Carver Inc., Summit, NJ) and heated to 85 °C for 30 sec. Then the copper plate with the fluidic design was placed on top the PMMA and pressed together at 4500 lbs for 3 min. After 3 minutes, the pressure was released, the copper plates with the PMMA turned by 180°, and the pressure reapplied for another 2 min. Turning the plates should eliminate uneven depths in the channel due to an uneven heat distribution on the hot press. The PMMA was then removed from the two copper plates and left to cool

down before holes were drilled at the inlets of each channel and the outlet of the main channel. With the channel side up, the PMMA pieces were placed under UV/ozone exposure for 10 min, together with plain PMMA pieces for SRB detection, or PMMA slides with electrodes for ECL and EC measurements. For bonding one PMMA piece with channel design, a plain or electrode covered PMMA piece were pressed together in the hot press at 65 °C and 4500 lbs for 3 min. in between two blank copper plates. Then the plates were turned again by 180 °C and pressed for another 2 min., resulting in a sealed microfluidic system, with overlapping electrodes, if required. Into the inlet and outlet holes, tubing was fastened with super glue.

3.2.3 DNA Hybridization Assay

For the formation of the hybridization assay, a Hybridization Buffer was used, consisting of 50% formamide, 10x SSC, 0.5 % ficoll (w/v), 0.3 M sucrose at a pH of 7.0. During detection on chip, a Running Buffer was used consisting of 20% formamide, 4xSSC, 0.2M sucrose, 0.2% ficoll (w/v), 0.8% dextran sulfase, and 0.1% sodium citrate at a pH of 7.0. The Capture DNA sequence was: 5'-biotin-AGA TTC GAA GAA CTC TGC GC-3'. The Target DNA sequence: 5'-AAGGACCAGCATCCTTGAGTA CTTTCT C AA CTG GAG CTA AAG TTG CAC GGA AGT AAT CA GCG CAG AGT TCT TCG AAT CT AG CTC TAC TGA TGG CAA CTG A-3'. The Reporter Probe was: 5‘-GTG CAA CT T TAG CTC CAG TT-[cholesterol]-3‘. The Capture Probe was linked to streptavidin on magnetic beads by washing 5 µl of magnetic beads with more than 50 µl of water, holding them in place inside an eppendorf tube with a magnet, and resuspending them in 3.75 µl of water. Then 1.25 µl of a 10 µM Capture Probe were added and incubated for 15 min. in shaker at room temperature. The beads were washed once more and resuspended in 3.75 µl water.

The hybridization assay itself consisted of 2.25 µl Hybridization Buffer, 2 µl Liposome solution (with Reporter Probe already attached to it), 1 µl target DNA, and 3.75 µl magnetic beads with capture probe solution (freshly prepared), incubated at room temperature for 15 min in a shaker.

3.2.4 Liposome Synthesis

Buffers required for liposome synthesis were: 10x HEPES buffer, consisting of 0.1 M HEPES, 2 M Sodium Chloride, 0.1% (w/v) Sodium Azide, pH adjusted to 7.5 with 4M NaOH, and volume brought to 1 liter; and 2 M Sucrose solution with 1% Sodium Azide. Both were mixed with a 1x HSS Buffer, which consisted of 200 ml MQ H_2O, 400 ml 2 M sucrose solution with 1% sodium azide, and 400 ml 10xHEPES, while the volume was brought to 4 liters with MQ H_2O.

The encapsulants were prepared differently. For the EC/fluorescent liposomes, the encapsulant consisted of 200 mM Potassium Ferricyanide, 200 mM Potassium Ferrocyanide, and 10 mM SRB. The required amounts of powder for each final concentration were dissolved and vortexed in 5 ml of MQ water and 0.9 ml of 0.2 M HEPES. After dissolving, the solution was increased to 10 ml, and either used immediately or stored in the refrigerator overnight for liposome fabrication. For 5 ml of encapsulant for ECL liposomes, 25 mM $Ru(bpy)_3^{2+}$, 0.5 ml of 0.2 M HEPES and 0.95 ml of 2 M Sucrose were used.

The liposome synthesis was started by dissolving 0.030 g DPPC, 0.015 g DPPG and 0.020 g cholesterol in 3 ml chloroform and 0.5 ml methanol, and sonicating for 1 min at 42 °C. 50 µl of crypto Reporter Probe (with cholesterol, and dissolved in 4:1 Formamide/Methanol) was added, and the solution sonicated for 4 min. Then 2 ml of the respective encapsulant, heated to 42 °C, was added, before the flask with the solution was attached to a rotary evaporator, set to 42 °C. The rotation was set to the highest rotation speed, and the pressure was lowered in 50 mbar/hPa steps down to 380 mbar/hPa. If too many air bubbles occurred, the pressure was increased again, but stayed at or under 600 mbar/hPa for 40 to 60 min. Then the pressure was increased, and the rotation stopped, before the flask was vortexed again to bring liposomes that might have fallen out of the solution into the solution again. Another 2 ml of encapsulant at 42 °C was added before the flask was attached to the rotary evaporator again. The rotation was set to maximum, and the pressure was lowered in 50 mbar/hPa steps down to 280 mbar/hPa and left at this pressure for 20 minutes, before the pressure pump was switched off and the rotation set to half speed for another 20 min.

Next, the liposome mix was inserted into an extruder, consisting of two syringes on each side of a filter. The solution was pushed back and forth for 21 times, first through a 1 µm pore size and then 0.4 µm (both filters from Whatman Nucleopore). After the extrusion, the liposome mix was run through a Sephadex G-50 column filled with a 1xHSS solution. This

allowed for separation of the liposomes and free dye. The isolated liposomes were pipetted into a dialysis membrane with 2 mL/cm volume capacity and sealed, before placing them into 800 ml of 1xHSS solution overnight.

3.3. Data Recording and Analysis

3.3.1 EC Standard Curves

EC standard curve data was recorded on chip after washing with water at 10 µl/min for 1 min and while 0.1 M KCl solution was applied at the RE channel at a flow rate of 5 µl/min. During measurements, the RE channel flow rate of the 0.1 M KCl solution was reduced to 0.8 µl/min. The analyte solution, consisting of $Ru(bpy)_3^{2+}$ at various concentrations with a coreactant/surfactant mix in 0.1 M PB, was injected at a flow rate of 5 µl/min. A voltage of 1.2 V was applied for 180 sec before the current was recorded with a potentiostat CV-50W (Basi, West Lafayette, IN, USA). The chip was then washed with the buffer solution (coreactant/surfactant in 0.1 M PB) before the same $Ru(bpy)_3^{2+}$ concentration was applied again and the recording repeated. Each concentration was measured in triplicate before the chip was washed, and a higher concentration of $Ru(bpy)_3^{2+}$ was measured in triplicate. For the standard curve, the values for each concentration were averaged and plotted against the concentration with their standard deviation.

3.3.2 ECL and SRB Liposome Recording

Prior to injection of the hybridization assay, the chip was washed thoroughly with water and Running Buffer in all channels at 20 µl/min for several minutes. For ECL and EC measurements, 0.1 M KCl solution in PBS was applied at the reference channel, and 60 mM OG solution connected to the OG channel but not injected yet. The needle of the syringe filled with OG solution was only hooked up to the tubing after the OG solution was pumped to the end of the needle and a droplet was clearly visible, to ensure injection without air bubbles. The hybridization mixture was drawn into a 10 µl syringe and quickly inserted into the inlet tubing. Then the main tubing was quickly connected to the Running Buffer-filled syringe, where solution had been flushed through already, to ensure no air bubble injection. In cases of air bubbles inside the tubing, Running Buffer was carefully pushed into the channel from the syringe, blocking the second inlet in the second fluidic design. This had to be done

with great care in order not to lose hybridization solution. The magnetic beads were then washed towards the magnet, which could be done at a high flow rate of up to 20 µl/min, but with great care not to lose beads. Once the magnetic beads reached the magnet, the flow needed to be decreased to less than 0.5 µl/min in the old fluidic design, and 1.5 µl/min in the new fluidic design, until all magnetic beads were accumulated over the magnet. After accumulation, 60 mM OG solution in 1xPBS from the OG channel was injected at 0.2 µl/min for the old fluidic design, and at 1 µl/min for the new one. Images of the background and signal were taken via the microscope camera. Once liberation occurred, pictures were taken in ten-second intervals at an exposure time of 1 sec and analyzed with ImageJ.

3.3.3 Optimization of Chemical Environment for ECL Enhancement

A sample volume of 40 µL, containing 250 µM $Ru(bpy)_3^{2+}$, one of the coreactants TPA, DABE, or NBEA, and one of the surfactants, Triton X-100 or Zonyl FSN in 0.1 M phosphate buffer (PB), was used for ECL and EC measurements, to determine the optimal coreactant concentration and a direct comparison between optimized systems. The microfabricated WE and CE were used in these experiments, with an Ag wire as reference electrode (RE). A CV-50W potentiostat (Basi, West Lafayette, IN, USA) was used to apply 1.2 V to the system for 30 s. The ECL signal was recorded via a Leica DM LB microscope (Leica Microsystems, Wetzlar, Germany) and a digital CoolSnap CCD camera (Photometrics, Tucson, AZ) which was operated by imaging software of Roper Scientific Inc. (Tuscon, AZ). An image of the WE was recorded every two seconds at an exposure time of 1 s. The images were converted to grey scale through ImageJ software, in which the signal intensity was determined. The resulting intensity values were integrated over time and normalized by the area of the electrode from which they were obtained, and compared to each other as intensity per unit area.

To compare the surfactant-free solution to the ones containing a surfactant, a 200 nm thick gold layer on a glass slide was used as WE. A Pt wire and Ag wire were used as CE and RE, respectively. ECL signal generation and recording were as previously described for the coreactant optimization. The value for NBAE and DBAE in surfactant free solution was normalized in relation to surfactant containing solutions, recorded under the same conditions.

For the dose-response curve and the low oxidation potential study, a three electrode setup consisting of a gold disc WE (diameter of 1.6 mm), a Pt wire CE (diameter of 0.5 mm), and

Ag wire RE (diameter of 2 mm) was employed. All electrodes were purchased from Basi (West Lafayette, IN, USA). An Autolab potentiostat (Metrohm, Herisau, Switzerland) was used to apply 1.2 V for 30 s. The luminescence was recorded via a spectrofluorimeter (Aminco Bowman Series 2, (AB2)) in bioluminescence mode with a PMT-voltage of 1000 V, and the integrated signal was determined via the AB2 software.

3.3.4 LOP Study

The concentration of $Ru(bpy)_3^{2+}$ was at1 μM, 50 mM for NBEA and DBAE, and 0.05wt% for Zonyl FSN, as previously optimized. Tris and Potassium Phosphate (PB) buffer were prepared at a concentration of 0.1 M each. 0.1 M PB was prepared with 0.1 M Potassium Phosphate Monobasic and 0.1 M Potassium Phosphate Dibasic to reach pH 7 and Tris by dissolving Tris in powdered form at the concentration of 0.1 M and then adjusting the pH to 8.5 with HCl. The three-electrode setup consisted of a gold disc WE (diameter of 1.6 mm) a Pt wire CE, and Ag/AgCl RE. An Autolab potentiostat was used to apply 1.2 V for 30 sec. The signal itself was recorded via an AB2 PMT, voltage at 1000 V, and the integrated signal was determined via AB2 software.

4. Results

4.1. Optimization of Chemical Environment for ECL Enhancement

The combination of $Ru(bpy)_3^{2+}$ with a coreactant such as tripropylamine (TPA) increases the ECL signal and allows detection in aqueous solutions under a constant potential, which is ideal for biological assays[3, 4, 187]. In coreactant-based ECL (Fig. 7), one of the coreactants' intermediate states upon reduction or oxidation can react with the ECL molecule, e.g. to form an excited state. The underlying mechanism for $Ru(bpy)_3^{2+}$ ECL can be either direct oxidation, catalytic oxidation, or reactions between the $Ru(bpy)_3^{2+}$ molecules and the amine cation radicals[13, 36–38, 40, 41, 188–194]. In the case of $Ru(bpy)_3^{2+}$, the ECL molecule is not consumed, and the process can be repeated.

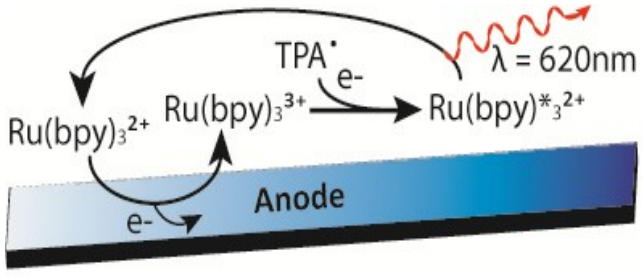

Fig. 7 ECL Mechanism

$Ru(bpy)_3^{2+}$ and the coreactant tripropyl amine (TPA) undergo electron transfer reactions at an electrode, leading to the excited, photon emitting state $Ru(bpy)^*_3{}^{2+}$.

For TPA, it was demonstrated that the surfactant Triton X-100 enhances the ECL signal[36], and an 8-fold increase in ECL efficiency in the presence of Triton X-100 was demonstrated by Workman et al. Surfactants are assumed to render gold and platinum electrode surfaces more hydrophobic, allowing more TPA molecules to reach the electrode surfaces, and consequently resulting in an increased coreactant oxidation rate[37]. The increased number of oxidized TPA molecules leads to a larger number of reacting and excited $Ru(bpy)_3^{2+}$ molecules. Even though micelle interactions could not be ruled out as cause for changes in ECL intensity, the stated and more likely explanation is the change in hydrophobicity of the electrode surface[3, 36, 195] Therefore, for $Ru(bpy)_3^{2+}$ ECL, TPA in combination with Triton X-100 is typically used in analytical applications, providing lower limits of detection and enhancing the sensitivity compared to a surfactant free solution.

However, in recent years, coreactants such as 2-(dibutylamino)ethanol (DBAE)[13] and N-Butyldiethanolamine (NBEA)[14] (Fig. 8) have been shown to enhance the ECL signal of $Ru(bpy)_3^{2+}$ even more than TPA. Han et al.[14] investigated multiple coreactants such as monoamines, e.g. 2-(dibutylamino)ethanol and N-butyldiethanolamine, and diamines, including N,N,N',N'-tetrakis-(2-hydroxyethyl)-ethylenediamine and N,N,N',N'-tetrakis-(2-hydroxypropyl)ethlenediamine. They found that monoamines lead to higher ECL signals than the diamines, with NBEA affording the highest so far published signal increase for $Ru(bpy)_3^{2+}$. The higher promotion of the amine oxidation by two hydroxyethyl groups instead of one is suggested to cause the increased ECL signal. It was also shown that the ECL process is directly related to the oxidation of NBEA. All of these studies demonstrate that investigations on alternative coreactants are valuable in reaching higher ECL intensities.

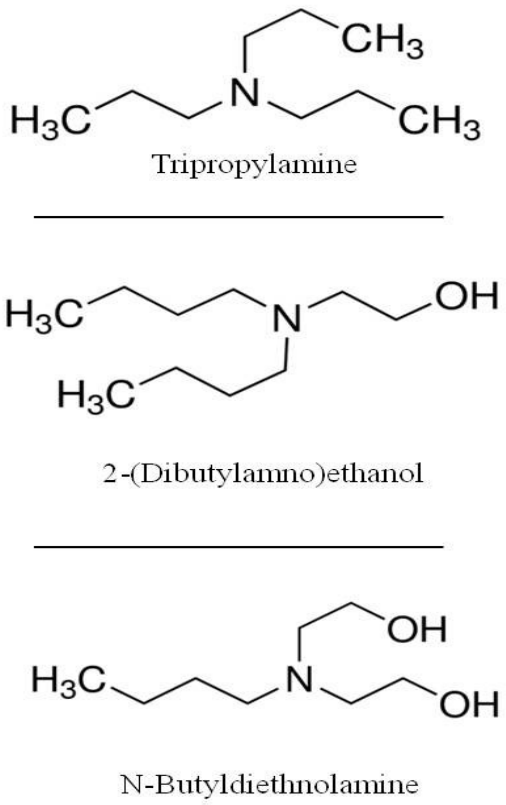

Fig. 8 Chemical structures of the coreactants Tripropylamine (TPA), 2- (Dibutylamino)ethanol (DBAE) and N-Butyldiethanolamine (NBEA)

Furthermore, alternative surfactants have been investigated. Zonyl FSN was shown to provide an approximately fifty-fold increase in ECL signal for $Ru(bpy)_3^{2+}$ with TPA compared to Triton X-100, supposedly due to an increase in TPA oxidation[37]. Even though

it has been demonstrated that DBAE and NBEA increase the ECL signal, no publication shows the two coreactants in combination with Triton X-100 or Zonyl FSN for $Ru(bpy)_3^{2+}$. Also, a comparative study is missing which would help elucidate the mechanisms of the complex ECL reactions. This study therefore investigated the effects of both surfactants, Triton X-100 and Zonyl FSN, in combination with the three coreactants, TPA, DBAE and N-Butyldiethanolamine, on $Ru(bpy)_3^{2+}$ ECL.

Electrochemiluminescence is an attractive analytical detection strategy for the detection of analytes, and has been studied extensively. It has been described previously that the ECL signal strongly depends on the coreactant concentration[13, 14]. It has also been found that, in addition to the original TPA coreactant, other amines can serve the same purpose. However, the mechanisms attributed to the various coreactants are different. Specifically, it was suggested that, for DBAE and NBEA, the direct oxidation of the coreactant is of great importance at low $Ru(bpy)_3^{2+}$ concentrations, and electrocatalytic oxidation of the coreactant by $Ru(bpy)_3^{2+}$ at higher $Ru(bpy)_3^{2+}$ concentrations[13, 14, 36, 38, 189–192]. This begged the question of how surfactants influence the various coreactant-based ECL reactions on gold surfaces. While Workman et al. have previously shown that surfactants increase the ECL signal due to an increase in hydrophobicity on the electrode surface and hindering of oxide layer formation, thus promoting access of TPA to the electrode, it is not clear that this mechanism holds true for other coreactant systems of the $Ru(bpy)_3^{2+}$-based ECL reaction[36]. A direct comparison within the same electrochemical and ECL set-up was necessary. Experiments were performed on microfabricated electrodes on PMMA (see Fig. 3), as, ultimately, ECL will be used in miniaturized (bio)assays. Since gold-plated PMMA is less sturdy than solid gold electrodes, additional knowledge was gained by using the more fragile electrode system.

Fig. 9 ECL Signal at the Working Electrode (WE)
Left: Brightfield image of the gold WE and CE
Middle: ECL signal for 250 µM $Ru(bpy)_3^{2+}$ with 100 mM TPA /0.4 mM Triton X-100
Right: ECL signal for 250 µM $Ru(bpy)_3^{2+}$ with 50 mM N-Butyldiethanolamine / 0.05 wt% Zonyl FSN

Initial studies looked at the $Ru(bpy)_3^{2+}$ ECL signal obtained for the combinations of the three coreactants, TPA, DBAE and NBEA, with the two surfactants Triton X-100 and Zonyl FSN, at varying coreactant concentrations (see Fig.10, Table 2 and Coreactant Optimization in the Supplementary Information). It was found that DBAE- and NBEA-based ECL require

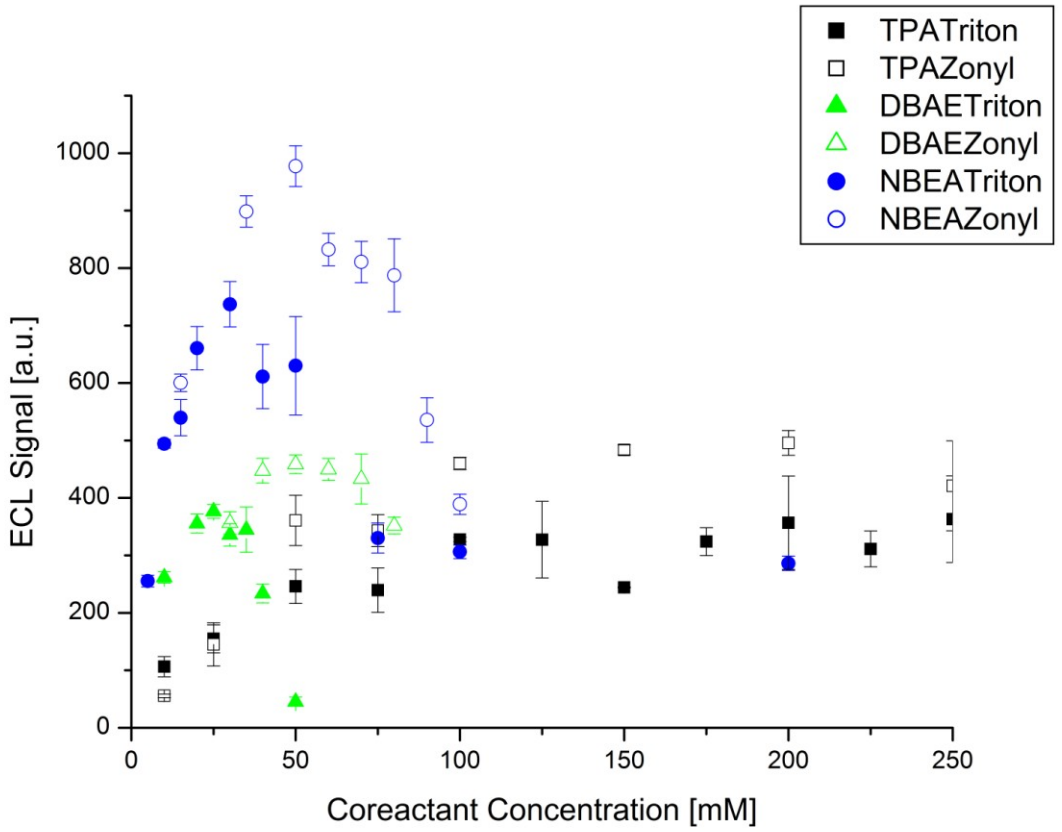

Fig. 10 $Ru(bpy)_3^{2+}$ ECL intensity vs. coreactant concentration for each of the six coreactant/surfactant systems.

Concentrations used were 250 µM $Ru(bpy)_3^{2+}$, 0.4 mM Triton X-100, and 0.05 wt% Zonyl FSN in 0.1 M phosphate buffer, at 1.2 V for 30 seconds, measured on a microfabricated gold working and counter electrode, with AG wire as reference electrode. Analyses were done in triplicates, and standard deviations are plotted here.

significantly less coreactant concentration than TPA-based ECL to reach the optimal ECL signal with the respective coreactant. This has also been shown previously, in cases where DBAE was used at 20 mM and NBEA at 15 mM, in contrast to 100 mM for TPA, with the goal of replacing the toxic TPA with more environmentally friendly coreactants [13, 14].

However, in the systems investigated in the present study, the coreactant concentration needed to be increased in the presence of both surfactants, compared to the previously published concentrations. Triton X-100 required, in general, less coreactant concentration to

reach optimal ECL intensity, but also led to a lower ECL signal compared to Zonyl FSN for each coreactant. Specifically, with Zonyl FSN as surfactant, the optimal coreactant concentration for DBAE and for NBEA was 50 mM; for TPA, 200 mM. For Triton X-100, the highest ECL signal could be observed at 100 mM TPA, 25 mM DBAE and 30 mM NBEA. This is significant, as lower coreactant concentrations lead to overall lower current flows and, in turn, higher stability of microfabricated electrodes (see further below).

A direct comparison between the coreactant surfactant systems with these optimized coreactant concentrations revealed that NBEA with Zonyl FSN leads to the highest ECL signal (Fig. 11 and Table 2).

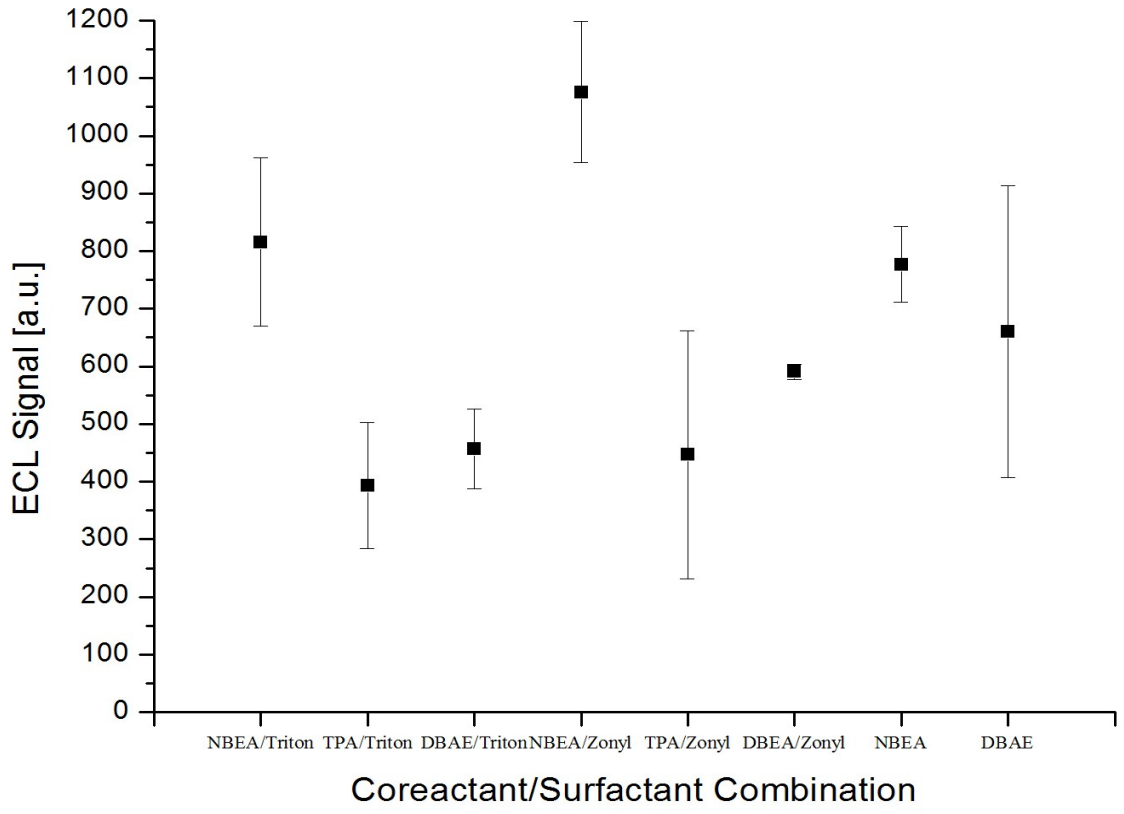

Fig. 11 ECL signal dependence on the optimized coreactant/surfactant system for 250 µM $Ru(bpy)_3^{2+}$

ECL signal of 250 µM $Ru(bpy)_3^{2+}$ with 30 mM NBEA/0.4 mM Triton X-100, 50 mM NBEA/0.05 wt% Zonyl FSN, 25 mM DBAE/0.4 mM Triton X-100, 50 mM DBAE/0.05 wt% Zonyl FSN, 100 mM TPA/0.4 mM Triton X-100, 200 mM TPA/0.05 wt% Zonyl FSN, 50 mM NBEA and 50 mM DBAE in 0.1 M phosphate buffer. Voltage of 1.2 for 30 seconds on microfabricated gold WE. Analyses were done on six replicates and standard deviations plotted here.

Also, the signal is stronger than the previously published highest increase by NBEA alone, or by TPA with either surfactant[14, 36, 37]. We obtained an ECL signal which shows an increase by factor of 1.4 over the previously most effective coreactant NBEA by itself, and a factor of 2.7 over the standard TPA/Triton system.

This proved that the role NBEA plays in the $Ru(bpy)_3^{2+}$ ECL pathway is not diminished by the surfactant, but instead enhanced. On the other hand, as the data indicates, DBAE in the presence of any of the two surfactants displayed a lower ECL signal than for DBAE alone. This is contradictory to the assumption that the surfactant's effect is solely to render the electrode surface more hydrophobic[3, 36, 37, 86, 195]. An increased hydrophobicity of the electrode explains the signal enhancement for the hydrophobic TPA. Furthermore, it would suggest to affect the coreactant DBAE in a lesser manner than TPA, due to the two $-CH_3$ groups and one -OH group of DBAE compared to the slightly more hydrophobic TPA with three $-CH_3$ groups. NBEA by this argumentation should either be more or similarly repelled from the electrode surface and its layer of surfactant as DBAE, leading to a lower number of coreactant molecules in close proximity to the electrode to participate in electron transfer reactions to support the ECL pathways of $Ru(bpy)_3^{2+}$.

As our data indicate the opposite, we suggest that besides the hydrophobic effect of the surfactant other aspect need to be taken into consideration. Both Triton X-100 and Zonyl FSN are present in a concentration above the critical micelle concentration (CMC)[196–198], ruling this factor out. However other factors are important. For example, amongst others, in the ECL cycle itself three major parts can influence the ECL signal. First (1), the oxidation of $Ru(bpy)_3^{2+}$ at the electrode, second (2) the formation of $Ru(bpy)_3^{2+}$-coreactant couples and reduction of $Ru(bpy)_3^{3+}$ and third (3) the radiative and nonradiarive relaxation to the ground state. For the first aspect, the oxidation of $Ru(bpy)_3^{2+}$, it would indeed appear that the hydrophobicity is the most important factor and would enhance the signal with the coreactant TPA the most and NBEA the least. Yet in the second part, the positively charged ruthenium complex and the less polar coreactant have to be brought into close proximity to enable an electron transfer from the tertiary amine. NBEA in this case with two OH-groups that have a negative partial charge will be able to approach the positively charged $Ru(bpy)_3^{2+}$ complex in closer proximity. This effect is smaller for DBAE and even less for TPA. Hence, in part (2) the electron transfer should be promoted just in the opposite order of the coreactants as in part (1). For the third factor, the radiative and nonradiarive relaxation to the ground state, the surfactant should play an important role, as the decay from the excited state is promoted by a

less polar (i.e. water-free) environment. Less water in the micelle means less quenching and higher light emission. Zonyl as a polyfluorinated detergent should supply a less water containing micelle than Triton X-100 which would then explain the trend for the higher ECL signal with Zonyl FSN instead of Triton X-100.

Since however the ECL signal is affected by all of the mentioned factors and even more interactions it is hard to conclude a general assumption. A likely explanation in our case, is that the effects of part (2) and (3) dominate the effect of part (1), leading to the signal enhancement for NBEA with Zonyl FSN.

Table 2: *Optimal coreactant concentration and ECL signal for different coreactant/surfactant systems. Concentrations used were 250 µM* $Ru(bpy)_3^{2+}$*, 0.4 mM Triton X-100 and 0.05 wt% Zonyl, and the coreactant concentration as stated in the first row. Signal was generated on microfabricated gold electrodes.*

	TPA/Triton	TPA/Zonyl	DBAE/Triton	DBAE/Zonyl	NBEA/Triton	NBEA/Zonyl
Optimal Coreactant Concentration [mM]	100	200	25	50	30	50
ECL Intensity [a.u.] integrated over 30 sec	393 ± 109.4	447 ± 214.9	457 ± 69.1	591 ± 13.6	816 ± 143.2	1076 ± 122.8

As indicated above, the ECL signal was recorded on microfabricated electrodes on PMMA to test for the capability and feasibility of incorporation into a microfluidic ECL detector. Microfluidic devices are especially necessary in cases with reduced sample volume, or where mobility and easy handling are required. However, reduction of sample sizes led, in general, to a decrease in signal, which needs to be compensated for in order to be compatible with large-scale detection devices in terms of sensitivity. ECL-based detection offers the benefit of low background noise, and is therefore highly promising for sensitive microfluidic devices. ECL requires the presence of electrodes, and the lifetime of a microfluidic device is mainly determined by the stability of its active components, such as the electrodes. Therefore, it is critical to prevent the fouling and delamination of the electrodes (in our case, the evaporated gold layer), which is inadvertently caused by excessively high current flow. Microfabricated electrodes from various fabrication batches were used for this study. Also, new electrodes were used for each experiment, so that contamination of surfactants could be avoided. While this leads to high standard deviations, as would be expected[199], the direct comparison of the

standard TPA/Triton X-100 and the optimal NBEA/Zonyl system showed a significantly lower current flow for the NBAE system, i.e. dropping from 91 µA (±27 µA) for TPA/Triton X-100 to 64 µA (±29 µA) for NBEA/Zonyl.

Finally, the NBEA/Zonyl FSN system was compared to the standard TPA/Triton X-100 $Ru(bpy)_3^{2+}$ ECL reaction. This time, experiments were done using a standard gold disc electrode, in order to obtain highly reliable and comparable sets of data, and avoiding batch-to-batch variations of microfabricated PMMA-coated electrodes. A dose response curve for $Ru(bpy)_3^{2+}$ showed an improvement in the limit of detection (LOD) by a factor of 250 (Fig. 12 and Table 3).

Table 3: *Limit of detection for $Ru(bpy)_3^{2+}$ with 50 mM NBEA/0.05 wt% Zonyl and 100 mM TPA/0.4 mM Triton (n=3). Signals were measured with either phosphate buffer or the complete ECL solution (without the ruthenium complex) to calculate the LOD.*

Solution used for background noise detection	LOD – NBEA/Zonyl	LOD – TPA/Triton
Phosphate Buffer	1.6 nM	58.42 nM
Coreactant/surfactants present in phosphate buffer	2.2 nM	0.59 µM

The LOD for $Ru(bpy)_3^{2+}$ with TPA/Triton X-100 was at 0.59 µM, but as low as 2.2 nM (3σ/slope) with NBEA/Zonyl FSN. Interestingly, it was observed that the background noise afforded by the ECL solution components (minus the ruthenium complex) is much more significant for the TPA/Triton X-100 solution than for the NBEA solution. The increased background intensity for TPA has already been discovered by Leland at al.[187] when they introduced TPA as a signal enhancing coreactant for $Ru(bpy)_3^{2+}$.

NBEA, on the other hand, does not show this negative effect in our study. Specifically, the background noise leads to an increase (worsening) of the LOD by a factor of 10 for the TPA/Triton X-100 system, whereas the LOD for the NBEA/Zonyl FSN system is not changed (Table 2). Moreover, the sensitivity, as calculated by the slope of the linear portion of the

dose-response curve, was $3.8*10^7$ M^{-1} for the new system, in comparison to only $8*10^5$ M^{-1} for the standard condition.

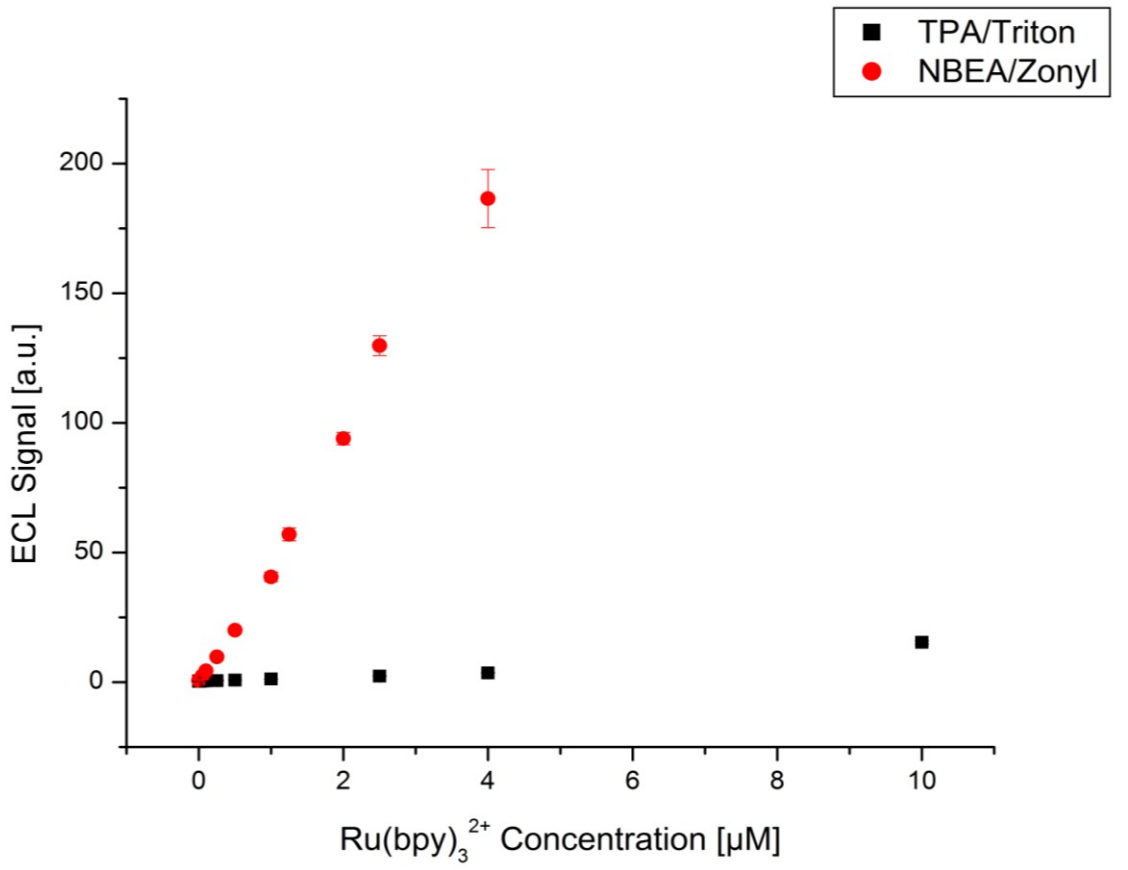

Fig. 12 Dose Response Curve for $Ru(bpy)_3^{2+}$ with 50 mM NBEA/0.05 wt% Zonyl (●) and 100 mM TPA/0.4 mM Triton X-100 (■) in 0.1 M phosphate buffer with 2 mm gold disc WE. Analyses were done in triplicate, and standard deviations are plotted here.

Both the decreased LOD and the increased sensitivity are important features for the development of analytical systems based on an ECL reaction. These findings are not only beneficial for future to-be-developed miniaturized ECL (bio)sensors, but also for existing assays, since no changes are required on the hardware components of an ECL (bio)sensor, but only a change in the chemical environment.

4.2. Low Oxidation Potential ECL

While conducting studies on the influence of Tris buffer on the $Ru(bpy)_3^{2+}$ ECL system, we found that it displays an ECL signal at potentials well below 1V. Investigated were solutions of 1 µM $Ru(bpy)_3^{2+}$ with 50 mM NBEA and 0.05 wt% Zonyl FNS in Tris buffer pH 8.5 at various potentials (Fig. 13). Even at potentials as low as 800 mV, a significant ECL signal was detectable. The LOP ECL signal itself showed that a plateau in LOP ECL signal was reached between 880 mV and 910 mV vs. Ag/AgCl, and a potential of 890 mV was consequently chosen for subsequent studies. The LOP occurs at the potential for the direct oxidation of NBEA, which was shown to be around 900 mV[13].

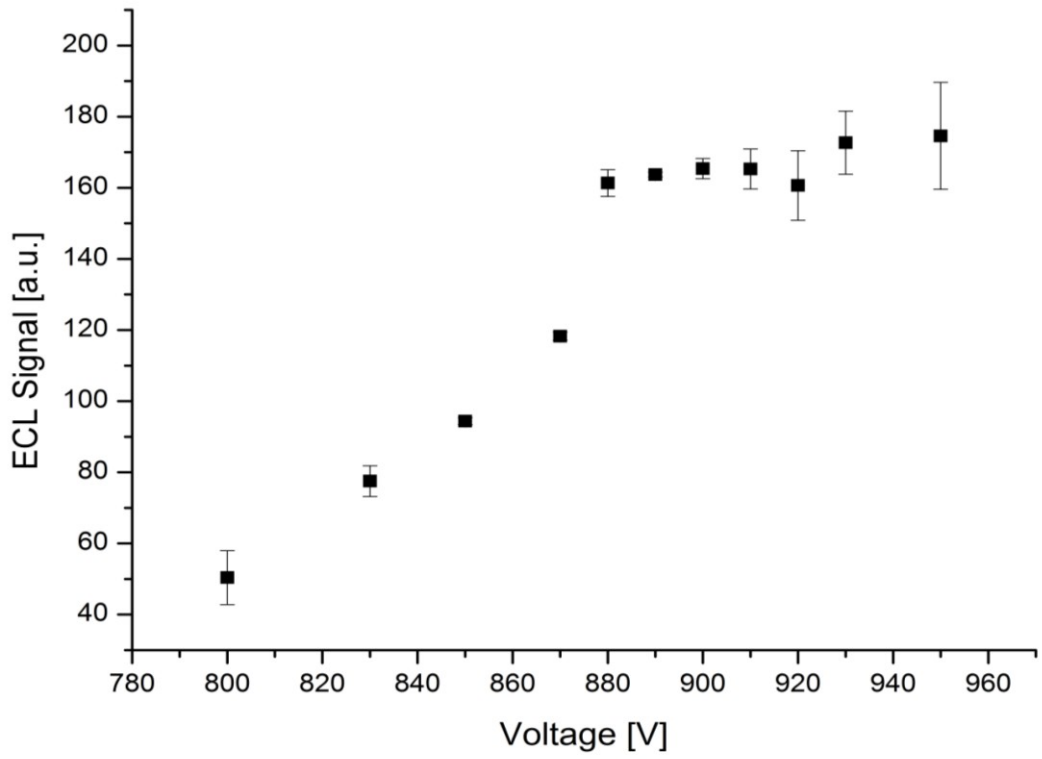

Fig. 13 ECL signal for 1 µM $Ru(bpy)_3^{2+}$ with 50 mM NBEA and 0.05 wt% Zonyl FNS in Tris Buffer pH 8.5 according to applied potential vs. Ag/AgCl. ECL signal was generated on an Au disc electrode vs. Ag/AgCl, and integrated over 30 sec. n=3.

Previously, no one had reported an LOP ECL signal with NBEA as coreactant. Therefore, we started with the investigation by comparing the signal to a more commonly used phosphate buffer system and changing the pH from a standard 7 to 8.5, which is still usable in biological assays. Furthermore, the influence of the surfactant Zonyl FSN was investigated. To complete the study, we tested DBAE for its LOP ECL capabilities as well, and compared it with TPA.

When recording the EC data for NBEA in the combinations of PB and Tris Buffer at the pHs 7 and 8.5, we observed strong peaks in current at well below 1 V for all systems except Tris buffer at a pH of 7 (Fig. 14).

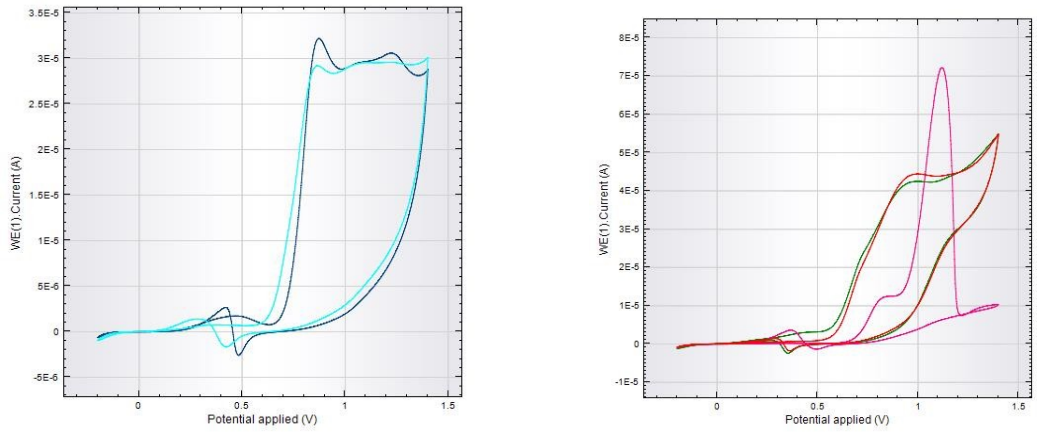

Fig. 14 CVs for 1 µM $Ru(bpy)_3^{2+}$ with the coreactant NBEA. Left: PB at pH of 7 (blue) and at a pH.8.5 (Cyan). Right: Tris buffer at a pH of 7 (Pink), at a pH of 8.5 (red) and at a pH of 8.5 in the absence of Zonyl FSN (green). Recorded at a Scan rate of 10 mV/sec vs. Ag/AgCl.

Indeed, 1 µM $Ru(bpy)_3^{2+}$ with the coreactant NBEA in Tris buffer at a pH of 7 did not lead to an LOP ECL signal, as could be expected from the CV data (Fig. 14 and 15). However, the LOP ECL signal for PB was minimal, and much weaker than would be expected from the CV data. This shows that, in ECL studies, EC data can be an indicator for the signal intensity, but cannot be directly translated, since too many interactions can occur between the different components that lead to electron transfer but do not support the formation of the excited photon-emitting state of $Ru(bpy)_3^{2+}$.

Only in Tris buffer, pH 8.5, was a clear LOP ECL signal detectable for NBEA (Fig. 15). Interestingly, the same LOP ECL intensity was observed in the presence and absence of the surfactant Zonyl FSN. This suggests that, even though the ECL signal at 1.2 V can be slightly increased with Zonyl FSN, a surfactant is neither beneficial nor detrimental to the LOP ECL of $Ru(bpy)_3^{2+}$ with NBEA.

TPA shows an LOP signal in PB, but only a slight signal in Tris. For DBAE, an LOP ECL signal was observable under all tested conditions. Only in Tris, pH 7, was the signal the highest for DBAE, albeit with high variations in signal.

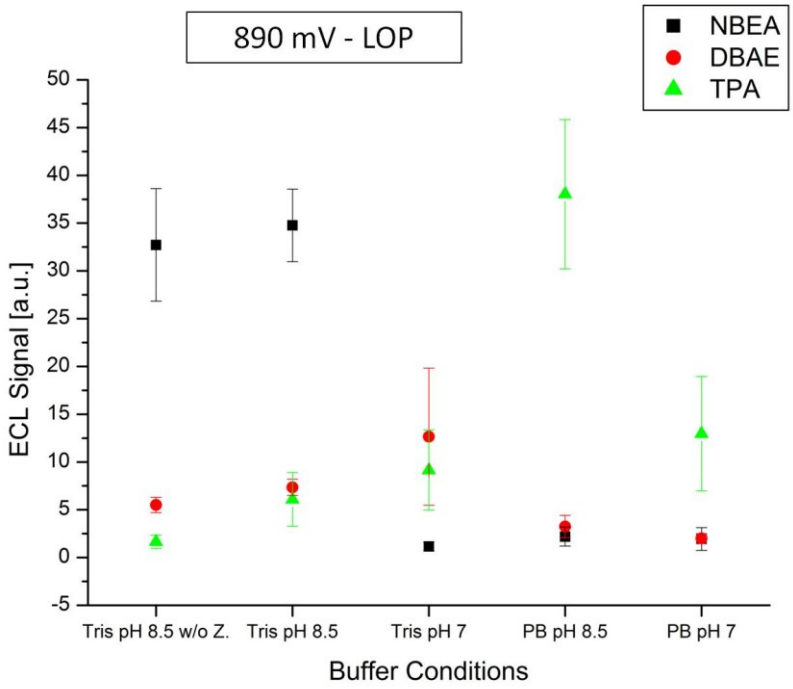

Fig. 15 LOP ECL signal for 1 µM $Ru(bpy)_3^{2+}$ with the coreactants NBEA (■), DBAE (●) and TPA (▲) and the surfactant Zonyl FSN under different buffer conditions. The investigated buffers were, from left to right: Tris buffer pH 8.5 without Zonyl (w/o z.), Tris buffer pH 8.5, Tris buffer pH 7, PB pH 8.5 and PB pH 7. ECL signal was recorded on a gold disc electrode at a potential of 890 mV.

We can conclude that the LOP ECL signal is not only dependent on the buffer system, but also on the pH. The same proved to be true for the ECL intensity at 1.2 V vs. Ag/AgCl (Fig. 16). It is therefore assumed that Tris interferes with the $Ru(bpy)_3^{2+}$ ECL pathway and, consequently, the enhanced production of the excited state. However, we could not obtain any information in the literature to prove this. Even though Tris can interfere with metals, and has been studied in the presence of metal ions such as Mg^{2+}, Ca^{2+}, Ba^{2+}, Mn^{2+}, Co^{2+}, Ni^{2+}, Cu^{2+}, Zn^{2+}, Cd^{2+}, and Pb^{2+} [200], we are not aware of any studies with $Ru(bpy)_3^{2+}$ nor of possible influences on ECL generation. However, it is known that Tris can form complexes with transition metal ions[201]. Those complexes are mostly formed through deprotonation of one of the OH-groups of Tris[201].

Not only did NBEA in Tris pH 8.5 display an LOP ECL signal, it also showed the highest ECL signal, at 1.2 V vs. Ag/AgCl from the investigated systems (Fig. 16).

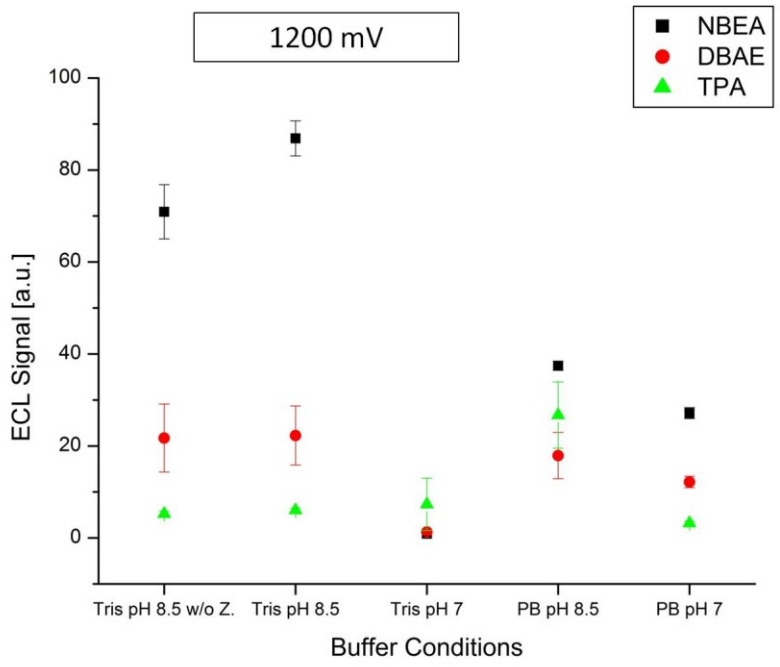

Fig. 16 LOP ECL signal for 1 µM $Ru(bpy)_3^{2+}$ with the coreactants NBEA (■), DBAE (●) and TPA (▲) and Zonyl FSN as surfactant under different buffer conditions. The investigated buffers were, from left to right: Tris buffer pH 8.5 without Zonyl (w/o z.), Tris buffer pH 8.5, Tris buffer pH 7, PB pH 8.5 and PB pH 7. ECL signal was recorded on a gold disc electrode at a potential of 1.2 V.

While the surfactant appears to be of no importance to the occurrence of LOP ECL, the buffer conditions themselves influence the signal intensity significantly. Specifically, the ECL signal with NBEA was enhanced when the buffer system was changed from PB to Tris buffer, i.e. the signal increased from a value of 37 (±4) to 87 (±7) at a pH of 8.5 and a voltage of 1.2 V, and from 2 (±1) to 35 (±4) at the LOP voltage. Consequently, multiple factors can interfere with the LOP ECL signal of $Ru(bpy)_3^{2+}$ and defined buffer and pH conditions are required.

Overall, it was determined that the optimal LOP ECL signal of the $Ru(bpy)_3^{2+}$/NBEA/Zonyl system is 40% lower than the optimal ECL signal at 1.2 V. However, it is still 2.7 times higher than the commonly-used TPA/Triton X-100 system at pH 7 in a phosphate buffer (Fig. 15 and 16), which thus makes it a viable option for all (bio)assay applications and very attractive for miniaturized systems.

4.3. Microfluidic ECL device using Liposome-based Amplification for DNA Detection

Microfluidic chips are highly diverse, and specifically designed and manufactured for the required application. Specifically, in our case, the microfluidic channels needed to overlap with a three-electrode system. Since the chip was intended for DNA detection via lysis of liposomes, multiple inlets were required to supply the captured DNA with washing and lysing solution. In addition, the chip had to be reusable after DNA detection.

Microfluidic Design

For preliminary measurements, a chip design was used that had been previously used in our lab for EC applications and had been designed by Dr. Nongnoot Wongkaew (Fig. 17). The chip used three inlets for each of the three channels: a) the main channel, into which the analyte was injected; b) the OG channel which, after washing via the main channel, inserted the liposome-lysing reagent Octyl β-D-glucopyranoside (OG); and c) the reference channel, which supplied the reference electrode with KCl solution.

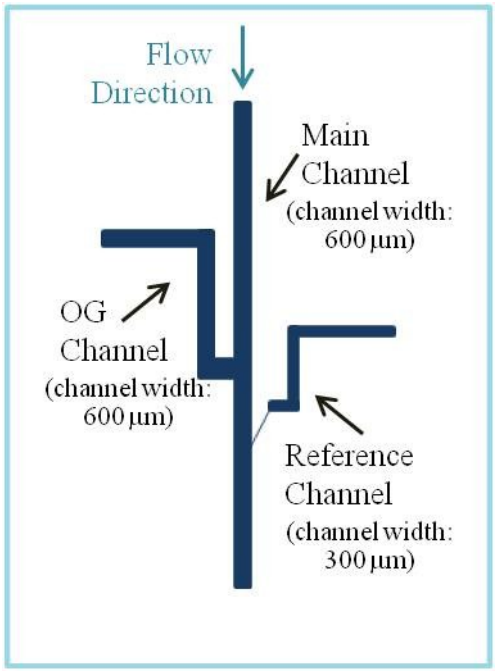

Fig. 17 Microfluidic Design

As a substrate, PMMA was employed. There is a large variety of substrates one can use for the fabrication of microfluidic systems, including PDMS, paper, glass, and silicon. All have certain advantages and disadvantages, and one needs to pick a substrate carefully with these requirements in mind. In our case, the attachment of conductive parts on a non-conductive substrate is essential, in combination with an easy method to form microfluidic channels into the substrate that is transparent for light. For PDMS and PMMA, there are established methods for attaching metal to them while retaining their transparency. PDMS, however, usually requires the use of a plasma oven to seal it to either glass or PDMS, and can be rather soft and easy to bend, increasing the risk of a discontinuous metal layer. PMMA is commercially and cheaply available and, combined with the tools and expertise in our lab, the better choice.

Incorporation of the micro channel system into the chip was achieved via hot embossing. In this common method for forming PMMA, a mask carrying the microfluidic design is pressed into the heated PMMA, to stamp the pattern into it. The hot press is also used to bind the PMMA piece with the microfluidic channels to the one with the electrodes, forming a sealed system. Usually, PMMA needs to be heated above its glass transition temperature for such treatment. However, a UV/ozone treatment allows manipulation well before the glass transition temperature T_g[202, 203]. For both steps, embossing and binding, the parameters, such as pressure and temperature, had to be optimized, as well as the conditions for UV/Ozone treatment itself.

Electrode Fabrication

ECL requires electrodes in bench-top devices as well as in microfluidic devices. The electrode system usually employed for ECL, and also EC, is a three electrode system, consisting of a working electrode (WE), a counter electrode (CE) and a reference electrode (RE). The ECL signal itself will be generated at the WE, set to the specific voltage required for the ECL pathway in relation to the RE. The different requirements and functions of the electrodes are reflected in their material of choice. For instance, as the analytical reactions take place at the WE, the WE material needs to be inert in order to be unaffected by the current going through it. Therefore, gold, platinum, and carbon are often used as WE. The counter, or auxiliary, electrode needs to be made out of an inert material as well. It is used as source and drain for the current, but does not participate in the electrochemical reaction. The current itself flows between the WE and the CE. The RE is the potential reference to the WE. Ideally, it should stay unaffected by current flow passing through it, and hold a constant potential. This can be achieved by either having a high input impedance, reducing the current flow, or use of a non-polarizable electrode where a small flow of current does not affect the potential. The classical reference electrodes are, for example, made of Ag/AgCl, saturated calomel, or mercury/mercury sulfate.

In bench-top devices, the realization of a three-electrode system is fairly easy. Numerous companies offer electrodes with known dimensions. In commercial large-scale ECL machines, the electrodes are already incorporated. In self-built microfluidic devices, however, incorporation of a working three-electrode system is a great challenge. Of course, one could think of a system where commercially available macro electrodes can be attached

to the chip: e.g., a platinum wire could be inserted into the microfluidic system through a drilled and sealed hole. Considering the price for those electrodes, a few hundred euros would be required for a complete system. Even if the same electrodes can be used while the chip is replaced, one is faced with problems, such as possible leaking on the places where the electrodes are inserted into the system, lower mobility, and the need for more highly-qualified personnel for operation. For general testing, a macro electrode system is still highly valuable, since it eliminates several complex factors, e.g. electrode delamination and flow effect. But for large scale manufacturing, it is not an option that is affordable, fast and easy to use. For autonomous microfluidic ECL systems, it is therefore essential that a three-electrode system is incorporated into each chip.

Specifically, for PMMA, the surface can be thiolated, enabling the linkage of gold to it[172, 199, 204]. For the thiolation (Fig. 18), a UV treatment is required to induce carboxyl (C(O)OH group) formation. Surface thiolation is achieved via further treatment with EDC (N-(3-Dimethylaminopropyl-N'-ethylcarbodyamide-hydroxychloride)), NHS (N-Hydroxysuccinimide) and cystamine ($C_3H_7NO_2S$).

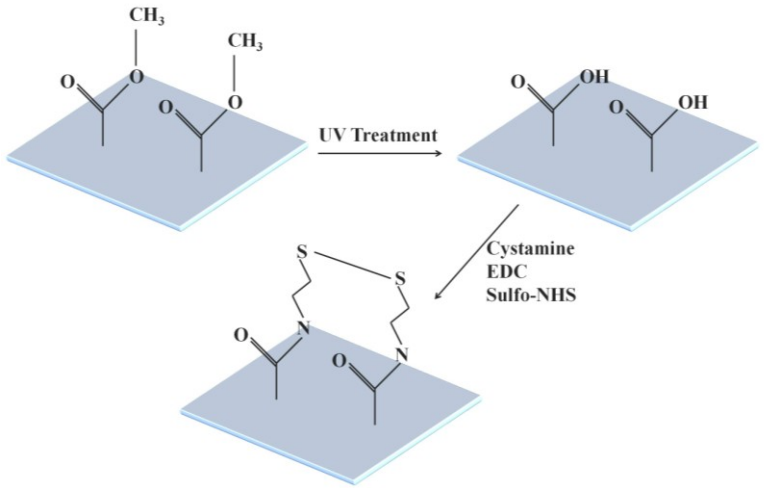

Fig. 18 Surface thiolation schematic of PMMA

The gold itself can then be evaporated under clean-room conditions via e-beam evaporation. Since gold forms strong bonds with free thiols, no further treatment is required. A layer of designated thickness can be evaporated and used for measurements.

Gold is therefore a good choice as WE and CE material, which require inert materials. However, for the RE, another metal is needed. For the first $Ru(bpy)_3^{2+}$ EC measurements with the device, silver was electroplated on a gold RE to form, together with the KCl solution in the reference channel, an Ag/AgCl RE. The initial electrode dimensions were 100 µm × 600 µm for the WE, 1200 µm × 600 µm for the CE, and 100 µm × 300 µm for the RE (Fig. 19). The connecting pads were glued to a copper wire with conductive glue, to allow attachment to the potentiostat supplying the required voltage.

The microfluidic channels needed to be aligned with the electrodes to close the three-electrode system and to allow for detection (Fig. 20). The analyte was inserted via the main channel, and detection accured on the WE.

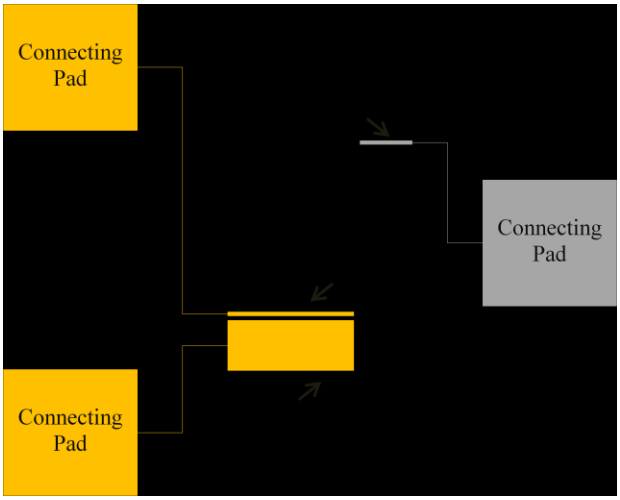

Fig. 19 Three electrode setup design on chip

Dimension:
WE = 100 µm × 600 µm
CE = 1200 µm × 600 µm
RE = 100 µm × 300 µm
The connecting pads do not participate in the ECL or EC reaction, but offer electric contact to the potentiostat.

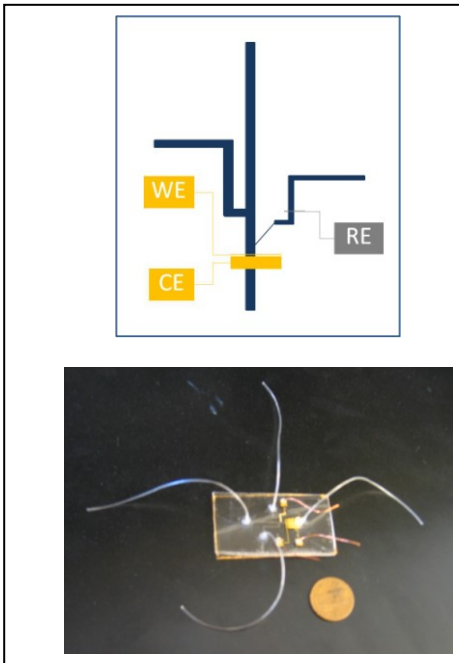

Fig. 20 Microfluidic Chip

Schematic drawing of fluidic and electrode overlap (top) and finished chip with tubing and copper wires (bottom).

Electrochemical (EC) Measurements

For our first insights into the behavior, handling and limitations of the chip, EC measurements were performed with the device as an initial step. $Ru(bpy)_3^{2+}$ is probably the most common ECL reagent in literature, and was also used for our assays. $Ru(bpy)_3^{2+}$ ECL is rarely used by itself in analytical applications, but in combination with a coreactant and sometimes with a surfactant, both intended to increase the ECL signal. Therefore, as first tests, three coreactants, TPA, DBAE and NBAE, were combined with the surfactants Triton X-100 and Zonyl FSN. Under a voltage of 1.2 V, the current on the WE was recorded depending on different $Ru(bpy)_3^{2+}$ concentrations, from which standard curves of $Ru(bpy)_3^{2+}$ under different coreactant/surfactant conditions were determined (Table 4 and EC Standard Curves in the Supplementary Information).

Table 4: *EC Detection of $Ru(bpy)_3^{2+}$, in different chemical environments*

			Measured Current Range			
Coreactant/Surfactant	LoD, [µM]	Sensitivity	min, [A]	Max, [A]	Value at 100 uM, [A]	Value at 500 uM, [A]
TPA/Triton X-100	47.2	1.81E-009	-1.76E-07	-1.73E-06	-3.22E-07	-1.09E-06
DBAE/Triton X-100	68.27	2.01E-08	-2.09E-06	-1.78E-05	-4.29E-06	-1.19E-05
N-BEA/Triton X-100	33.97	2.98E-08	-1.38E-06	-1.61E-05	-5.18E-06	-1.61E-05
TPA/Zonyl FSN	4.68	8.31E-09	-1.97E-07	-4.25E-06	-8.63E-07	-4.25E-06
DBAE/Zonyl FSN	22.87	8.05E-09	-6.00E-07	-4.52E-06	-1.12E-06	-4.52E-06
N-BEA/Zonyl FSN	15.51	3.78E-08	-9.47E-07	-1.91E-05	-2.97E-06	-1.91E-05

It was found that, for EC, Zonyl FSN leads to lower limits of detection for every coreactant, compared to the more commonly used surfactant Triton X-100. However, more importantly, it revealed weaknesses of the chip itself. While conducting the measurements for the EC comparison and preliminary ECL measurements, it was found that delamination of the gold occurred for some chips. When the ΔE of 1.2 V were applied and ECL solution containing the $Ru(bpy)_3^{2+}$/coreactant/surfactant mix was flown through the channels, it could sometimes be observed that the gold of the WE as well as the gold of the CE detached from the PMMA (Fig. 21). A correlation was observed between the current and detachment: when the current reached about $2*10^{-5}$ A, the connection between electrode and connection pad failed, and the chip was unusable. It was therefore likely that the WE was too small, and the high voltage and resulting current led to the detachment and instability of the electrode system.

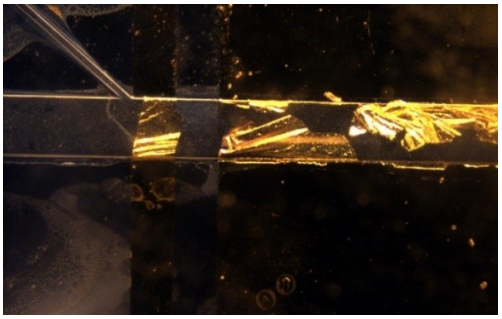

Fig. 21 Detachment of gold WE and CE

The RE suffered in stability over time as well. The electroplated silver could be washed away over time. The destruction of the electrodes was a significant problem for reliability and reusability of the device. In addition, the connection of the connecting pads to the potentiostat

via glued copper wires was hard to realize. Furthermore, it was frequently observed that the thin connection from the electrode to the connecting pad broke during bonding of the chip due to thermal stress, leaving the electrodes isolated.

Changes in Electrode and Microfluidic Design

The instability of the WE, due to its size, and the RE, due to its fabrication method, required a novel electrode design and, in the case of the RE, a new fabrication approach, both of which were accomplished by Dr. Olivier Bolduc, as well as subsequent changes in the fluidic pattern. All electrodes were increased in width to sustain the high current running through them when ECL reagents are used. Specifically, the WE and RE width were increased from 100 to 300 µm, and the CE from 1200 to 5000 µm. The channel length, and therefore the length of the exposed electrodes, remained the same. The connection to the connecting pads, as well as the connecting pads themselves, were redesigned (Fig. 22). Multiple and thicker connections were used, since it increased the chance of one connection being intact, even when others broke during thermal stress. The connecting pad was expanded, and moved towards the edge of the PMMA in order to be connected to the potentiostat's clamps directly. This eliminated the vulnerable connection via copper wire that would eventually break or loosen from the glue.

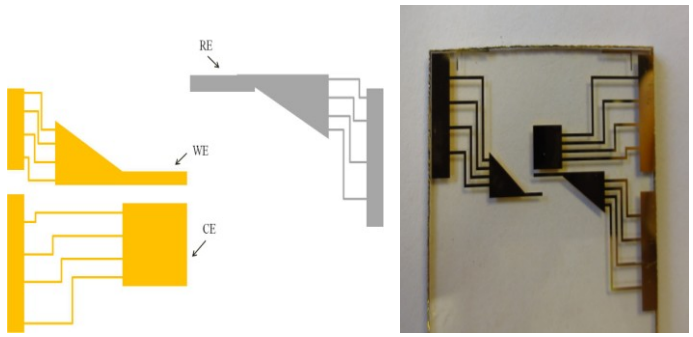

Fig. 22 New three-electrode system

Left: Schematic drawing of the electrode arrangement. Au WE and CE, as well as Ag RE and connecting pads, are increased in size. Right: picture of the three-electrode systems on PMMA.

The realization of a silver electrode, without a layer of gold underneath, was accomplished by adding a second evaporation step in the clean room fabrication of the chip. Originally, a 200 nm thick layer of gold was evaporated onto the whole PMMA slice, revealing the three gold electrodes after lithography and etching steps. In the new approach, however, two metal evaporations were conducted, one with gold and one with silver, to receive a gold WE and CE and a silver RE. With the application of a 0.1 M KCl solution in the RE channel in contact with the silver RE, an Ag/AgCl RE was realized with the new system as well. In order not to

have the gold and silver layer overlap, which would result in all three electrodes being of the same material, it was necessary to cover first one half of the chip and then the other for the second evaporation (Fig. 23). In our case, aluminum foil was used to cover the PMMA.

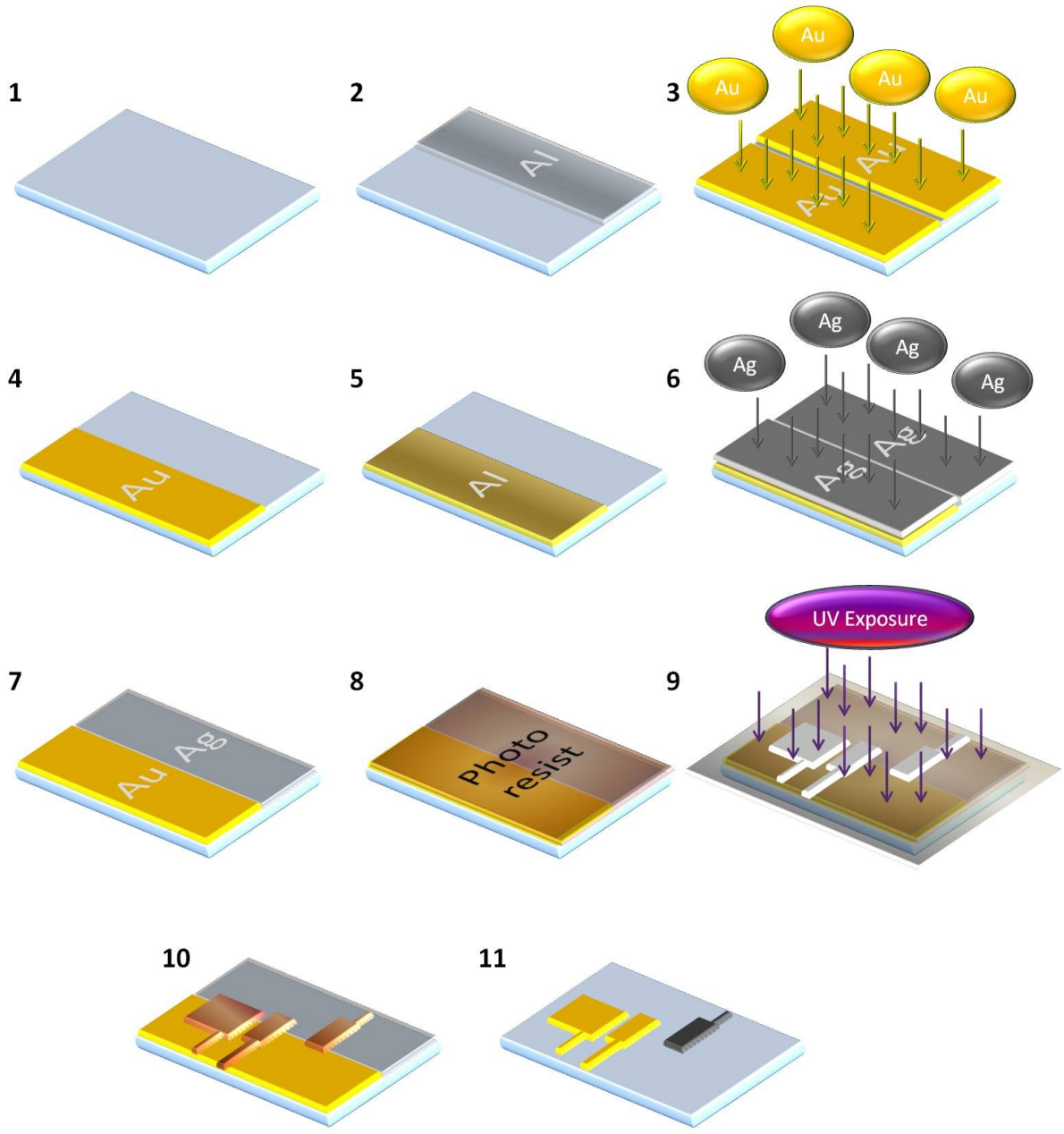

Fig. 23 Schematic of electrode fabrication with gold WE and CE and silver RE

A thiolated PMMA sheet (1) is covered on one half with Al foil (2) before gold evaporation (3), allowing only one side of the PMMA to be covered with gold (4). Next, the half of the gold PMMA side is covered with Al foil (5) before silver evaporation (6), leading to a PMMA slide which is coated with gold on one half and with silver on the other (7). Photoresist is spun on the metal covered slide and baked (8) before a mask with the electrode design is used for UV exposure (9). Upon washing, the dissolvable photoresist can be washed from the slide, remaining only at the places the electrodes should be (10). With gold etchant, the gold and the silver not covered by photoresist can be etched from the PMMA, while with an additional UV exposure of the whole slide, the remaining photoresist can be removed in an additional wash step, leading to the final three electrode system (11).

After both evaporations, the PMMA was then covered on one half with a 200 nm layer of Au, the other with a 200 nm layer of Ag. Subsequent lithography via UV exposure through a mask and metal etching revealed the three electrodes in two different metals. This enhanced the stability of the RE, and reduced degeneration due to liquid flow and could be observed in following measurements.

Beside the electrodes, it was also necessary to change the channel design as well. The well-established fluorescent molecule Sulforhodamine B (SRB) was used for first investigations of the microfluidic channels. SRB has maximal absorbance at 565 nm and maximal fluorescence emission at 585 nm. While testing the chip with a hybridization assay with magnetic beads and SRB encapsulating liposomes, it became obvious that the fluidics needed to be improved. In the assay (as described in more detail later) the liposomes were coupled to an analyte DNA, which itself was attached to magnetic beads to allow fixation in the chip (Fig. 27). It became obvious that, when changing the solution, the change in pressure led to the analyte solution moving back towards the inlet of the main channel, but also into the OG channel (Fig. 24). Furthermore, it became difficult to wash the solution in the main channel

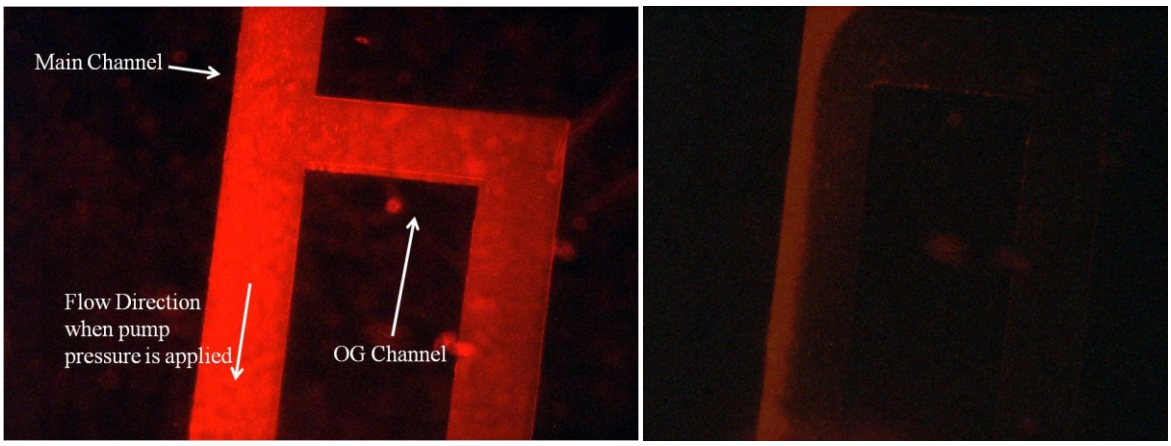

Fig. 24 SRB fluorescence signal pre- liposome lysis inside the microfluidic channels.

(Left) liposome solution reaches OG channel, which is filled with running buffer.
(Right) solution in OG channel has been washed out, while liposome solution is still present in the main channel (signal on the left side of the channel).

out when the OG solution was applied. In response to this, a second inlet at the main channel was introduced, so that a constant pressure could be applied. To solve the side flow into the OG channel, the connection between them was reduced in size and angled.

In addition, it was determined that accumulation of the magnetic beads over a magnet placed underneath the main channel required a very low flow rate. Increasing the flow rate to over 0.5 µl/min in the main channel and 0.2 µl/min in the OG channel pushed the magnetic beads beyond the magnet and, in most cases, led to a complete loss of the magnetic beads, together with the analyte. It was easily observable under brightfield conditions (Fig. 25), where the edge of the magnet was clearly visible as well as the magnetic beads. As can be seen in Fig. 24, a higher flow rate led to a washing out of the magnetic beads before detection of the analyte was possible.

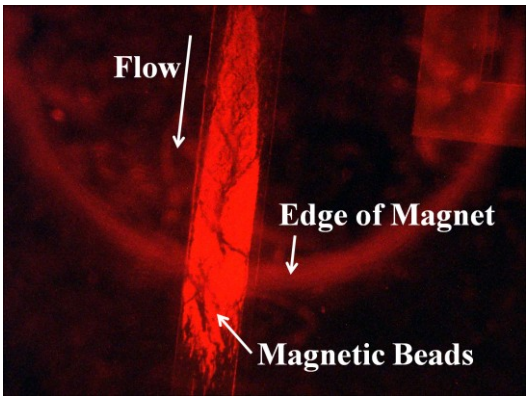

Fig. 25 Magnetic bead removal on chip.

Magnetic beads, previously assembled at the magnet, are being washed out downstream due to too high a flow rate.

As such low flow rates are inefficient for fast assays, as the required assay times was over 40 minutes, it was necessary to change the diameter of the accumulation zone (Fig. 26). While the diameter in most parts of the main channel was unchanged, the channel was expanded to twice its width at the site where the magnet was placed. This allowed for faster flow rates, as the local flow in the accumulation zone was reduced due to the wider channel width. The flow rate could be increased to 1.5 µl/min in the main channel and 1 µl/min in the OG channel without the risk of losing the magnetic beads.

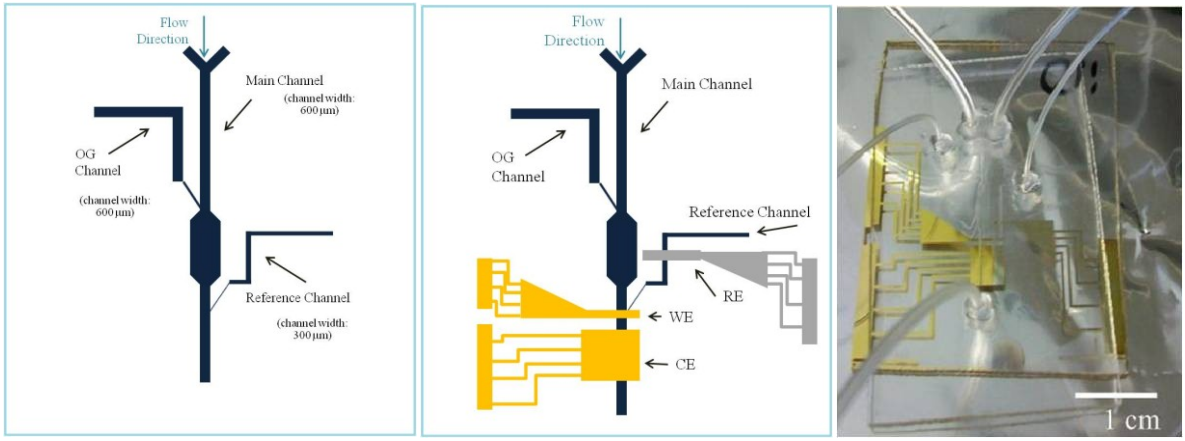

Fig. 26 Second microfluidic and electrode design.

Left: Microfluidic design
Middle: Microfluidic channels are overlapped with new electrode design.
Right: Finished chip with tubing and exposed connecting pads on the sides of the PMMA.

Hybridization Assay

The microfluidic device is intended for pathogen detection in water samples, although the device will not be limited to this application. Any kind of DNA or RNA can be theoretically detected with the device if the necessary parameters are adjusted, e.g. the DNA or RNA sequences need to be specific for the analyte. There are numerous options one can choose for the detection of DNA in a microfluidic device. However, it is important that the DNA is immobilized so the detection can happen, and, furthermore, that all unbound DNA or targeting molecules are removed so as to not lead to a false signal. One common method to immobilize the DNA inside the chip is to attach it directly to the substrate or, as in our case, the electrodes. This method requires a thorough cleaning of the channels if the chip is to be used for more than one assay. A more elegant method to reach reusability is by linking the analyte to magnetic beads. The magnetic beads, and therefore the analyte, can be held in place inside the chip with an external magnet till all unbound DNA is washed out. After the specific signal is recorded, the magnet is simply removed, allowing for the bound DNA to be washed out. The chip is therefore easily recyclable.

For our applications, the DNA should not only be linked to one ECL reagent. To enhance the signal, we chose to employ liposome-encapsulating ECL molecules. The surface of liposomes can be modified to link to biomolecules (e.g. DNA, proteins, and biotin). Therefore, in our case, the DNA can be linked to the magnetic beads for immobilization and at the same time to liposomes for signal increase. Fig. 27 shows the general idea of the assay, in which the analyte DNA (Target DNA) is linked to Capture DNA, which is attached to magnetic beads (MB) via

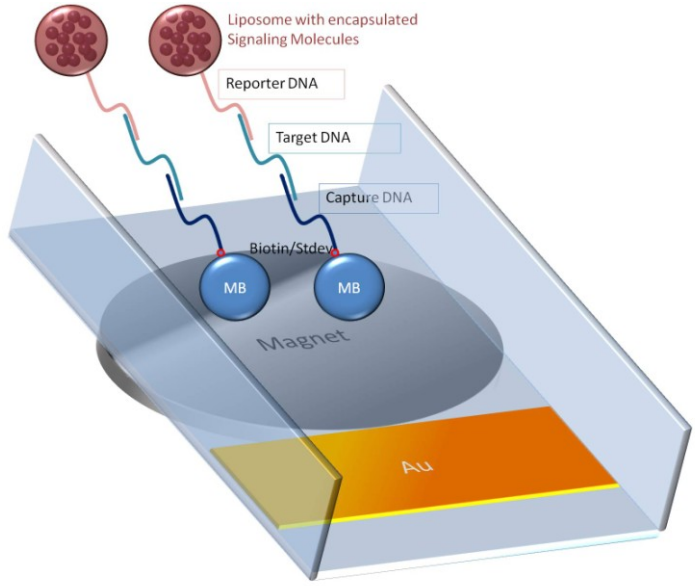

Fig. 27 Schematic hybridization Assay inside the microfluidic device.

The target DNA is linked to liposomes and magnetic beads, and held in place by a magnet placed underneath the chip and in front of the electrodes.

a biotin-strepdavidin bonding. The target DNA is linked with a reporter probe DNA that has been incorporated into the surface of the liposomes. In our approach, the *C. parvum*-specific DNA sequence is attached to the surface of the liposomes via a cholesterol tag. Cholesterol is one of the lipids of which the bilayer consists. The lipids themselves are not randomly distributed over the sphere, but form clusters of the same kind of lipid (Fig. 28). A DNA linked to a cholesterol-tag and added upon formation of the bilipid structure can then be incorporated into the cholesterol cluster, leaving the DNA linked to the liposome, but exposed to a complementary DNA strand.

Inside the liposomes, ECL molecules, as well as fluorescent and EC molecules, were encapsulated that would lead to a signal upon release from the lipsomes. Liposomes are vesicles consisting of lipids and can be broken apart by, among other things, the influence of a surfactant. Previous studies revealed that a surfactant with good liposome-lysing capabilities is Octyl β-D-glucopyranoside (OG). When introduced to the immobilized liposomes, after the unbound liposomes have been washed out inside the channel, the OG solution destroys the tight vesicle structure and the signaling molecules can be detected.

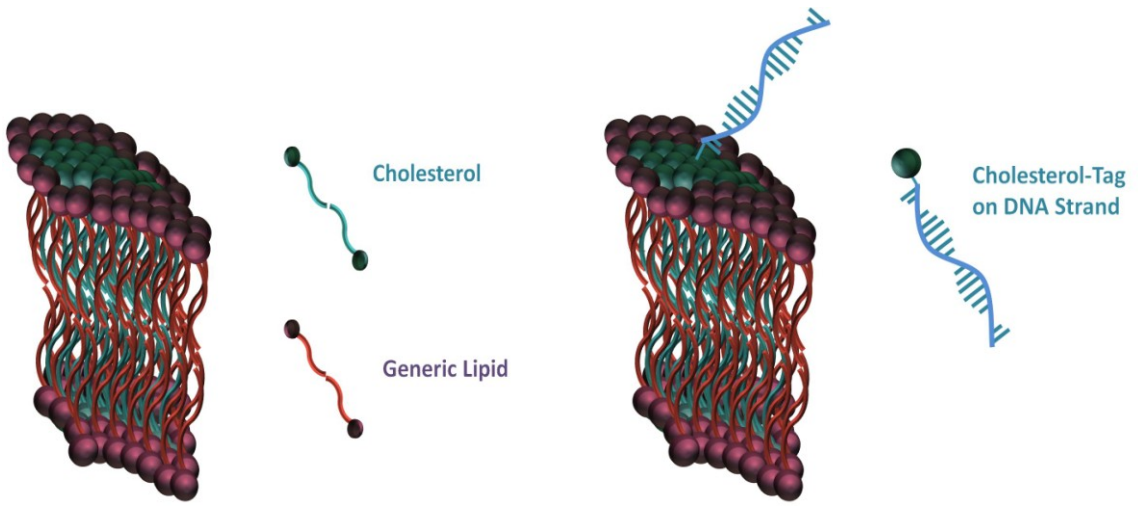

Fig. 28 Schematic of lipid arrangement in a bilipid liposome structure.

The different lipids, such as cholesterol, are not individually distributed over the liposome surface, but arrange themselves in patches. A DNA strand with a cholesterol tag can be stably incorporated into the cholesterol patch and connected to other DNA strands.

DNA Detection on Chip

Incorporating $Ru(bpy)_3^{2+}$ into liposomes is rarely demonstrated in the literature[141, 143, 146], and, to our knowledge, has never been incorporated into a microfluidic system. Therefore, it was a logical consequence to start with a more established liposome system to test the hybridization assay conditions and the chip. SRB (sulforhodamine B) was used frequently in our lab as liposome encapsulant and marker. Furthermore, fluorescence detection offered the advantage of focusing on the microfluidic system and the assay, instead of the electrode fabrication that would enhance the complexity and the cost per chip. A *C. parvum*-specific liposome encapsulating 150 mM SRB was the first kind of liposome with which a positive liberation on chip was achieved (Fig. 29), which included tests on the hybridization assay and the flow on chip.

The best results were achieved when the different hybridization components were mixed under the following conditions and incubated for 15 min:

1. 2.25 µl Hybridization Buffer
2. 2 µl Liposome Solution (with Reporter Probe already attached to it)
3. 1 µl target DNA
4. 3.75 µl magnetic bead with capture probe (prepared from 5 µl of magnetic bead and 1.25 µl of 10 µM Capture Probe, washed, incubated and resuspended in 3.75 µl of water)

Before applying the solution to the chip, a thorough wash step with water and Running Buffer was done via filled syringes hooked up to syringe pumps. Since the total hybridization assay volume is only 9 µl, a 10 microliter syringe was used for injection into the inlet tubing of the chip. With running buffer, the hybridization mixture was pushed through the tubing into the main channel, where the magnetic beads accumulated over the magnet, placed underneath the chip. After accumulation and washing of the unbound components, 60 mM OG solution in 1xPBS was inserted, also via syringe pump, leading to the release of SRB and detection in the channel downstream of the accumulated magnetic beads. Through removal of the magnet after detection, the chip could be cleaned and reused.

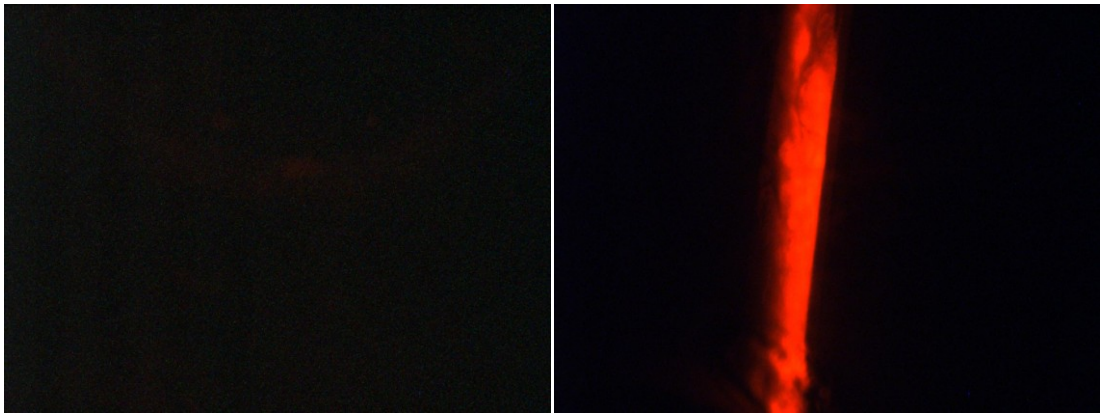

Fig. 29 Liberation of SRB after liposome lysis.

Left: background before lysis.
Right: SRB signal inside the microfluidic channel after lysis of liposomes linked to *C.* parvum DNA with OG solution.

After successful DNA detection via SRB encapsulating liposomes, the next step was detection via EC reagent encapsulating liposomes. As EC reagent, 200 mM ferri/ferro hexacyanide was used. Ferri/ferro hexacyanide requires a significantly lower voltage than $Ru(bpy)_3^{2+}$, only 400 mV instead of 1.2 V, and is a well studied EC system.

This required the fabrication of new liposomes. Since it was uncertain if the electrochemical detection of *C. parvum* would be successful, liposomes were employed that, besides 200 mM ferri/ferro hexacyanide, also contained 10 mM SRB. This setup allowed for visual

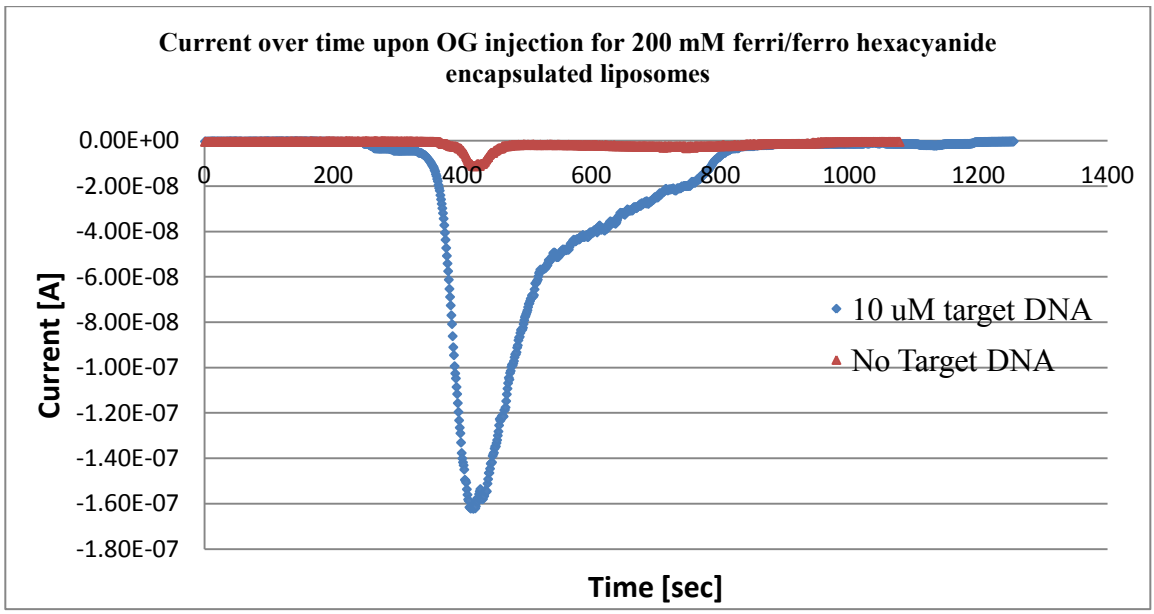

Fig. 30 EC detection of *C. parvum* DNA.

EC signal (blue) upon lysis of 200 mM ferri/ferro hexacyanide encapsulated liposomes and negative control (red).

confirmation of liberation with the established SRB. Experimental condition of fluid injection remained the same as for fluorescent detection. At the WE, an increase in current could be observed after liposome lysis. A clear increase compared to the background signal, as well as to a blank (Fig. 30). The signal increased 20 times compared to the blank when taking the area underneath the curve as the value measured, and about an order of magnitude when taking the current itself.

The increase in fluorescent signal could, furthermore, be perfectly matched to an increase in current upon lysis (Fig. 31).

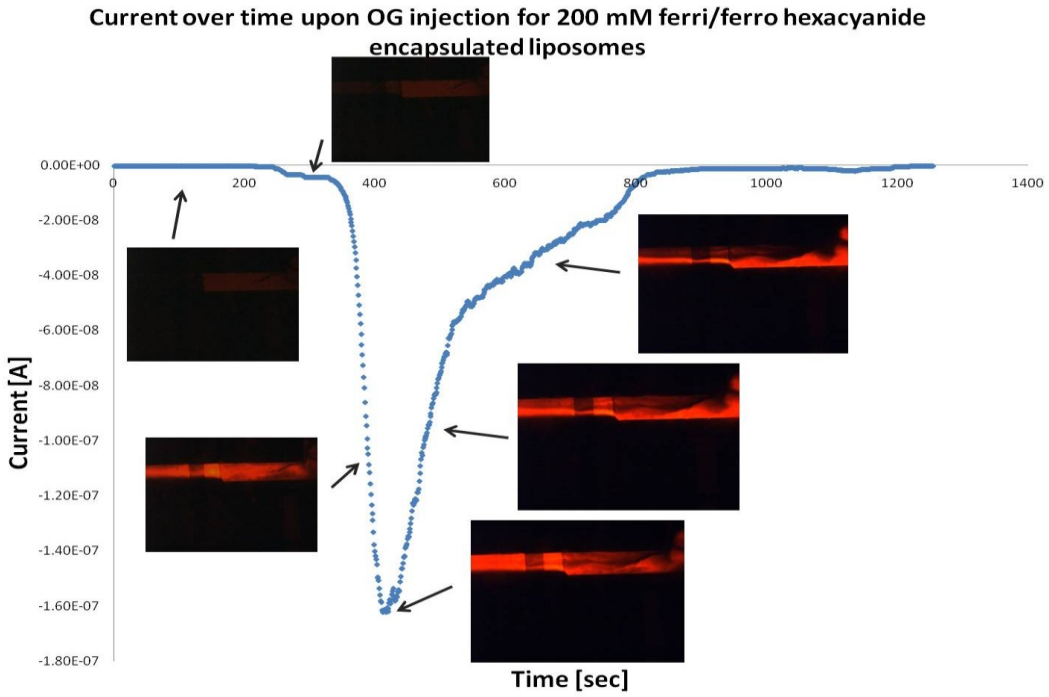

Fig. 31 EC detection of *C. parvum* DNA with fluorescent signal by SRB

200 mM ferri/ferro hexacyanide and 10 mM SRB were encapsulated into liposomes and can be detected at the same time

For $Ru(bpy)_3^{2+}$ encapsulating liposomes, we had to start even with the right encapsulant, since information for $Ru(bpy)_3^{2+}$ liposomes is lacking. For liposome encapsulants, the right osmotic pressure is important, and needs to be adjusted according to the pressure outside of the liposomes, given by the surrounding buffer. It the difference in osmolality between the inside and outside of the liposomes is too strong, more than 50 mol/kg, the liposomes are not stable. Usually, for stabilization, a mixture of HEPES and sucrose is used. However, when dissolving $Ru(bpy)_3^{2+}$ in HEPES solution, a color change occurred. The solution turned

darker, compared to a dilution in water (Fig. 32). Since such a color change could indicate a complexation of $Ru(bpy)_3^{2+}$ and possibly influence the ECL, experiments were required to determine such an effect. Therefore the following solutions were tested:

a) 250 µM $Ru(bpy)_3^{2+}$ in N-Butyldiethanolamine/Triton X-100 Buffer (prepared right before the experiment); blue data set in Fig. 33.

b) 250 µM $Ru(bpy)_3^{2+}$ in N-Butyldiethanolamine/Triton X-100 Buffer diluted from a 25 mM $Ru(bpy)_3^{2+}$ solution in **water**; red data set in Fig. 33.

c) 250 µM $Ru(bpy)_3^{2+}$ in N-Butyldiethanolamine/Triton X-100 Buffer diluted from a 25 mM $Ru(bpy)_3^{2+}$ solution in **water/HEPES mix**; green data set in Fig. 33.

Both b) and c) were stored in the refrigerator. For all solutions, a potential of 1.2 V was applied, and pictures were taken of the signal at different exposure times to rule out a false result by overexposure of the camera. All solutions were tested three times, while the chip was rinsed in between tests with N-Butyldiethanolamine/Triton X-100 Buffer. Also, the signal for plain buffer was recorded to obtain the background signal (purple data set in Fig. 33). The EC signal is in the same order for all solutions, but more importantly, this was also the case for the ECL signal for the different solutions (Fig. 33), where the averaged pixel intensity is shown for various exposure times. The data shows that there is no negative influence of HEPES on the light emission of $Ru(bpy)_3^{2+}$. This holds true even when the $Ru(bpy)_3^{2+}$ was stored in the HEPES solution for a longer period of time. The liposomes could, therefore, be fabricated with the standard protocol, using HEPES.

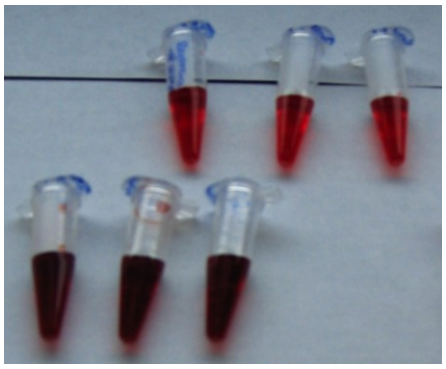

Fig. 32 25 mM $Ru(bpy)_3^{2+}$ in water (top) and HEPES buffer (bottom)

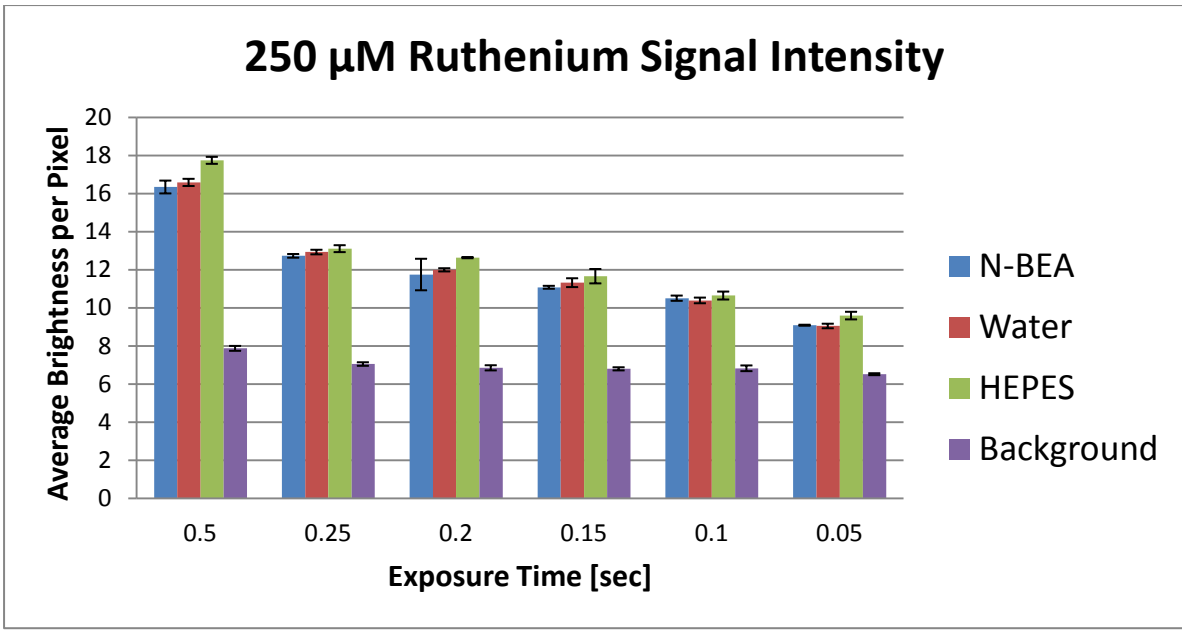

Fig. 33 ECL signal of 250 µM $Ru(bpy)_3^{2+}$ with N-Butyldiethanolamine/Triton X-100 Buffer in different media.

Blue: 250 µM $Ru(bpy)_3^{2+}$ dissolved in N-Butyldiethanolamine/Triton X-100 Buffer.
Red: 250 µM $Ru(bpy)_3^{2+}$ in N-Butyldiethanolamine/Triton X-100 Buffer diluted down from 25 mM $Ru(bpy)_3^{2+}$ in water.
Green: 250 µM $Ru(bpy)_3^{2+}$ in N-Butyldiethanolamine/Triton X-100 Buffer diluted down from 25 mM $Ru(bpy)_3^{2+}$ in a water/HEPES solution.
Purple: Background signal of N-Butyldiethanolamine/Triton X-100 Buffer.

The concentration of encapsulant should be as high as possible, and 25 mM $Ru(bpy)_3^{2+}$ were still dissolvable and used for liposome fabrication. For 5 ml of encapsulant, 0.5 ml of 0.2 M HEPES and 0.95 ml of 2M Sucrose led to an osmolality of 531 mmol/kg. The first two batches of $Ru(bpy)_3^{2+}$ liposomes were prepared with 10 mM SRB as well, since it had proven useful for the EC liposomes to confirm the liberation with the established fluorescent system. Unfortunately, even though fluorescent detection was possible, no EC nor ECL signal was observable. The fluorescent detection established that the hybridization assay worked. However, not even lysed liposomes themselves led to an ECL signal. Failure of the electrode connection was also ruled out by testing plain $Ru(bpy)_3^{2+}$ solutions on the same electrodes and obtaining an ECL signal in those cases. Either the SRB interfered with the $Ru(bpy)_3^{2+}$, or an encapsulation of $Ru(bpy)_3^{2+}$ had not been possible.

Another attempt was made to fabricating 25 mM $Ru(bpy)_3^{2+}$ liposomes, but without SRB present. Indeed, in a plain $Ru(bpy)_3^{2+}$ solution, it was possible to encapsulate $Ru(bpy)_3^{2+}$ inside the liposomes. In a hybridization assay on chip, it was possible to liberate and detect $Ru(bpy)_3^{2+}$ at the WE (Fig. 34).

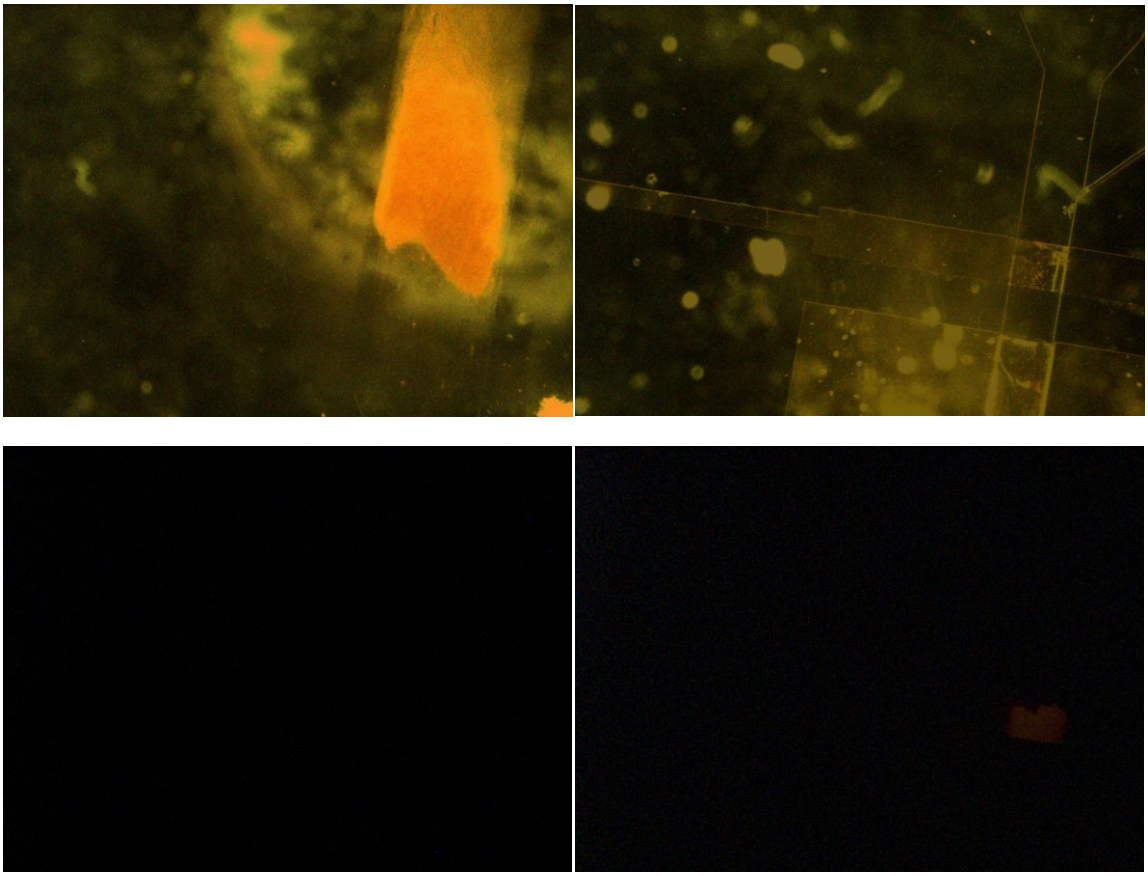

Fig. 34 ECL detection of *C. parvum* DNA at $\Delta E_{applied}$ = 1200mV vs. Ag/AgCl.
1: Assembly of magnetic beads linked to the target DNA and $Ru(bpy)_3^{2+}$ liposomes.
2: Bright field image of the WE and main channel.
3: Background signal, when 1.2 V have been applied but lysis has not been initiated.
4: ECL signal of $Ru(bpy)_3^{2+}$ at the WE upon liposome lysis via 60 mM OG solution with NBEA and Triton X-100.

Based on the identification of the right hybridization assay and flow conditions, and with the use of the synthesized liposomes, the limits of detection for the various detection techniques were investigated in subsequent measurements by Dr. Olivier Bolduc. For the limits of detection for *C.parvum*, it was found that for SRB the $LOD_{Fluorescence}$ was 46 nM; for 200 mM ferri/ferro hexacyanide encapsulating liposomes ($\Delta E_{applied}$ = 400mV) a LOD_{EC} of 9 nM was found; and with the use of 250 µM $Ru(bpy)_3^{2+}$ encapsulating liposomes ($\Delta E_{applied}$ = 1200mV), the LOD_{ECL} was 13 nM[205]. Dr. Olivier Bolduc furthermore investigated the signal enhancement factor obtained by employing liposomes instead of a one-to-one analyte to

signaling molecule labeling approach, based on the synthesized 200 mM ferri/ferro hexacyanide encapsulating liposomes in comparison to 1µM $[Fe(CN)_6]^{4-}$. It was found that the data suggest an amplification factor of 5000.

After low signal intensities or, in case of ECL, a non-existent signal at the beginning of the studies, the identification of the appropriate liposome, hybridization and flow conditions was of great importance. The proof of principle for DNA detection via the three different techniques, fluorescence, EC, and ECL, was only possible after a stable accumulation of the magnetic beads at flow rates of over 1 µl/min. This furthermore allowed for the assay time on chip to be reduced to less than 10 minutes on chip, not counting the incubation time, which took place outside the chip. Due to the employment of magnetic beads and thorough washing, the chip was reusable. All these important factors make this a promising novel ECL microfluidic biosensor.

5. Conclusion

ECL detection is gaining in importance for biological and clinical sensing, due to its virtually zero background, high photon yields, and high sensitivity capabilities. However, not many microfluidic ECL systems detecting DNA have been realized so far. One limiting factor is the identification of signal-enhancing strategies to gain an advantage over other detection methods. Since coreactants and surfactants are known to be capable of enhancing the ECL intensity, coreactant-based $Ru(bpy)_3^{2+}$ ECL was investigated here with the tertiary amines TPA, DBAE and NBEA, under the influence of the surfactants Triton X-100 and Zonyl FSN. As already demonstrated for TPA, the addition of a surfactant had an enhancing effect, also for NBEA/$Ru(bpy)_3^{2+}$ ECL. NBEA with Zonyl FSN is more effective than NBEA by itself for $Ru(bpy)_3^{2+}$ ECL, and the most effective coreactant/surfactant combination reported so far. However, for DBAE, the signal decreased in the presence of a surfactant, which is surprising considering the chemical structure of the three investigated coreactants. The findings suggest that the surfactant interacts in a more complicated manner with the coreactant/$Ru(bpy)_3^{2+}$ system than the general belief of the formation of a hydrophobic layer on the surface of the electrode. Additional factors have to be taken into account, such as the formation of ruthenium/coreactant couples that are more likely to occur when both molecules can be brought in close proximity with each other. This is easier to achieve with NBEA under the investigated conditions, as with two OH-groups that have a negative partial charge, NBEA molecules will be able to approach the positively charged $Ru(bpy)_3^{2+}$ complex in closer proximity. Consequently, a general assumption on electrode hydrophobicity influence upon the ECL signal cannot be made, but needs to be investigated for each coreactant system individually. We therefore suggest that possible coreactants that have previously been shown to have a lower ECL signal than TPA, and therefore have not been further investigated, may be worth further testing upon use of Zonyl FSN. This is especially interesting if additional benefits can result, such as a change in potential, higher ECL rates, or a shift in emission wavelength, due to the influence of different surfactants. Also, we can conclude that, in general, unless a system is sensitive to the presence of a surfactant, this easy substitute in the chemical environment of the ECL reaction can prove beneficial to many ECL assays already described in literature, without adding more time or costs to the assay preparation.

Even though NBEA as coreactant is the least represented in literature compared to the common TPA, and even the multiple occasions where DBAE was employed, NBEA also proved to be the best choice as coreactant when investigating low oxidation potential ECL.

NBEA had not been previously reported to display the capability of LOP ECL. However, as demonstrated here, an ECL signal was observed at voltages well below 1 V, and optimal at 890 mV under basic pH values and the use of Tris buffer instead of a potassium-based-buffer. In the end, the signals obtained for the optimized LOP ECL resulted in a signal almost three times higher than those obtained for normal ECL at 1.2V vs. Ag/AgCl using TPA as co-reactant, which is in standard use in (bio)assays. The use of Tris buffer at alkaline conditions, however, did not only prove beneficial for LOP ECL, but also at the standard 1.2 V vs. Ag/AgCl. While standard ECL is performed with TPA as coreactant, Triton X-100 as surfactant in a phosphate-based buffer and at 1.2V, a change to Tris, pH 8.5, NBEA as coreactant and Zonyl FSN as surfactant led to about a 3 times higher ECL signal at 1.2V. Here, it was observed that Tris was the clearly preferred buffer component, which we assume is due to metal complexing capability that positively influences the Ruthenium ECL pathway. Further studies, however, are needed to confirm the exact mechanism. We can also conclude that the occurrence of strong oxidation peaks in electrochemical CV studies do not necessarily translate into an LOP ECL signal. This is important to note, as many studies investigating LOP possibilities don't always correlate electrochemical and ECL signals. In further studies, it will need to be identified how beneficial the lower voltage proves for the stability and lifetime of microelectrodes.

We furthermore demonstrated ECL detection of DNA inside a microfluidic system with an integrated three electrode system, consisting of a gold WE and CE and an Ag/AgCl RE. Using the appropriate encapsulant conditions, it was possible to form liposomes that encapsulated the ECL reagent $Ru(bpy)_3^{2+}$ and led to a controlled released inside the chip under identified hybridization conditions. First tests led to changes in fluidic and electrode design to perform faster assays without the risk of losing the analyte solution. In the end, on chip detection and preparation for reusability was achieved in less than ten minutes, instead of forty minutes. With even further changes to the microfluidic system, as e.g. an even wider assembly area in front of the electrodes allowing for faster flow rates, an even faster assay time can be reached. Furthermore, a wider assembly area would allow for on-chip incubation of the hybridization assay, avoiding external incubation and sample preparation time. The chip furthermore allowed for fluorescent and EC detection, as successfully demonstrated. Since, in subsequent tests, ECL had better limits of detection than fluorescence, but not as good as EC detection, it will be necessary to enhance the detection limit and sensitivity for ECL by employing a more light-sensitive detector. While the microscope with CCD camera was valuable for preliminary data to gain insight on the signal distribution over the electrodes,

and a magnified view on the electrode itself to detect detachments early, a more powerful CCD camera, such as a cooled CCD camera or a high voltage photomultiplier tube (PMT) would be highly valuable to lower the limit of detection. In terms of miniaturization, a microsized PIN photodiode should be employed that can be directly attached on top the electrodes and ensure stable handling.

With detection on microfabricated electrodes, and the identification of signal enhancing strategies, we demonstrated that ECL is well suited to incorporation into microfluidic devices. One key step was the use of $Ru(bpy)_3^{2+}$ encapsulating liposomes, as well as the change in chemical environment. The LOD enhancement of a factor of 250 gained by employing the newly investigated N-Butyldiethanolamine/Zonyl FSN system, compared to the commonly used TPA/Triton system, is not only valuable to our system, but likely beneficial to all analytical ECL applications. For ECL sensors with limited sample size but stringent requirements in terms of sensitivity, such as ECL microfluidic DNA biosensors, this easy substitution of coreactant/surfactant conditions will prove highly valuable for future and existing ECL sensors, and further the use of ECL-based microfluidic applications. The studies demonstrated a significant step towards wide spread applications of sensitive ECL based microfluidic point-of-care systems.

Bibliography

1. Tokel N, Bard A (1972) Electrogenerated chemiluminescence. IX. Electrochemistry and emission from systems containing tris (2, 2'-bipyridine) ruthenium (II) dichloride. J Am Chem Soc 1853:2862–2863.

2. Kulmala S, Suomi J (2003) Current status of modern analytical luminescence methods. Anal Chim Acta 500:21–69. doi: 10.1016/j.aca.2003.09.004

3. Richter MM (2004) Electrochemiluminescence (ECL). Chem Rev 104:3003–36. doi: 10.1021/cr020373d

4. Miao W (2008) Electrogenerated chemiluminescence and its biorelated applications. Chem Rev 108:2506–53. doi: 10.1021/cr068083a

5. Bertoncello P, Stewart AJ, Dennany L (2014) Analytical applications of nanomaterials in electrogenerated chemiluminescence. Anal Bioanal Chem 406:5573–87. doi: 10.1007/s00216-014-7946-x

6. Forster RJ, Bertoncello P, Keyes TE (2009) Electrogenerated chemiluminescence. Annu Rev Anal Chem (Palo Alto Calif) 2:359–85. doi: 10.1146/annurev-anchem-060908-155305

7. Auroux P-A, Iossifidis D, Reyes DR, Manz A (2002) Micro total analysis systems. 2. Analytical standard operations and applications. Anal Chem 74:2637–52.

8. Baker CA, Duong CT, Grimley A, Roper MG (2009) Recent advances in microfluidic detection systems. Bioanalysis 1:967–975. doi: 10.4155/bio.09.86.Recent

9. Nahavandi S, Baratchi S, Soffe R, Tang S-Y, Nahavandi S, Mitchell A, Khoshmanesh K (2014) Microfluidic platforms for biomarker analysis. Lab Chip 14:1496–514. doi: 10.1039/c3lc51124c

10. Reyes DR, Iossifidis D, Auroux P-A, Manz A (2002) Micro total analysis systems. 1. Introduction, theory, and technology. Anal Chem 74:2623–36.

11. Segerink LI, Eijkel JCT (2014) Nanofluidics in point of care applications. Lab Chip 14:3201–5. doi: 10.1039/c4lc00298a

12. Kirschbaum SEK, Baeumner AJ (2015) A review of electrochemiluminescence (ECL) in and for microfluidic analytical devices. Anal Bioanal Chem 407:3911–3926. doi: 10.1007/s00216-015-8557-x

13. Liu X, Shi L, Niu W, Li H, Xu G (2007) Environmentally friendly and highly sensitive ruthenium(II) tris(2,2'-bipyridyl) electrochemiluminescent system using 2-(dibutylamino)ethanol as co-reactant. Angew Chem Int Ed Engl 46:421–4. doi: 10.1002/anie.200603491

14. Han S, Niu W, Li H, Hu L, Yuan Y, Xu G (2010) Effect of hydroxyl and amino groups on electrochemiluminescence activity of tertiary amines at low tris(2,2'-

bipyridyl)ruthenium(II) concentrations. Talanta 81:44–7. doi: 10.1016/j.talanta.2009.11.037

15. Chen X-M, Wu G-H, Chen J-M, Jiang Y-Q, Chen G-N, Oyama M, Chen X, Wang X-R (2010) A novel electrochemiluminescence sensor based on bis(2,2'-bipyridine)-5-amino-1,10-phenanthroline ruthenium(II) covalently combined with graphite oxide. Biosens Bioelectron 26:872–6. doi: 10.1016/j.bios.2010.07.083

16. Crespo G a, Mistlberger G, Bakker E (2012) Electrogenerated chemiluminescence for potentiometric sensors. J Am Chem Soc 134:205–7. doi: 10.1021/ja210600k

17. Guo Z, Gai P (2011) Development of an ultrasensitive electrochemiluminescence inhibition method for the determination of tetracyclines. Anal Chim Acta 688:197–202. doi: 10.1016/j.aca.2010.12.043

18. Guo Z, Hao T, Shi L, Gai P, Duan J, Wang S, Gan N (2012) A highly sensitive electrochemiluminescence method combined with molecularly imprinted solid phase extraction for the determination of phenolphthalein in drug, slimming food and human plasma. Food Chem 132:1092–1097. doi: 10.1016/j.foodchem.2011.11.056

19. Hu T, Liu X, Liu S, Wang Z, Tang Z (2014) Toward understanding of transfer mechanism between electrochemiluminescent dyes and luminescent quantum dots. Anal Chem 86:3939–46. doi: 10.1021/ac5004823

20. Lei Y, Lin Y, Zheng Y, Dai M, Wang K, Lin X (2013) Design of a Solid-State Electrochemiluminescence Biosensor for Detection of PML/RARa Fusion Gene Using Ru(bpy)2þ 3 -AuNPs Aggregations on Gold Electrode. Electroanalysis 25:1388–1394. doi: 10.1002/elan.201200623

21. Sun S, Li F, Liu F, Yang X, Fan J, Song F, Sun L, Peng X (2012) Synthesis and ECL performance of highly efficient bimetallic ruthenium tris-bipyridyl complexes. Dalton Trans 41:12434–8. doi: 10.1039/c2dt31603j

22. Sun S, Yang Y, Liu F, Fan J, Kehr J, Sun L, Peng X (2010) ECL performance of ruthenium tris-bipyridyl complexes covalently linked with phenothiazine through different bridge. Dalton Trans 39:8626–30. doi: 10.1039/c0dt00279h

23. Sun S, Yang Y, Liu F, Fan J, Peng X, Kehr J, Sun L (2009) Intra- and intermolecular interaction ECL study of novel ruthenium tris-bipyridyl complexes with different amine reductants. Dalton Trans 7969–74. doi: 10.1039/b905404a

24. Sun S, Yang Y, Liu F, Pang Y, Fan J, Sun L, Peng X (2009) Study of highly efficient bimetallic ruthenium tris-bipyridyl ECL labels for coreactant system. Anal Chem 81:10227–31. doi: 10.1021/ac9020903

25. Walker EK, Vanden Bout D a, Stevenson KJ (2012) Carbon optically transparent electrodes for electrogenerated chemiluminescence. Langmuir 28:1604–10. doi: 10.1021/la2042394

26. Wang S, Milam J, Ohlin AC, Rambaran VH, Clark E, Ward W, Seymour L, Casey WH,

Holder AA, Miao W (2009) Electrochemical and Electrogenerated Chemiluminescent Studies of a Trinuclear Interactions with Calf Thymus DNA. 81:4068–4075.

27. Wang S, Wei J, Hao T, Guo Z (2012) Determination of ractopamine in pork by using electrochemiluminescence inhibition method combined with molecularly imprinted stir bar sorptive extraction. J Electroanal Chem 664:146–151. doi: 10.1016/j.jelechem.2011.11.011

28. Wei Q, Han L, Jiang Y, Lin X, Duan Y, Chen G (2012) (R = CH 3 , n = 1; R = H, n = 1 and 2) with Amine (TPrA and DBAE) as the Coreactant and Determination of Sudan I. Inorg Chem 4:11117–11125.

29. Wei Q-H, Lei Y-F, Duan Y-N, Xiao F-N, Li M-J, Chen G-N (2011) Mono- and dinuclear Ru(II) complexes of 1,4-bis(3-(2-pyridyl)pyrazol-1-ylmethyl)benzene): synthesis, structure, photophysical properties and electrochemiluminescent determination of diuretic furosemide. Dalton Trans 40:11636–42. doi: 10.1039/c1dt11163a

30. Xue L, Guo L, Qiu B, Lin Z, Chen G (2009) Mechanism for inhibition of Ru(bpy)32+/DBAE electrochemiluminescence system by dopamine. Electrochem commun 11:1579–1582. doi: 10.1016/j.elecom.2009.05.059

31. Parveen S, Zhang W, Yuan Y, Hu L, Gilani M, Rehman AU, Xu G (2012) Electrogenerated chemiluminescence of Ru(phen)(3)(2+)/2-(dibutylamino)ethanol system. J Electroanal Chem 688:45–48.

32. Wu S, Zhou Z, Xu L, Su B, Fang Q (2014) Integrating bipolar electrochemistry and electrochemiluminescence imaging with microdroplets for chemical analysis. Biosens Bioelectron 53:148–53.

33. Sentic M, Milutinovic M, Kanoufi F, Manojlovic D, Arbault S, Sojic N (2014) Mapping electrogenerated chemiluminescence reactivity in space mechanistic insight into model systems used in immunoassays. Chem Sci 5:2568.

34. Jiang X, Ding W, Luan C (2013) Molecularly imprinted polymers for the selective determination of trace bisphenol A in river water by electrochemiluminescence. Can J Chem 6:1–6.

35. Li MJ, Shi YQ, Lan TY, Yang HH, Chen GN (2013) Solid-state electrochemiluminescence of two iridium complexes. J Electroanal Chem 702:25–30.

36. Workman S, Richter MM (2000) The effects of nonionic surfactants on the tris(2,2'-bipyridyl)ruthenium(II)--tripropylamine electrochemiluminescence system. Anal Chem 72:5556–61.

37. Li F, Zu Y (2004) Effect of Nonionic Fluorosurfactant on the Electrogenerated Chemiluminescence of the System : Lower Oxidation Potential and Higher Emission Intensity. Anal Chem 76:1768–1772.

38. Zu Y, Bard AJ (2001) Dependence of Light Emission of the Tris (2 , 2 ′) bipyridylruthenium (II)/ Tripropylamine System on Electrode Surface Hydrophobicity.

Anal Chem 73:3960–3964.

39. Zu Y, Li F (2005) Characterization of the low-oxidation-potential electrogenerated chemiluminescence of tris(2,2′-bipyridine)ruthenium(II) with tri-n-propylamine as coreactant. Anal Chim Acta 550:47–52. doi: 10.1016/j.aca.2005.06.055

40. Factor B, Muegge B, Workman S, Bolton E, Bos J, Richter MM (2001) Surfactant Chain Length Effects on the Light Emission of Tris (2 , 2 ′ -bipyridyl) ruthenium (II)/. Anal Chem 73:4621–4624.

41. Zu Y, Bard AJ (2000) Role of Direct Coreactant Oxidation in the Ruthenium Tris (2 , 2 ′) bipyridyl / Tripropylamine System and the Effect of Halide Ions on the Emission Intensity. Anal Chem 72:3223–3232.

42. Schnuriger M, Tague E, Richter MM (2011) Electrogenerated chemiluminescence properties of bisalicylideneethylenediamino (salen) metal complexes. Inorganica Chim Acta 379:158–162. doi: 10.1016/j.ica.2011.10.010

43. Zhou M, Robertson GP, Roovers J (2005) Comparative study of ruthenium(II) tris(bipyridine) derivatives for electrochemiluminescence application. Inorg Chem 44:8317–25. doi: 10.1021/ic0510112

44. Swanick KN, Price JT, Jones ND, Ding Z (2012) Synthesis, structure, electrochemistry, and electrochemiluminescence of thienyltriazoles. J Org Chem 77:5646–55. doi: 10.1021/jo300802h

45. Walker EK, Vanden Bout D a., Stevenson KJ (2011) Aqueous Electrogenerated Chemiluminescence of Self-Assembled Double-Walled Tubular J-Aggregates of Amphiphilic Cyanine Dyes. J Phys Chem C 115:2470–2475. doi: 10.1021/jp1108015

46. Reid EF, Burn PL, Lo S-C, Hogan CF (2013) Solution and solid-state electrochemiluminescence of a fac-tris(2-phenylpyridyl)iridium(III)-cored dendrimer. Electrochim Acta 100:72–77. doi: 10.1016/j.electacta.2013.03.094

47. Yu L, Huang Z, Liu Y, Zhou M (2012) Photophysics, electrochemistry and electrochemiluminescence of water-soluble biscyclometalated iridium (III) complexes. J Organomet Chem 718:14–21. doi: 10.1016/j.jorganchem.2012.08.006

48. Stagni S, Palazzi A, Zacchini S, Ballarin B, Bruno C, Marcaccio M, Paolucci F, Monari M, Carano M, Bard AJ (2006) A new family of ruthenium(II) polypyridine complexes bearing 5-aryltetrazolate ligands as systems for electrochemiluminescent devices. Inorg Chem 45:695–709. doi: 10.1021/ic0514905

49. Myung N, Ding Z, Bard AJ (2002) Electrogenerated Chemiluminescence of CdSe Nanocrystals. nanoletters 2:1315–1319.

50. Bae Y, Myung N, Bard AJ (2004) Electrochemistry and Electrogenerated Chemiluminescence of CdTe Nanoparticles. nanoletters 4:1153–1161m.

51. Myung N, Bae Y, Bard AJ (2003) Effect of Surface Passivation on the Electrogenerated

Chemiluminescence of CdSe / ZnSe Nanocrystals. nanoletters 3:1053–1055.

52. Chen Y, Yang M, Xiang Y, Yuan R, Chai Y (2013) Ligase chain reaction amplification for sensitive electrochemiluminescent detection of single nucleotide polymorphisms. Anal Chim Acta 796:1–6. doi: 10.1016/j.aca.2013.07.057

53. Cheng L, Liu X, Lei J, Ju H (2010) Low-potential electrochemiluminescent sensing based on surface unpassivation of CdTe quantum dots and competition of analyte cation to stabilizer. Anal Chem 82:3359–64. doi: 10.1021/ac100315a

54. Hua L, Zhou J, Han H (2010) Direct electrochemiluminescence of CdTe quantum dots based on room temperature ionic liquid film and high sensitivity sensing of gossypol. Electrochim Acta 55:1265–1271. doi: 10.1016/j.electacta.2009.10.038

55. Jie G, Huang H, Sun X, Zhu J (2008) Electrochemiluminescence of CdSe quantum dots for immunosensing of human prealbumin. Biosens Bioelectron 23:1896–1899. doi: 10.1016/j.bios.2008.02.028

56. Jie G, Yuan J (2012) Novel Magnetic Fe3O4@CdSe Composite Quantum Dot-Based Electrochemiluminescence Detection of Thrombin by a Multiple DNA Cycle Amplification Strategy. Anal Chem 84:2811–2817.

57. Liu X, Cheng L, Lei J, Liu H, Ju H (2010) Formation of Surface Traps on Quantum Dots by Bidentate Chelation and Their Application in Low-Potential Electrochemiluminescent Biosensing. Chemistry 16:10764–10770.

58. Hu T, Li T, Yuan L, Liu S, Wang Z (2012) Anodic electrogenerated chemiluminescence of quantum dots size and stabilizer matter. Nanoscale 4:5447.

59. Yang M, Chen Y, Xiang Y, Yuan R, Chai Y (2013) In situ energy transfer quenching of quantum dot electrochemiluminescence for sensitive detection of cancer biomarkers. Biosens Bioelectron 50:393–398.

60. Gan N, Zhou J, Xiong P, Li T, Jiang S, Cao Y (2013) An Ultrasensitive Electrochemiluminescence Immunoassay for Carbohydrate Antigen 19-9 in Serum Based on Antibody Labeled Fe 3 O 4 Nanoparticles as Capture Probes and Graphene / CdTe Quantum Dot Bionanoconjugates as Signal Amplifiers. Int J Mol Sci 14:10397–10411.

61. Ji J, He L, Shen Y, Hu P, Li X, Jiang L, Zhang J, Li L, Zhu J (2014) High-Efficient Energy Funneling Based on Electrochemiluminescence Resonance Energy Transfer in Graded-Gap Quantum Dots Bilayers for Immunoassay. Anal Chem 86:3284–3290.

62. Qian J, Zhang C, Cao X, Liu S (2010) Versatile Immunosensor Using a Quantum Dot Coated Silica Nanosphere as a Label for Signal Amplification. Anal Chem 82:6422–6429.

63. Wang S, Harris E, Shi J, Chen A, Parajuli S (2010) Electrogenerated chemiluminescence determination of C-reactive protein with carboxyl CdSe / ZnS core / shell quantum dots. Phys Chem Chem Phys 12:10073–10080.

64. Yan P, Zhang J, Tang Q, Deng A, Li J (2014) A quantum dot based electrochemiluminescent immunosensor for the detection of pg level phenylethanolamine A using gold nanoparticles as substrates and electron transfer accelerators. Analyst 139:4365–4372. doi: 10.1039/C4AN00378K

65. Yuan L, Hua X, Wu Y, Pan X, Liu S (2011) Polymer-Functionalized Silica Nanosphere Labels for Ultrasensitive Detection of Tumor Necrosis Factor-alpha. Anal Chem 83:6800–6809.

66. Zhang Y, Li L, Yang H, Ding Y, Su M, Zhu J, Yan M, Yu J, Song X (2013) Gold-silver nanocomposite-functionalized graphene sensing platform for an electrochemiluminescent immunoassay of a tumor marker. RSC Adv 3:14701.

67. Huang H, Tan Y, Shi J, Zhu J (2010) DNA aptasensor for the detection of ATP based on quantum dots electrochemiluminescence. Nanoscale 2:606–612.

68. Liu Y-M, Zhou M, Liu Y-Y, Huang K-J, Cao J-T, Zhang J-J, Shi G-F, Chen Y-H (2014) A novel sandwich electrochemiluminescence aptasensor based on molybdenum disulfide nanosheet-graphene composites and Au nanoparticles for signal amplification. Anal Methods 6:4152.

69. Jie G, Zhang J, Jie G, Wang L (2014) A novel quantum dot nanocluster as versatile probe for electrochemiluminescence and electrochemical assays of DNA and cancer cells. Biosens Bioelectron 52:69–75.

70. Hu X, Wang R, Ding Y, Zhang X, Jin W (2010) Electrochemiluminescence of CdTe quantum dots as labels at nanoporous gold leaf electrodes for ultrasensitive DNA analysis. Talanta 80:1737–1743. doi: 10.1016/j.talanta.2009.10.015

71. Jie G, Wang L, Yuan J, Zhang S (2011) Versatile electrochemiluminescence assays for cancer cells based on dendrimer/CdSe-ZnS-quantum dot nanoclusters. Anal Chem 83:3873–3880.

72. Jie G, Zhao Y, Niu S (2013) Amplified electrochemiluminescence detection of cancer cells using a new bifunctional quantum dot as signal probe. Biosens Bioelectron 50:368–372.

73. Jie G, Yuan J, Zhang J (2012) Quantum dots-based multifunctional dendritic superstructure for amplified electrochemiluminescence detection of ATP. Biosens Bioelectron 31:69–76. doi: 10.1016/j.bios.2011.09.047

74. Shi C, Shan X, Pan Z, Xu J, Lu C, Bao N, Gu H (2012) Quantum Dot (QD)-Modified Carbon Tape Electrodes for Reproducible Electrochemiluminescence (ECL) Emission on a Paper- Based Platform. Anal Chem 84:3033–3038.

75. Sun L, Bao L, Hyun B, Bartnik AC, Zhong Y, Reed JC, Pang D, Abrun D, Malliaras GG, Wise FW (2009) Electrogenerated Chemiluminescence from PbS Quantum Dots. nanoletters 9:789–793.

76. Deng S, Zhang T, Zhang Y, Shan D, Zhang X (2014) Chronopotentiometric synthesis of

quantum dots with efficient surface-derived near-infrared electrochemiluminescence for ultrasensitive microchip-based ion-selective sensing. RSC Adv 4:29239. doi: 10.1039/c4ra03211j

77. Wang J, Han H (2013) Near-infrared electrogenerated chemiluminescence from quantum dots. Rev Anal Chem 32:91–101. doi: 10.1515/revac-2012-0043

78. Wang J, Han H, Jiang X, Huang L, Chen L, Li N (2012) Quantum Dot-Based Near-Infrared Electrochemiluminescent Immunosensor with Gold Nanoparticle-Graphene Nanosheet Hybrids and Silica Nanospheres Double-Assisted Signal Amplification. Anal Chem 84:4893–4899.

79. Wang J, Jiang X, Han H, Li N (2011) Cathodic electrochemiluminescence from self-designed near-infrared-emitting CdTe CdS ZnS quantum dots on bare Au electrode. Electrochem commun 13:359–362.

80. Han H, Sheng Z, Liang J (2007) Electrogenerated chemiluminescence from thiol-capped CdTe quantum dots and its sensing application in aqueous solution. Anal Chim Acta 596:73–78. doi: 10.1016/j.aca.2007.05.039

81. Lei Bao, Liangfeng Sun, Zhi Ling Zhang, Peng Jiang, Frank W. Wise, Ḥctor D. Abruña DWP (2011) Energy-Level-Related Response of Cathodic Electrogenerated-Chemiluminescence of Self-Assembled CdSe/ZnS Quantum Dot Films. J Phys Chem C 18822–18828.

82. Wan F, Yu J, Yang P, Ge S, Yan M (2011) An electrochemiluminescence sensor for determination of durabolin based on CdTe QD films by layer-by-layer self-assembly. Anal Bioanal Chem 807–814.

83. Hua L, Han H, Chen H (2009) Enhanced electrochemiluminescence of CdTe quantum dots with carbon nanotube film and its sensing of methimazole. Electrochim Acta 54:1389–1394. doi: 10.1016/j.electacta.2008.08.044

84. Hu L, Xu G (2010) Applications and trends in electrochemiluminescence. Chem Soc Rev 39:3275–304. doi: 10.1039/b923679c

85. Liu D-Y, Xin Y-Y, He X-W, Yin X-B (2011) A sensitive, non-damaging electrochemiluminescent aptasensor via a low potential approach at DNA-modified goldelectrodes. Analyst 136:479–485. doi: 10.1039/C0AN00607F

86. Chen Z, Zu Y (2009) Electrogenerated Chemiluminescence of the Tris (2 , 2 ′ -bipyridine) ruthenium (II)/ Tertiary Amine Systems : Effects of Electrode Surface Hydrophobicity on the Low-Oxidation-Potential Emission. 21877–21882.

87. Jiang P, Yan L, Liu Y-H, Yuan H-Y, Xiao D (2009) Enhanced Electrogenerated Chemiluminescence of Tris(2,2′-bipyridyl) Ruthenium(II)/tripropylamine in the Presence of Pyridine and Its Analogues. Electroanalysis 21:1611–1616. doi: 10.1002/elan.200804585

88. Zou G, Liang G, Zhang X (2011) Strong anodic near-infrared electrochemiluminescence

from CdTe quantum dots at low oxidation potentials. Chem Commun (Camb) 47:10115–7. doi: 10.1039/c1cc13168k

89. Liang G-X, Li L-L, Liu H-Y, Zhang J-R, Burda C, Zhu J-J (2010) Fabrication of near-infrared-emitting CdSeTe/ZnS core/shell quantum dots and their electrogenerated chemiluminescence. Chem Commun (Camb) 46:2974–6. doi: 10.1039/c000564a

90. Ding Z, Quinn BM, Haram SK, Pell LE, Korgel B a, Bard AJ (2002) Electrochemistry and electrogenerated chemiluminescence from silicon nanocrystal quantum dots. Science 296:1293–7. doi: 10.1126/science.1069336

91. Wang S, Harris E, Shi J, Chen A, Parajuli S, Jing X, Miao W (2010) Electrogenerated chemiluminescence determination of C-reactive protein with carboxyl CdSe/ZnS core/shell quantum dots. Phys Chem Chem Phys 12:10073–80. doi: 10.1039/c0cp00545b

92. Zheng H, Zu Y (2005) Emission of tris(2,2'-bipyridine)ruthenium(II) by coreactant electrogenerated chemiluminescence: from O2-insensitive to highly O2-sensitive. J Phys Chem B 109:12049–53. doi: 10.1021/jp050350d

93. Chen Z, Zu Y (2008) Selective detection of uric acid in the presence of ascorbic acid based on electrochemiluminescence quenching. J Electroanal Chem 612:151–155. doi: 10.1016/j.jelechem.2007.09.018

94. Zheng H, Zu Y (2005) Highly efficient quenching of coreactant electrogenerated chemiluminescence by phenolic compounds. J Phys Chem B 109:16047–51. doi: 10.1021/jp052843o

95. Hill CM, Clayton D a, Pan S (2013) Combined optical and electrochemical methods for studying electrochemistry at the single molecule and single particle level: recent progress and perspectives. Phys Chem Chem Phys 15:20797–807. doi: 10.1039/c3cp52756e

96. Yuan Y, Wei S, Liu G, Xie S, Chai Y, Yuan R (2014) Ultrasensitive electrochemiluminescent aptasensor for ochratoxin A detection with the loop-mediated isothermal amplification. Anal Chim Acta 811:70–5. doi: 10.1016/j.aca.2013.11.022

97. Li T, Jeon K-S, Suh YD, Kim M-G (2011) A label-free, direct and noncompetitive FRET immunoassay for ochratoxin A based on intrinsic fluorescence of an antigen and antibody complex. Chem Commun (Camb) 47:9098–100. doi: 10.1039/c1cc12604k

98. Wu S, Duan N, Ma X, Xia Y, Wang H, Wang Z, Zhang Q (2012) Multiplexed fluorescence resonance energy transfer aptasensor between upconversion nanoparticles and graphene oxide for the simultaneous determination of mycotoxins. Anal Chem 84:6263–70. doi: 10.1021/ac301534w

99. Hun X, Liu F, Mei Z, Ma L, Wang Z, Luo X (2013) Signal amplified strategy based on target-induced strand release coupling cleavage of nicking endonuclease for the ultrasensitive detection of ochratoxin A. Biosens Bioelectron 39:145–51. doi: 10.1016/j.bios.2012.07.005

100. Low WS, Kadri NA, Abas WABBW (2014) Computational fluid dynamics modelling of

microfluidic channel for dielectrophoretic BioMEMS application. ScientificWorldJournal 2014:961301. doi: 10.1155/2014/961301

101. Wang S, Ge L, Zhang Y, Song X, Li N, Ge S, Yu J (2012) Battery-triggered microfluidic paper-based multiplex electrochemiluminescence immunodevice based on potential-resolution strategy. Lab Chip 12:4489–98. doi: 10.1039/c2lc40707h

102. Li W, Li M, Ge S, Yan M, Huang J, Yu J (2013) Battery-triggered ultrasensitive electrochemiluminescence detection on microfluidic paper-based immunodevice based on dual-signal amplification strategy. Anal Chim Acta 767:66–74. doi: 10.1016/j.aca.2012.12.053

103. Delaney JL, Doeven EH, Harsant AJ, Hogan CF (2013) Use of a mobile phone for potentiostatic control with low cost paper-based microfluidic sensors. Anal Chim Acta 790:56–60. doi: 10.1016/j.aca.2013.06.005

104. Delaney JL, Hogan CF, Tian J, Shen W (2011) Electrogenerated chemiluminescence detection in paper-based microfluidic sensors. Anal Chem 83:1300–6. doi: 10.1021/ac102392t

105. Ge L, Yan J, Song X, Yan M, Ge S, Yu J (2012) Three-dimensional paper-based electrochemiluminescence immunodevice for multiplexed measurement of biomarkers and point-of-care testing. Biomaterials 33:1024–31. doi: 10.1016/j.biomaterials.2011.10.065

106. Zhang M, Ge L, Ge S, Yan M, Yu J, Huang J, Liu S (2013) Three-dimensional paper-based electrochemiluminescence device for simultaneous detection of Pb2+ and Hg2+ based on potential-control technique. Biosens Bioelectron 41:544–50. doi: 10.1016/j.bios.2012.09.022

107. Yan J, Ge L, Song X, Yan M, Ge S, Yu J (2012) Paper-based electrochemiluminescent 3D immunodevice for lab-on-paper, specific, and sensitive point-of-care testing. Chemistry 18:4938–45. doi: 10.1002/chem.201102855

108. Hosono H, Satoh W, Toya M, Morimoto K, Fukuda J, Suzuki H (2008) Microanalysis system with automatic valve operation, pH regulation, and detection functions. Sensors Actuators B Chem 132:614–622. doi: 10.1016/j.snb.2007.12.054

109. Hosono H, Satoh W, Fukuda J, Suzuki H (2007) On-chip handling of solutions and electrochemiluminescence detection of amino acids. Sensors Actuators B Chem 122:542–548. doi: 10.1016/j.snb.2006.06.030

110. Sardesai NP, Kadimisetty K, Faria R, Rusling JF (2013) A microfluidic electrochemiluminescent device for detecting cancer biomarker proteins. Anal Bioanal Chem 405:3831–8. doi: 10.1007/s00216-012-6656-5

111. Redha ZM, Baldock SJ, Fielden PR, Goddard NJ, Brown BJT, Haggett BGD, Andres R, Birch BJ (2009) Hybrid Microfluidic Sensors Fabricated by Screen Printing and Injection Molding for Electrochemical and Electrochemiluminescence Detection.

Electroanalysis 21:422–430. doi: 10.1002/elan.200804415

112. Wang S, Ge L, Yan M, Yu J, Song X, Ge S, Huang J (2013) 3D microfluidic origami electrochemiluminescence immunodevice for sensitive point-of-care testing of carcinoma antigen 125. Sensors Actuators B Chem 176:1–8. doi: 10.1016/j.snb.2012.08.035

113. Pittet P, Lu G-N, Galvan J-M, Ferrigno R, Blum LJ, Leca-Bouvier B (2007) PCB-based integration of electrochemiluminescence detection for microfluidic systems. Analyst 132:409–11. doi: 10.1039/b701296a

114. Pittet P, Lu G-N, Galvan J-M, Ferrigno R, Stephan K, Blum LJ, Leca-Bouvier B (2008) A novel low-cost approach of implementing electrochemiluminescence detection for microfluidic analytical systems. Mater Sci Eng C 28:891–895. doi: 10.1016/j.msec.2007.10.030

115. Deng S, Ju H (2013) Electrogenerated chemiluminescence of nanomaterials for bioanalysis. Analyst 138:43–61. doi: 10.1039/c2an36122a

116. Martinez AW, Phillips ST, Butte MJ, Whitesides GM (2007) Patterned paper as a platform for inexpensive, low-volume, portable bioassays. Angew Chem Int Ed Engl 46:1318–20. doi: 10.1002/anie.200603817

117. Ge L, Yu J, Ge S, Yan M (2014) Lab-on-paper-based devices using chemiluminescence and electrogenerated chemiluminescence detection. Anal Bioanal Chem 406:5613–5630.

118. Yan J, Yan M, Ge L, Yu J, Ge S, Huang J (2013) A microfluidic origami electrochemiluminescence aptamer-device based on a porous Au-paper electrode and a phenyleneethynylene derivative. Chem Commun (Camb) 49:1383–5. doi: 10.1039/c2cc37402a

119. Zhang M, Ge L, Ge S, Yan M, Yu J, Huang J, Liu S (2013) Biosensors and Bioelectronics Three-dimensional paper-based electrochemiluminescence device for simultaneous detection of Pb 2 þ and Hg 2 þ based on potential-control technique. Biosens Bioelectron 41:544–550. doi: 10.1016/j.bios.2012.09.022

120. Zhan W, Alvarez J, Crooks RM (2003) A two-channel microfluidic sensor that uses anodic electrogenerated chemiluminescence as a photonic reporter of cathodic redox reactions. Anal Chem 75:313–8.

121. Zhan W, Alvarez J, Crooks RM (2002) Electrochemical sensing in microfluidic systems using electrogenerated chemiluminescence as a photonic reporter of redox reactions. J Am Chem Soc 124:13265–70.

122. Zhan W, Alvarez J, Sun L, Crooks RM (2003) A multichannel microfluidic sensor that detects anodic redox reactions indirectly using anodic electrogenerated chemiluminescence. Anal Chem 75:1233–8.

123. Wu M-S, Shi H-W, He L-J, Xu J-J, Chen H-Y (2012) Microchip device with 64-site electrode array for multiplexed immunoassay of cell surface antigens based on

electrochemiluminescence resonance energy transfer. Anal Chem 84:4207–13. doi: 10.1021/ac300551e

124. Qiu H, Yan J, Sun X, Liu J, Cao W, Yang X, Wang E (2003) Microchip Capillary Electrophoresis with an Integrated Indium Tin Oxide Electrode-Based Electrochemiluminescence Detector. Anal Chem 75:5435–5440.

125. Guo L, Qiu B, Xue L, Chen G (2009) CE with a new electrochemiluminescent detection system for separation and detection of proteins labeled with tris(1,10-phenanthroline) ruthenium(II). Electrophoresis 30:2390–6. doi: 10.1002/elps.200800715

126. Yin X-B, Du Y, Yang X, Wang E (2005) Microfluidic chip with electrochemiluminescence detection using 2-(2-aminoethyl)-1-methylpyrrolidine labeling. J Chromatogr A 1091:158–162. doi: 10.1016/j.chroma.2005.07.046

127. Mavré F, Anand RK, Laws DR, Chow K-F, Chang B-Y, Crooks J a, Crooks RM (2010) Bipolar electrodes: a useful tool for concentration, separation, and detection of analytes in microelectrochemical systems. Anal Chem 82:8766–74. doi: 10.1021/ac101262v

128. Chang BY, Mavré F, Chow KF, Crooks JA, Crooks RM (2010) Snapshot voltammetry using a triangular bipolar microelectrode. Anal Chem 82:5317–5322.

129. Chow K-F, Mavré F, Crooks JA, Chang B-Y, Crooks RM (2009) A large-scale, wireless electrochemical bipolar electrode microarray. J Am Chem Soc 131:8364–5. doi: 10.1021/ja902683f

130. Mavré F, Chow K-F, Sheridan E, Chang B-Y, Crooks JA, Crooks RM (2009) A Theoretical and Experimental Framework for Understanding Electrogenerated Chemiluminescence (ECL) Emission at Bipolar Electrodes. Anal Chem 81:6218–6225.

131. Arora A, Eijkel JCT, Morf WE, Manz A (2001) A Wireless Electrochemiluminescence Detector Applied to Direct and Indirect Detection for Electrophoresis on a Microfabricated Glass Device. Anal Chem 73:3282–3288.

132. Zhang X, Chen C, Li J, Zhang L, Wang E (2013) New Insight into a Microfluidic-Based Bipolar System for an Electrochemiluminescence Sensing Platform. Anal Chem 85:5335–5339.

133. Chang B-Y, Chow K-F, Crooks J a, Mavré F, Crooks RM (2012) Two-channel microelectrochemical bipolar electrode sensor array. Analyst 137:2827–33. doi: 10.1039/c2an35382b

134. Wu M-S, Xu B-Y, Shi H-W, Xu J-J, Chen H-Y (2011) Electrochemiluminescence analysis of folate receptors on cell membrane with on-chip bipolar electrode. Lab Chip 11:2720–4. doi: 10.1039/c1lc20143c

135. Wu M-S, Yuan D-J, Xu J-J, Chen H-Y (2013) Electrochemiluminescence on bipolar electrodes for visual bioanalysis. Chem Sci 4:1182. doi: 10.1039/c2sc22055e

136. Kim Y, Kim J (2014) Modification of Indium Tin Oxide with Dendrimer-Encapsulated

Nanoparticles To Provide Enhanced Stable Electrochemiluminescence of Ru(bpy)3 2+/Tripropylamine While Preserving Optical Transparency of Indium Tin Oxide for Sensitive Electrochemiluminescence-B. Anal. Chem. 86:

137. Lin Y, Dai H, Xu G, Yang T, Yang C, Tong Y, Yang Y, Chen G (2013) Enhanced luminol electrochemiluminescence triggered by an electrode functionalized with dendrimers modified with titanate nanotubes. Microchim Acta 180:563–572. doi: 10.1007/s00604-013-0963-1

138. Li J, Xu Q, Fu C, Zhang Y (2013) A dramatically enhanced electrochemiluminescence assay for CA125 based on dendrimer multiply labeled luminol on Fe3O4 nanoparticles. Sensors Actuators B Chem 185:146–153.

139. Zhuo Y, Gui G, Chai Y, Liao N, Xiao K, Yuan R (2014) Sandwich-format electrochemiluminescence assays for tumor marker based on PAMAM dendrimer-L-cysteine-hollow gold nanosphere nanocomposites. Biosens Bioelectron 53:459–464.

140. Qi H, Qiu X, Xie D, Ling C, Gao Q, Zhang C (2013) Ultrasensitive Electrogenerated Chemiluminescence Peptide-Based Method for the Determination of Cardiac Troponin I Incorporating Ampli fi cation of Signal Reagent ‑ Encapsulated Liposomes. Anal Chem 85:3886–3894.

141. Zhan W, Bard AJ (2007) Immunoassay of Human C-Reactive Protein by Using Ru (bpy) 32 + -Encapsulated Liposomes as Labels. Anal Chem 79:7109–7113.

142. Miao W, Bard AJ (2003) Determination of Immobilized DNA and C-Reactive Protein on Au (111) Electrodes Using Tris (2 , 2 ′ -bipyridyl) ruthenium (II) Labels. Anal Chem 75:5825–5834.

143. Wang H, Sun D, Tan Z, Gong W, Wang L (2011) Electrochemiluminescence immunosensor for α-fetoprotein using Ru(bpy)3(2+)-encapsulated liposome as labels. Colloids Surf B Biointerfaces 84:515–9. doi: 10.1016/j.colsurfb.2011.02.008

144. Liu L, Bao J, Fang M, Li L, Dai Z (2009) Electrogenerated chemiluminescence for the sensitive detection of leucine using Ru(bpy)32+ immobilized on dendritic Pd nanoparticle. Sensors Actuators B Chem 139:527–531. doi: 10.1016/j.snb.2009.02.066

145. Ma F, Zhang Y, Qi H, Gao Q, Zhang C, Miao W (2012) Ultrasensitive electrogenerated chemiluminescence biosensor for the determination of mercury ion incorporating G4 PAMAM dendrimer and Hg(II)-specific oligonucleotide. Biosens Bioelectron 32:37–42. doi: 10.1016/j.bios.2011.11.011

146. Yoon C-H, Cho J-H, Oh H-I, Kim M-J, Lee C-W, Choi J-W, Paek S-H (2003) Development of a membrane strip immunosensor utilizing ruthenium as an electro-chemiluminescent signal generator. Biosens Bioelectron 19:289–296. doi: 10.1016/S0956-5663(03)00207-0

147. Shashi K, Satinder K, Bharat P (2012) A COMPLETE REVIEW ON: LIPOSOMES. Int Res J Pharm 3:10–16.

148. Venkatanarayanan A, Crowley K, Lestini E, Keyes TE, Rusling JF, Forster RJ (2012) High sensitivity carbon nanotube based electrochemiluminescence sensor array. Biosens Bioelectron 31:233–9. doi: 10.1016/j.bios.2011.10.022

149. Pal S, Kim MJ, Tak YK, Kwon HT, Song JM (2009) Interdigitated microelectrode array-coupled bipolar semiconductor photodiode array (IMEA-PDA) microchip for on-chip electrochemiluminescence detection. Biomed Microdevices 11:971–980. doi: 10.1007/s10544-009-9314-8

150. Sun F, Chen F, Fei W, Sun L, Wu Y (2012) A novel strategy for constructing electrochemiluminescence sensor based on CdS-polyamidoamine incorporating electrodeposited gold nanoparticle film and its application. Sensors Actuators B Chem 166-167:702–707. doi: 10.1016/j.snb.2012.03.043

151. Tai JH, Ewert MS, Belliot G, Glass RI, Monroe SS (2003) Development of a rapid method using nucleic acid sequence-based amplification for the detection of astrovirus. J Virol Methods 110:119–127. doi: 10.1016/S0166-0934(03)00108-3

152. Mac Kenzie WR, Hoxie NJ, Proctor ME, Gradus MS, Blair KA, Peterson DE, Kazmierczak JJ, Addiss DG, Fox KR, Rose JB (1994) A massive outbreak in Milwaukee of cryptosporidium infection transmitted through the public water supply. N Engl J Med 331:161–7. doi: 10.1056/NEJM199407213310304

153. Benamrouz S, Conseil V, Creusy C, Calderon E, Dei-Cas E, Certad G (2012) Parasites and malignancies, a review, with emphasis on digestive cancer induced by Cryptosporidium parvum (Alveolata: Apicomplexa). Parasite 19:101–15.

154. Certad G, Creusy C, Guyot K, Mouray A, Chassat T, Delaire B, Pinon A, Sitja-Bobadilla A, Alvarez-Pellitero P, Praet M, Cuvelier C, Dei-Cas E (2010) Fulminant cryptosporidiosis associated with digestive adenocarcinoma in SCID mice infected with Cryptosporidium parvum TUM1 strain. Int J Parasitol 40:1469–75. doi: 10.1016/j.ijpara.2010.07.007

155. Certad G, Ngouanesavanh T, Guyot K, Gantois N, Chassat T, Mouray A, Fleurisse L, Pinon A, Cailliez J-C, Dei-Cas E, Creusy C (2007) Cryptosporidium parvum, a potential cause of colic adenocarcinoma. Infect Agent Cancer 2:22. doi: 10.1186/1750-9378-2-22

156. Certad G, Creusy C, Ngouanesavanh T, Guyot K, Gantois N, Mouray A, Chassat T, Flament N, Fleurisse L, Pinon A, Delhaes L, Dei-Cas E (2010) Development of Cryptosporidium parvum-Induced Gastrointestinal Neoplasia in Severe Combined Immunodeficiency (SCID) Mice: Severity of Lesions Is Correlated with Infection Intensity. Am J Trop Med Hyg 82:257–265. doi: 10.4269/ajtmh.2010.08-0309

157. Sulżyc-Bielicka V, Kuźna-Grygiel W, Kołodziejczyk L, Bielicki D, Kładny J, Stępień-Korzonek M, Telatyńska-Śmieszek B (2007) Cryptosporidiosis in Patients with Colorectal Cancer. J Parasitol 93:722–724. doi: 10.1645/GE-1025R1.1

158. Chappell C, Okhuysen P, Sterling C, DuPont H (1996) Cryptosporidium parvum: Intensity of infection and oocyst excretion patterns in healthy volunteers. J Infect Dis

173:232–236.

159. Edwards K a, Bolduc OR, Baeumner AJ (2012) Miniaturized bioanalytical systems: enhanced performance through liposomes. Curr Opin Chem Biol 16:444–52. doi: 10.1016/j.cbpa.2012.05.182

160. Mansoori MA, Agrawal S, Jawade S, Khan MI (2012) A review on liposome. Internathinal J Adv Res pharmaccutical bio Sci 2:453–464.

161. Mufamadi MS, Pillay V, Choonara YE, Du Toit LC, Modi G, Naidoo D, Ndesendo VMK (2011) A review on composite liposomal technologies for specialized drug delivery. J Drug Deliv 2011:939851. doi: 10.1155/2011/939851

162. Samad A, Sultana Y, Aqil M (2007) Liposomal drug delivery systems: an update review. Curr Drug Deliv 4:297–305.

163. Tikshdeep C, Sonia A, Bharat P, Abhishek C (2012) Liposome Drug Delivery : A Review. Int J Pharm Chem Sci 1:754–764.

164. Edwards K a, Curtis KL, Sailor JL, Baeumner AJ (2008) Universal liposomes: preparation and usage for the detection of mRNA. Anal Bioanal Chem 391:1689–702. doi: 10.1007/s00216-008-1992-1

165. Connelly JT, Kondapalli S, Skoupi M, Parker JSL, Kirby BJ, Baeumner AJ (2012) Micro-total analysis system for virus detection: microfluidic pre-concentration coupled to liposome-based detection. Anal Bioanal Chem 402:315–23. doi: 10.1007/s00216-011-5381-9

166. Edwards K a, Wang Y, Baeumner AJ (2010) Aptamer sandwich assays: human α-thrombin detection using liposome enhancement. Anal Bioanal Chem 398:2645–54. doi: 10.1007/s00216-010-3920-4

167. Edwards K a, Meyers KJ, Leonard B, Baeumner AJ (2013) Superior performance of liposomes over enzymatic amplification in a high-throughput assay for myoglobin in human serum. Anal Bioanal Chem 405:4017–26. doi: 10.1007/s00216-013-6807-3

168. Edwards K a, Baeumner AJ (2006) Optimization of DNA-tagged liposomes for use in microtiter plate analyses. Anal Bioanal Chem 386:1613–23. doi: 10.1007/s00216-006-0743-4

169. Edwards K a, Duan F, Baeumner AJ, March JC (2008) Fluorescently labeled liposomes for monitoring cholera toxin binding to epithelial cells. Anal Biochem 380:59–67. doi: 10.1016/j.ab.2008.05.027

170. Edwards K a, Baeumner AJ (2009) Liposome-enhanced lateral-flow assays for the sandwich-hybridization detection of RNA. Methods Mol Biol 504:185–215. doi: 10.1007/978-1-60327-569-9_13

171. Lee M, Durst R a, Wong RB (1998) Development of flow-injection liposome immunoanalysis (FILIA) for imazethapyr. Talanta 46:851–9.

172. Nugen SR, Asiello PJ, Connelly JT, Baeumner AJ (2009) PMMA biosensor for nucleic acids with integrated mixer and electrochemical detection. Biosens Bioelectron 24:2428–33. doi: 10.1016/j.bios.2008.12.025

173. Akthong PR, Ntaramat AI, Atanabanangkoon KR (2010) Luminol Encapsulated Liposome as a Signal Generator for the Detection of Specific Antigen-antibody Reactions and Nucleotide Hybridization. Anal Sci 26:767–772.

174. Nakonechny F, Firer MA, Nitzan Y, Nisnevitch M (2010) Intracellular Antimicrobial Photodynamic Therapy : A Novel Technique for Efficient Eradication of Pathogenic Bacteria. Photochem Photobiol 86:1350–1355. doi: 10.1111/j.1751-1097.2010.00804.x

175. Suita T, Kamidate T, Yonaiyama M, Watanabe H (1997) Characterization of Horseradish Peroxidase-Encapsulated Liposomes Prepared by an Extrusion Technique. Anal Sci 13:577–581.

176. Suita T, Kamidate T (1999) Preparation of Antibody-Coupled Liposomes Containing Horseradish Peroxidase as a Marker Molecule. Anal Sci 15:349–352.

177. Qi H, Qiu X, Xie D, Ling C, Gao Q, Zhang C (2013) Ultrasensitive Electrogenerated Chemiluminescence Peptide-Based Method for the Determination of Cardiac Troponin I Incorporating Ampli fi cation of Signal Reagent ‑ Encapsulated Liposomes. Anal Chem 85:3886–3894.

178. Mao L, Yuan R, Chai Y, Zhuo Y, Xiang Y (2011) Signal-enhancer molecules encapsulated liposome as a valuable sensing and amplification platform combining the aptasensor for ultrasensitive ECL immunoassay. Biosens Bioelectron 26:4204–8. doi: 10.1016/j.bios.2011.02.035

179. Gan N, Hou J, Hu F, Cao Y, Li T, Guo Z, Wang J (2011) A Renewable and Ultrasensitive Electrochemiluminescence Immunosenor Based on Magnetic RuL@SiO2-Au~RuL-Ab2 Sandwich-Type Nano-Immunocomplexes. Sensors 11:7749–7762. doi: 10.3390/s110807749

180. Mao L, Yuan R, Chai Y, Zhuo Y, Jiang W (2011) Potential controlling highly-efficient catalysis of wheat-like silver particles for electrochemiluminescence immunosensor labeled by nano-Pt@Ru and multi-sites biotin/streptavidin affinity. Analyst 136:1450–1455. doi: 10.1039/c0an00867b

181. Dykes GM (2001) Dendrimers: a review of their appeal and applications. J Chem Technol Biotechnol 76:903–918. doi: 10.1002/jctb.464

182. Fischer M, Vögtle F (1999) Dendrimers: From Design to Application—A Progress Report. Angew Chemie Int Ed 38:884–905.

183. Gajbhiye V, Palanirajan VK, Tekade RK, Jain NK (2009) Dendrimers as therapeutic agents: a systematic review. J Pharm Pharmacol 61:989–1003. doi: 10.1211/jpp/61.08.0002

184. Bharali DJ, Khalil M, Gurbuz M, Simone TM, Mousa S (2009) Nanoparticles and cancer

therapy: a concise review with emphasis on dendrimers. Int J Nanomedicine 4:1–7.

185. Zhou M, Roovers J (2001) Dendritic Supramolecular Assembly with Multiple Ru(II) Tris(bipyridine) Units at the Periphery: Synthesis, Spectroscopic, and Electrochemical Study. Macromolecules 34:244–252. doi: 10.1021/ma001463s

186. Lee DN, Kim JK, Park HS, Jun YM, Hwang RY, Lee W-Y, Kim BH (2005) Polyamidoamine dendrimers functionalized with electrochemiluminescent polypyridyl Ru(II) complexes. Synth Met 150:93–100. doi: 10.1016/j.synthmet.2005.01.014

187. Leland JK, Powell MJ (1990) Electrogenerated Chemiluminescence: An Oxidative-Reduction Type ECL Reaction Sequence Using Tripropyl Amine. 137:3127–3131.

188. Cole C, Muegge BD, Richter MM (2003) Effects of poly(ethylene glycol) tert-octylphenyl ether on tris(2-phenylpyridine)iridium(III)-tripropylamine electrochemiluminescence. Anal Chem 75:601–4.

189. Kanoufi F, Zu Y, Bard AJ (2001) Homogeneous Oxidation of Trialkylamines by Metal Complexes and Its Impact on Electrogenerated Chemiluminescence in the Trialkylamine/Ru(bpy) 3 2+ System. J Phys Chem B 105:210–216. doi: 10.1021/jp002880+

190. Gross EM, Pastore P, Wightman RM (2001) High-Frequency Electrochemiluminescent Investigation of the Reaction Pathway between Tris(2,2‘-bipyridyl)ruthenium(II) and Tripropylamine Using Carbon Fiber Microelectrodes. J Phys Chem B 105:8732–8738. doi: 10.1021/jp011434z

191. Miao W, Choi J-P, Bard AJ (2002) Electrogenerated Chemiluminescence 69: The Tris(2,2‘-bipyridine)ruthenium(II), (Ru(bpy) 3 2+)/Tri- n -propylamine (TPrA) System Revisited - A New Route Involving TPrA •+ Cation Radicals. J Am Chem Soc 124:14478–14485. doi: 10.1021/ja027532v

192. Wightman R, Forry S, Maus R, Badocco D, Pastore P (2004) Rate-determining step in the electrogenerated chemiluminescence from tertiary amines with tris(2,2 ’-bipyridyl)ruthenium(II). J Phys Chem B 108:19119–19125. doi: 10.1021/jp0360341

193. Yin X-B, Sha B-B, Zhang X-H, He X-W, Xie H (2008) The Factors Affecting the Electrochemiluminescence of Tris(2,2′-bipyridyl)Ruthenium(II)/Tertiary Amines. Electroanalysis 20:1085–1091. doi: 10.1002/elan.200704156

194. Xu G, Pang H-L, Xu B, Dong S, Wong K-Y (2005) Enhancing the electrochemiluminescence of tris(2,2’-bipyridyl)ruthenium(II) by ionic surfactants. Analyst 130:541–544.

195. Factor B, Muegge B, Workman S, Bolton E, Bos J, Richter MM (2001) Surfactant Chain Length Effects on the Light Emission of Tris (2 , 2 ′ -bipyridyl) ruthenium (II). Anal Chem 73:4621–4624.

196. Holloway PW (1973) A simple procedure for removal of triton X-100 from protein samples. Anal Biochem 53:304–308. doi: 10.1016/0003-2697(73)90436-3

197. Papendick SL, Downs KR, Vo KD, Hamilton SK, Dawson GKW, Golding SD, Gilcrease PC (2011) Biogenic methane potential for Surat Basin, Queensland coal seams. Int J Coal Geol 88:123–134. doi: 10.1016/j.coal.2011.09.005

198. Vakarelski IU, Marston JO, Thoroddsen ST (2013) Foam-Film-Stabilized Liquid Bridge Networks in Evaporative Lithography and Wet Granular Matter. Langmuir 29:4966–4973. doi: 10.1021/la400662n

199. Wongkaew N, He P, Kurth V, Surareungchai W, Baeumner AJ (2013) Multi-channel PMMA microfluidic biosensor with integrated IDUAs for electrochemical detection. Anal Bioanal Chem 405:5965–74. doi: 10.1007/s00216-013-7020-0

200. Fischer BE, Haring UK, Tribolet R, Sigel H (1979) Metal Ion/Buffer Interactions. Stability of Binary and Ternary Complexes Containing 2-Amino-2(hydroxymethyl)-1,3-propanediol (Tris) and Adenosine 5'-Triphosphate (ATP). Eur J Biochem 94:523–530. doi: 10.1111/j.1432-1033.1979.tb12921.x

201. Masi D, Mealli C, Sabat M, Sabatini A, Vacca A, Zanobini F (1984) Bonding Capabilities of the Biochemical Buffer TRIS toward Copper(II) Ion. Structure and Magnetic Properties of Binuclear and Tetranuclear Systems. Helv Chim Acta 67:1818–1826. doi: 10.1002/hlca.19840670719

202. Tsao CW, Hromada L, Liu J, Kumar P, DeVoe DL (2007) Low temperature bonding of PMMA and COC microfluidic substrates using UV/ozone surface treatment. Lab Chip 7:499–505. doi: 10.1039/b618901f

203. Kettner P, Pelzer RL, Glinsner T, Farrens S, Lee D (2006) New Results on Plasma Activated Bonding of Imprinted Polymer Features for Bio MEMS Applications. J Phys Conf Ser 34:65–71. doi: 10.1088/1742-6596/34/1/011

204. Wongkaew N, Kirschbaum SEK, Surareungchai W, Durst RA, Baeumner AJ (2012) A Novel Three-Electrode System Fabricated on Polymethyl Methacrylate for On-Chip Electrochemical Detection. Electroanalysis 24:1903–1908. doi: 10.1002/elan.201200336

205. Bolduc OR (2013) 2012-2013 CNF Technical Report - Developing a novel electrochemiluminescent (ECL) microfluidic biosensor involving liposome based amplification. 2012-2013 CNF Tech. Rep.

Supplementary Information

EC Standard Curves

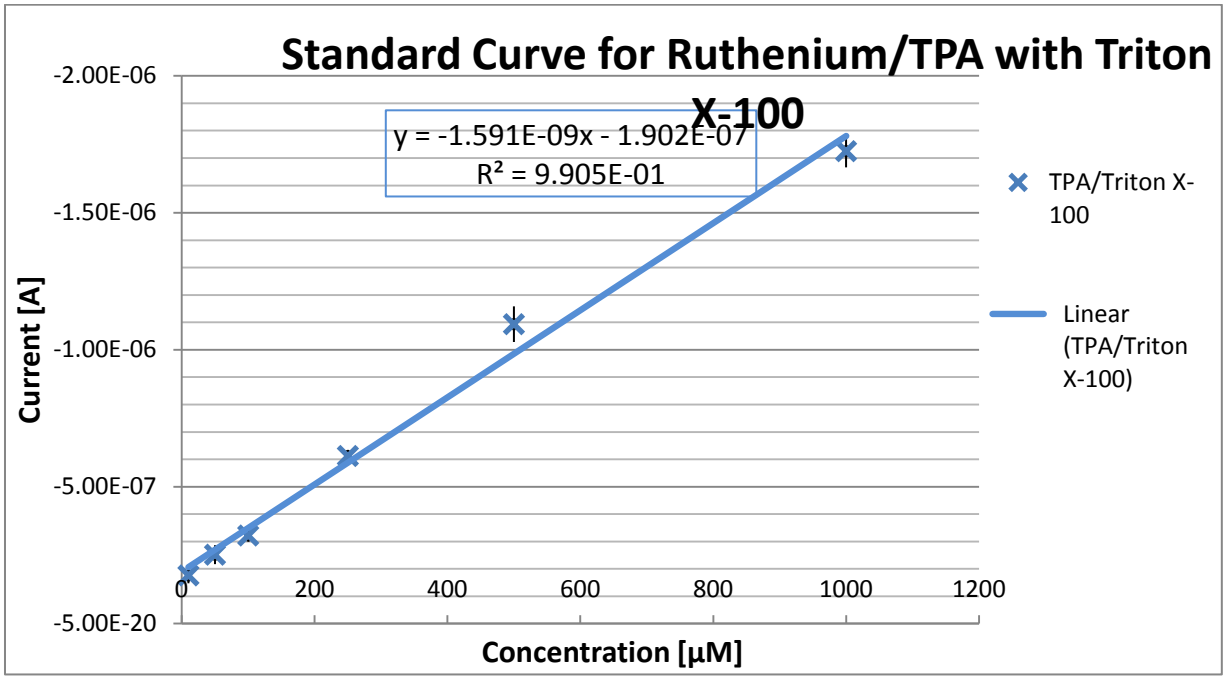

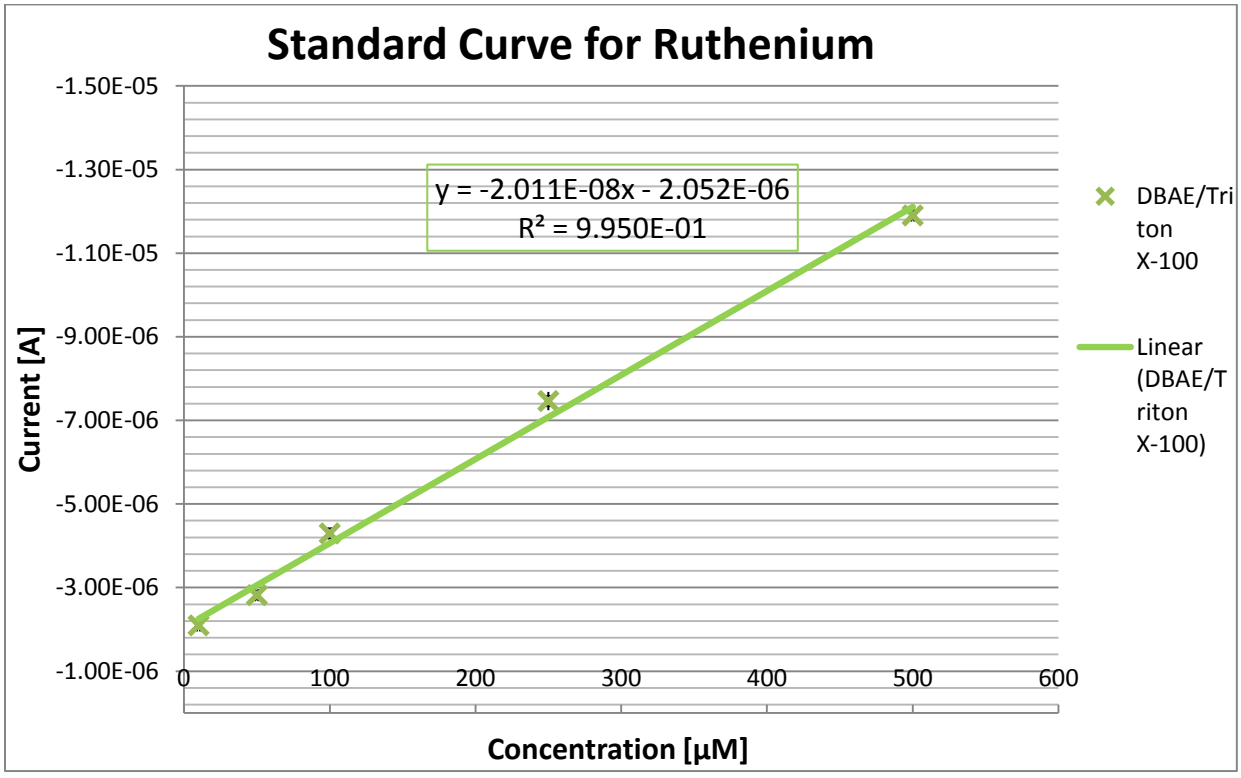

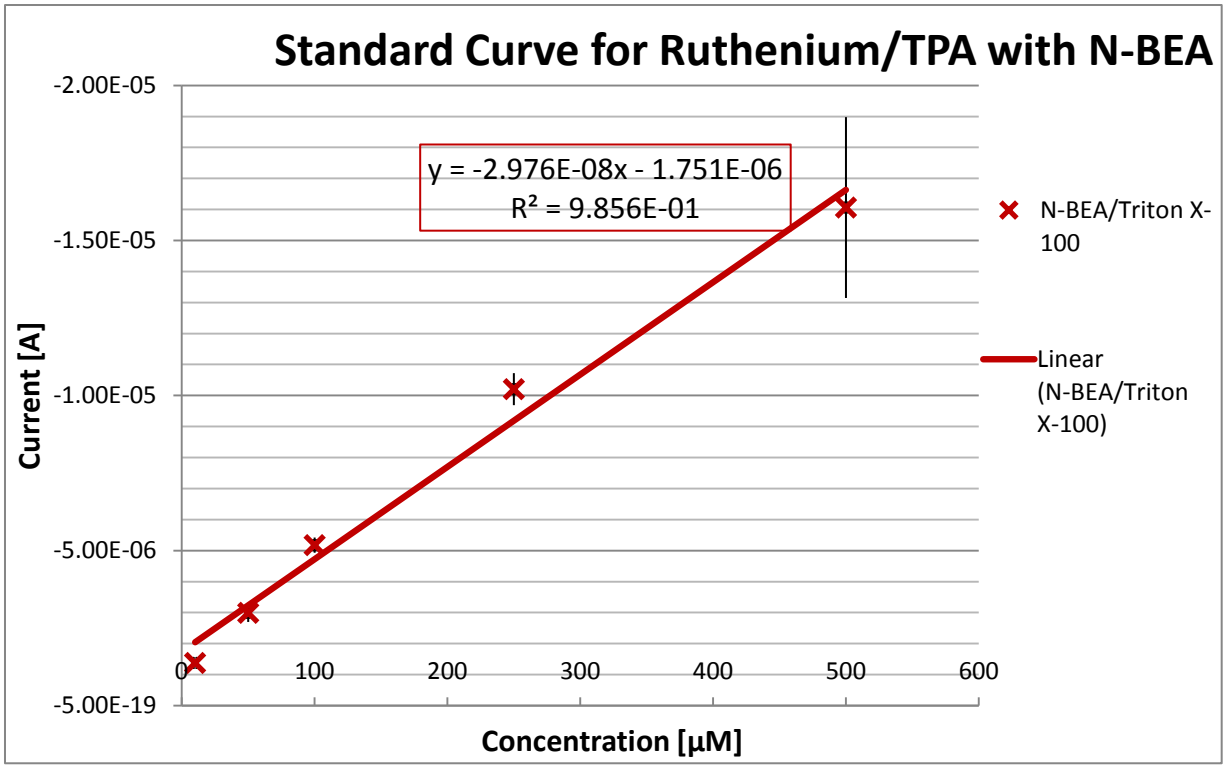
Standard Curve for Ruthenium/TPA with N-BEA
y = -2.976E-08x - 1.751E-06
R² = 9.856E-01
-2.00E-05
-1.50E-05
-1.00E-05
-5.00E-06
-5.00E-19
Current [A]
0
100
200
300
400
500
600
Concentration [µM]
N-BEA/Triton X-100
Linear (N-BEA/Triton X-100)

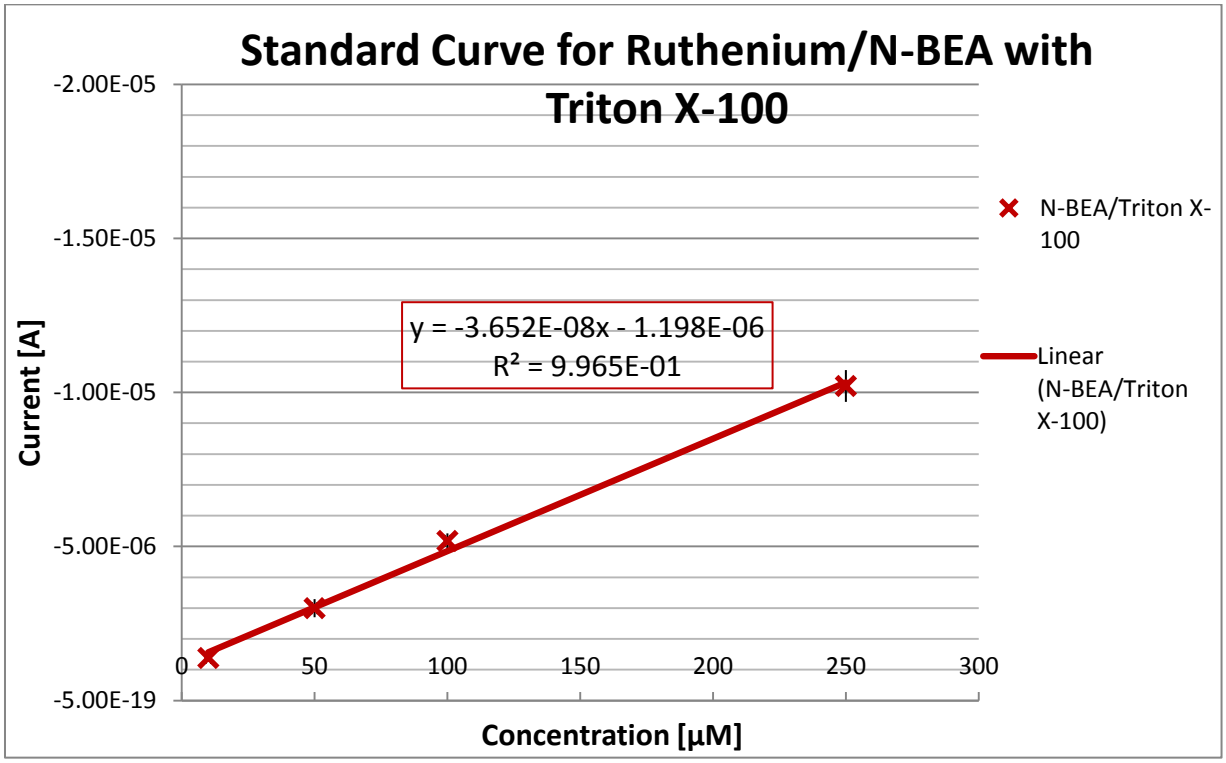
Standard Curve for Ruthenium/N-BEA with Triton X-100
y = -3.652E-08x - 1.198E-06
R² = 9.965E-01
-2.00E-05
-1.50E-05
-1.00E-05
-5.00E-06
-5.00E-19
Current [A]
0
50
100
150
200
250
300
Concentration [µM]
N-BEA/Triton X-100
Linear (N-BEA/Triton X-100)

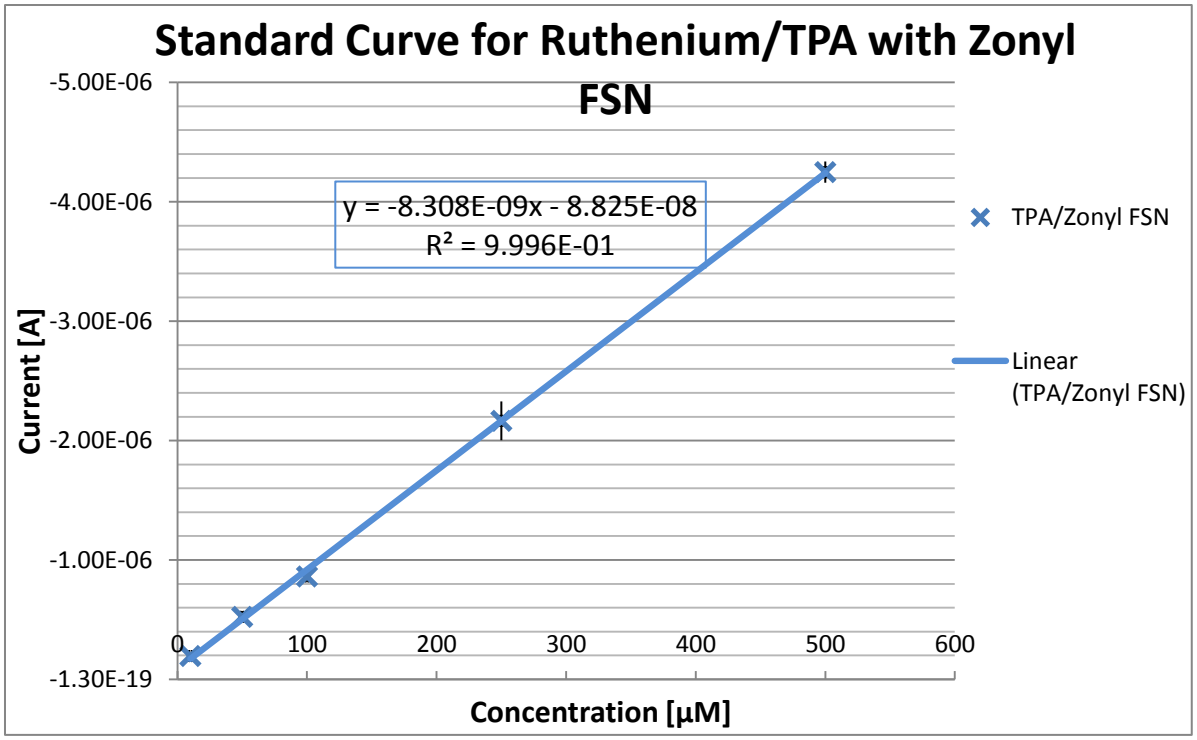
Standard Curve for Ruthenium/TPA with Zonyl FSN
y = -8.308E-09x - 8.825E-08
R² = 9.996E-01
TPA/Zonyl FSN
Linear (TPA/Zonyl FSN)
Current [A]
Concentration [µM]
-5.00E-06
-4.00E-06
-3.00E-06
-2.00E-06
-1.00E-06
-1.30E-19
0
100
200
300
400
500
600

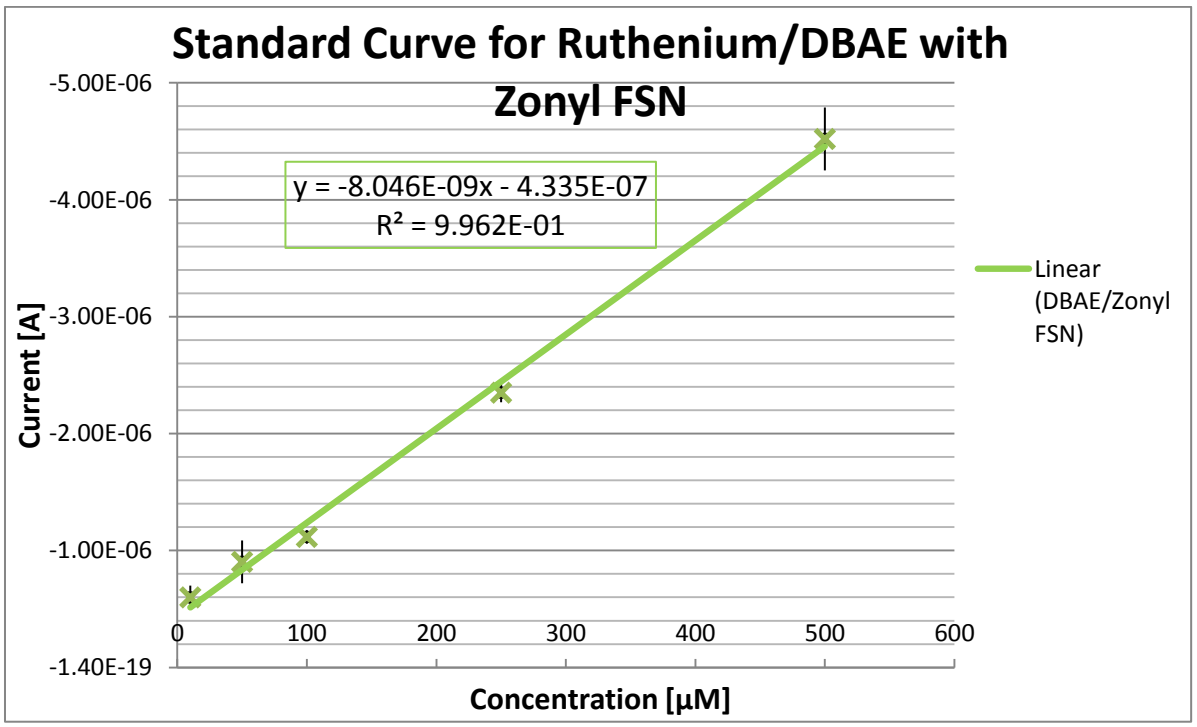
Standard Curve for Ruthenium/DBAE with Zonyl FSN
y = -8.046E-09x - 4.335E-07
R² = 9.962E-01
Linear (DBAE/Zonyl FSN)
Current [A]
Concentration [µM]
-5.00E-06
-4.00E-06
-3.00E-06
-2.00E-06
-1.00E-06
-1.40E-19
0
100
200
300
400
500
600

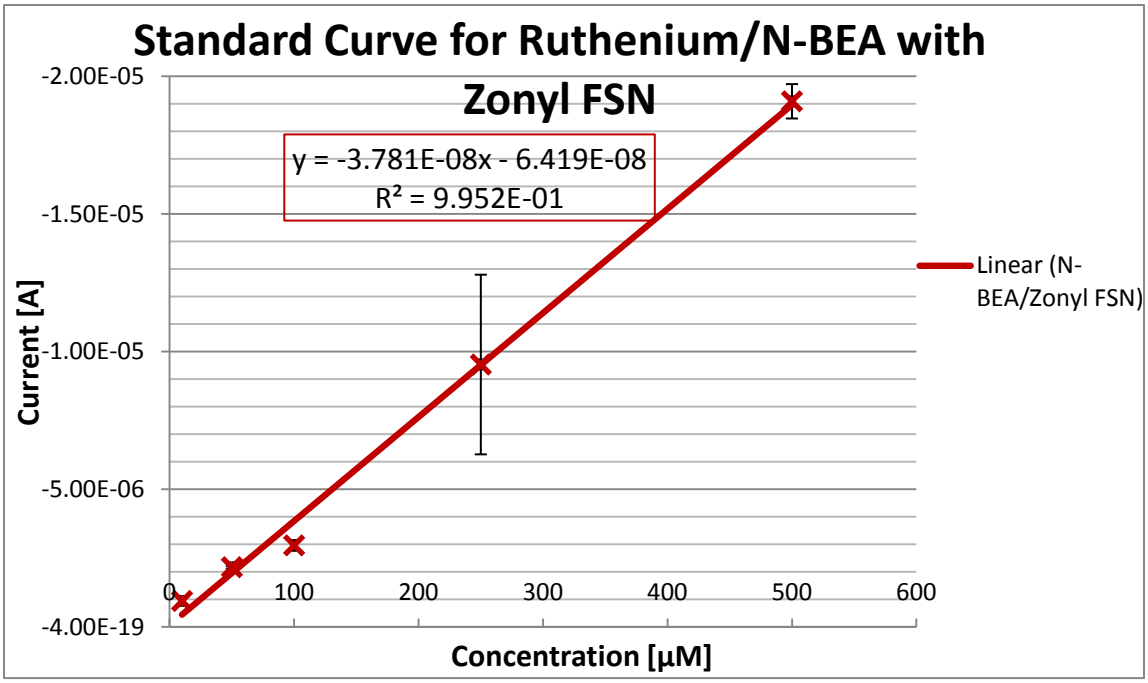
Standard Curve for Ruthenium/N-BEA with Zonyl FSN
y = -3.781E-08x - 6.419E-08
R² = 9.952E-01
-2.00E-05
-1.50E-05
-1.00E-05
-5.00E-06
-4.00E-19
Current [A]
0
100
200
300
400
500
600
Concentration [µM]
Linear (N-BEA/Zonyl FSN)

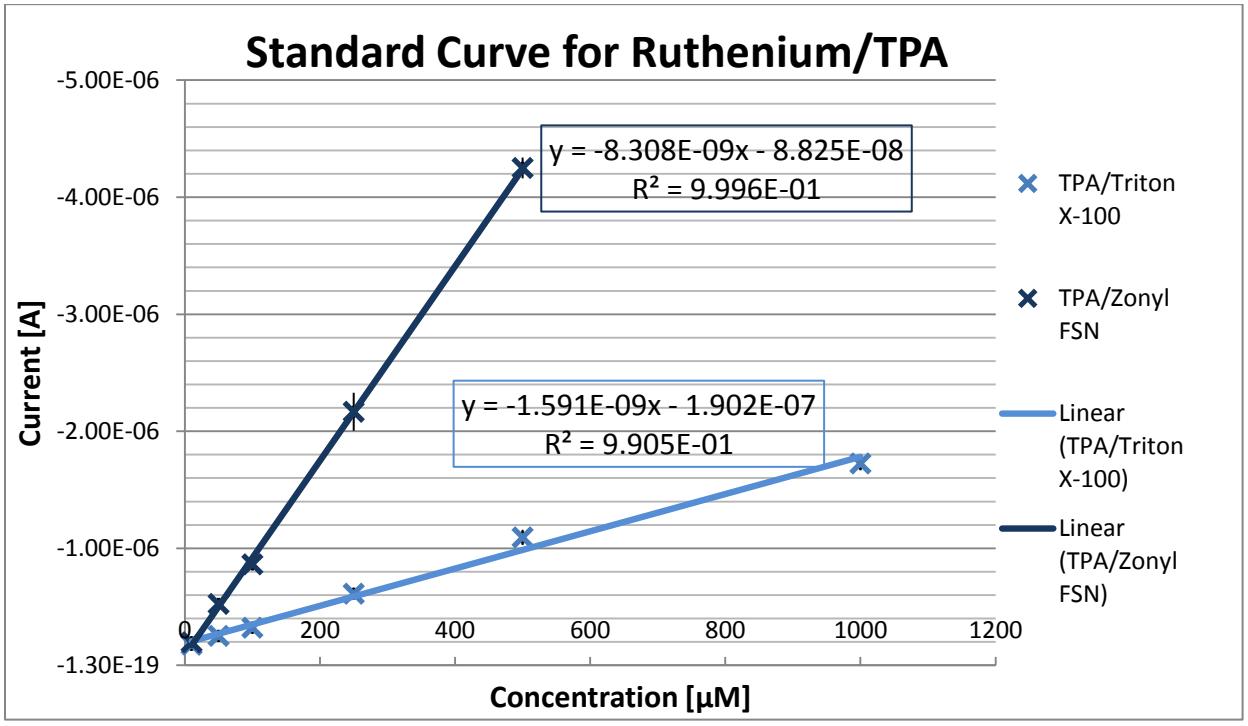
Standard Curve for Ruthenium/TPA
y = -8.308E-09x - 8.825E-08
R² = 9.996E-01
y = -1.591E-09x - 1.902E-07
R² = 9.905E-01
-5.00E-06
-4.00E-06
-3.00E-06
-2.00E-06
-1.00E-06
-1.30E-19
Current [A]
0
200
400
600
800
1000
1200
Concentration [µM]
TPA/Triton X-100
TPA/Zonyl FSN
Linear (TPA/Triton X-100)
Linear (TPA/Zonyl FSN)

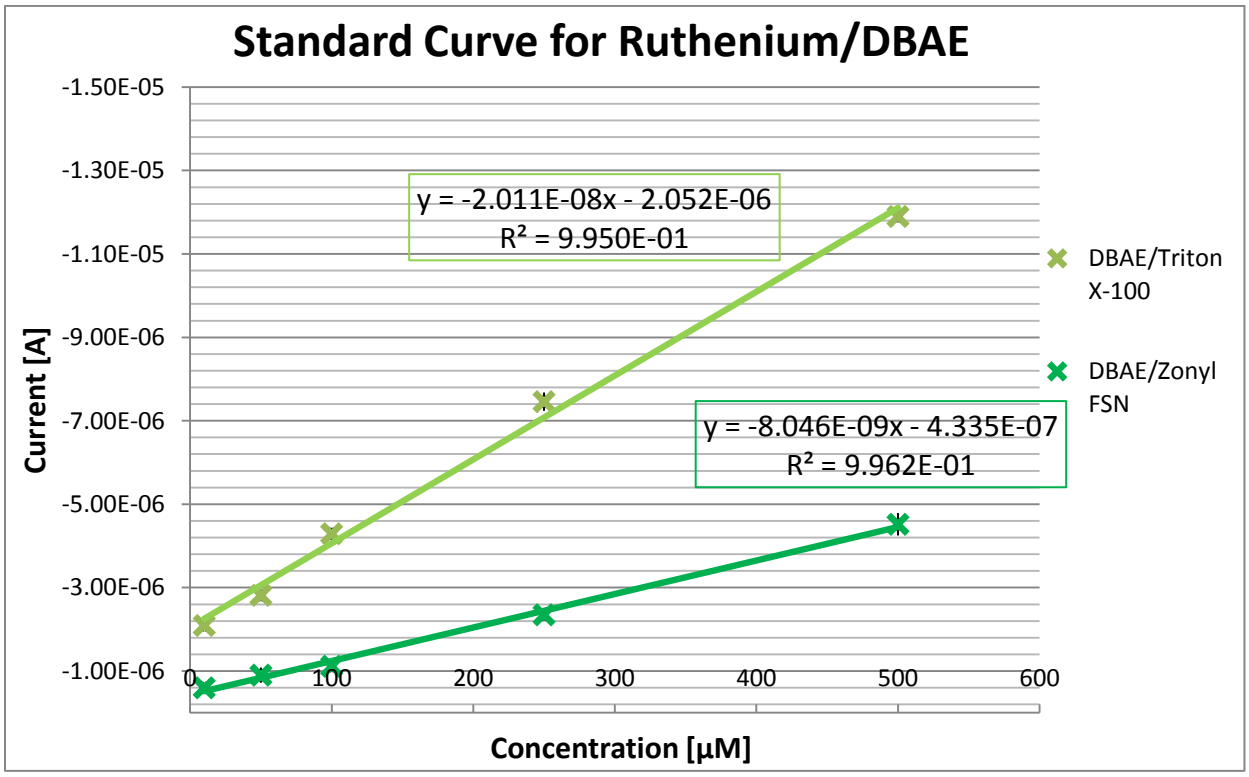
Standard Curve for Ruthenium/DBAE
-1.50E-05
-1.30E-05
-1.10E-05
-9.00E-06
-7.00E-06
-5.00E-06
-3.00E-06
-1.00E-06
Current [A]
y = -2.011E-08x - 2.052E-06
R² = 9.950E-01
y = -8.046E-09x - 4.335E-07
R² = 9.962E-01
0
100
200
300
400
500
600
Concentration [µM]
DBAE/Triton X-100
DBAE/Zonyl FSN

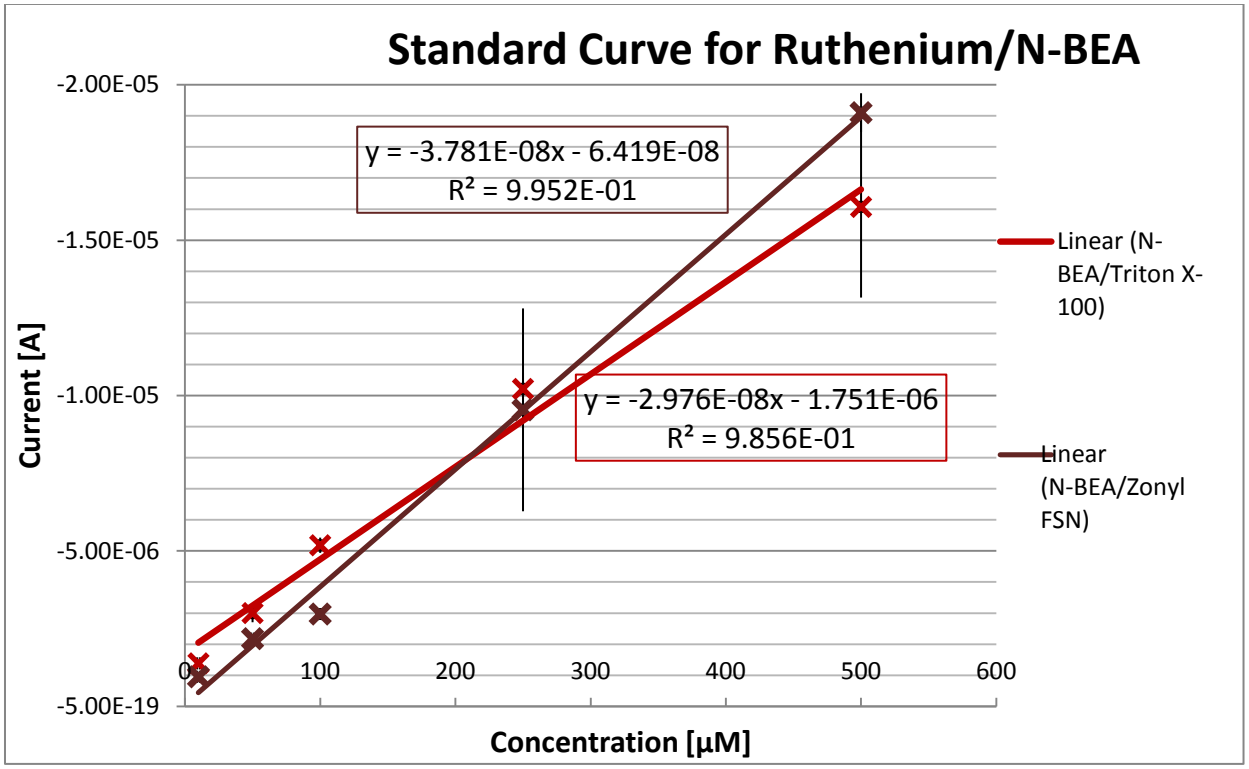
Standard Curve for Ruthenium/N-BEA
-2.00E-05
-1.50E-05
-1.00E-05
-5.00E-06
-5.00E-19
Current [A]
y = -3.781E-08x - 6.419E-08
R² = 9.952E-01
y = -2.976E-08x - 1.751E-06
R² = 9.856E-01
0
100
200
300
400
500
600
Concentration [µM]
Linear (N-BEA/Triton X-100)
Linear (N-BEA/Zonyl FSN)

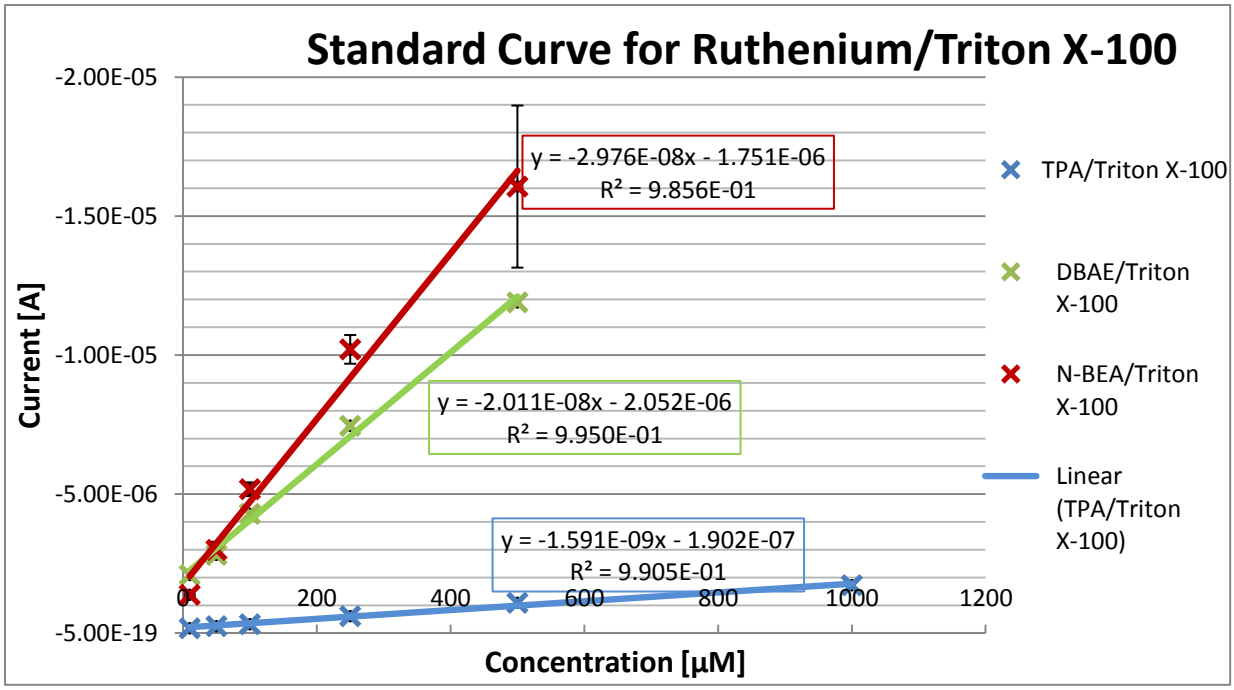
Standard Curve for Ruthenium/Triton X-100
-2.00E-05
-1.50E-05
-1.00E-05
-5.00E-06
-5.00E-19
Current [A]
0
200
400
600
800
1000
1200
Concentration [µM]
y = -2.976E-08x - 1.751E-06
R² = 9.856E-01
y = -2.011E-08x - 2.052E-06
R² = 9.950E-01
y = -1.591E-09x - 1.902E-07
R² = 9.905E-01
TPA/Triton X-100
DBAE/Triton X-100
N-BEA/Triton X-100
Linear (TPA/Triton X-100)

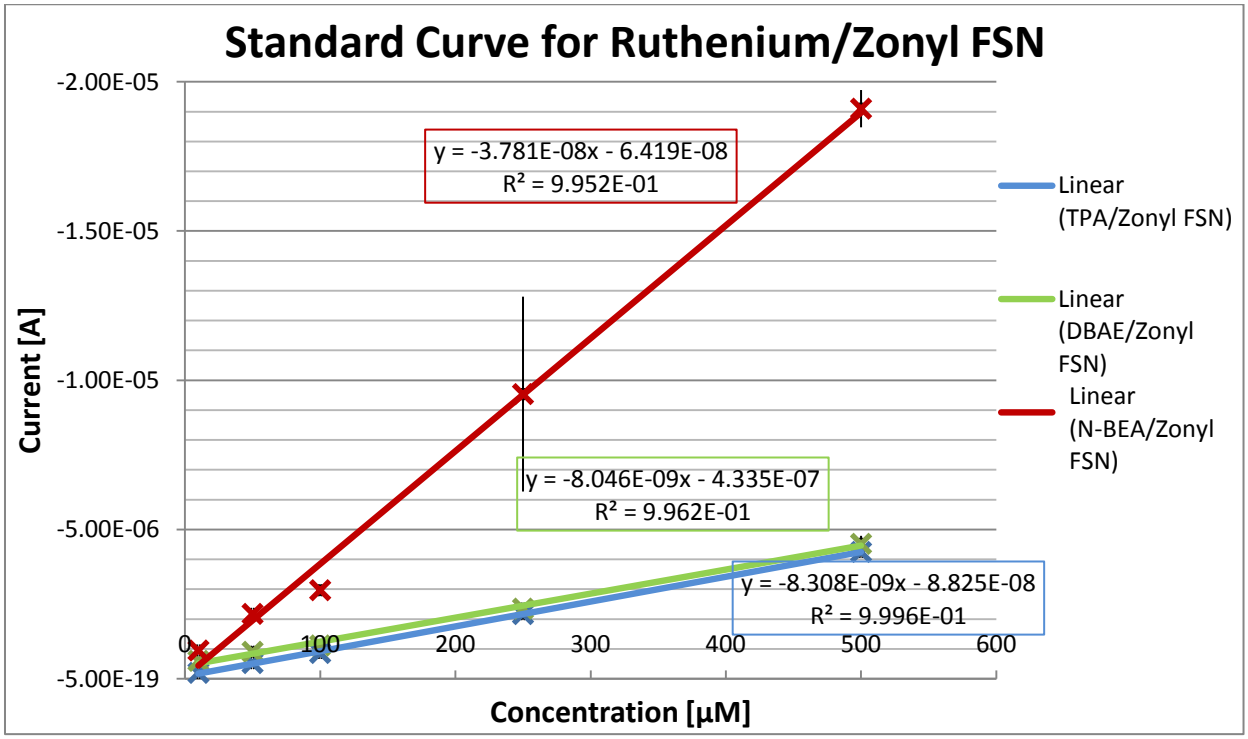
Standard Curve for Ruthenium/Zonyl FSN
-2.00E-05
-1.50E-05
-1.00E-05
-5.00E-06
-5.00E-19
Current [A]
0
100
200
300
400
500
600
Concentration [µM]
y = -3.781E-08x - 6.419E-08
R² = 9.952E-01
y = -8.046E-09x - 4.335E-07
R² = 9.962E-01
y = -8.308E-09x - 8.825E-08
R² = 9.996E-01
Linear (TPA/Zonyl FSN)
Linear (DBAE/Zonyl FSN)
Linear (N-BEA/Zonyl FSN)

Coreactant Optimization

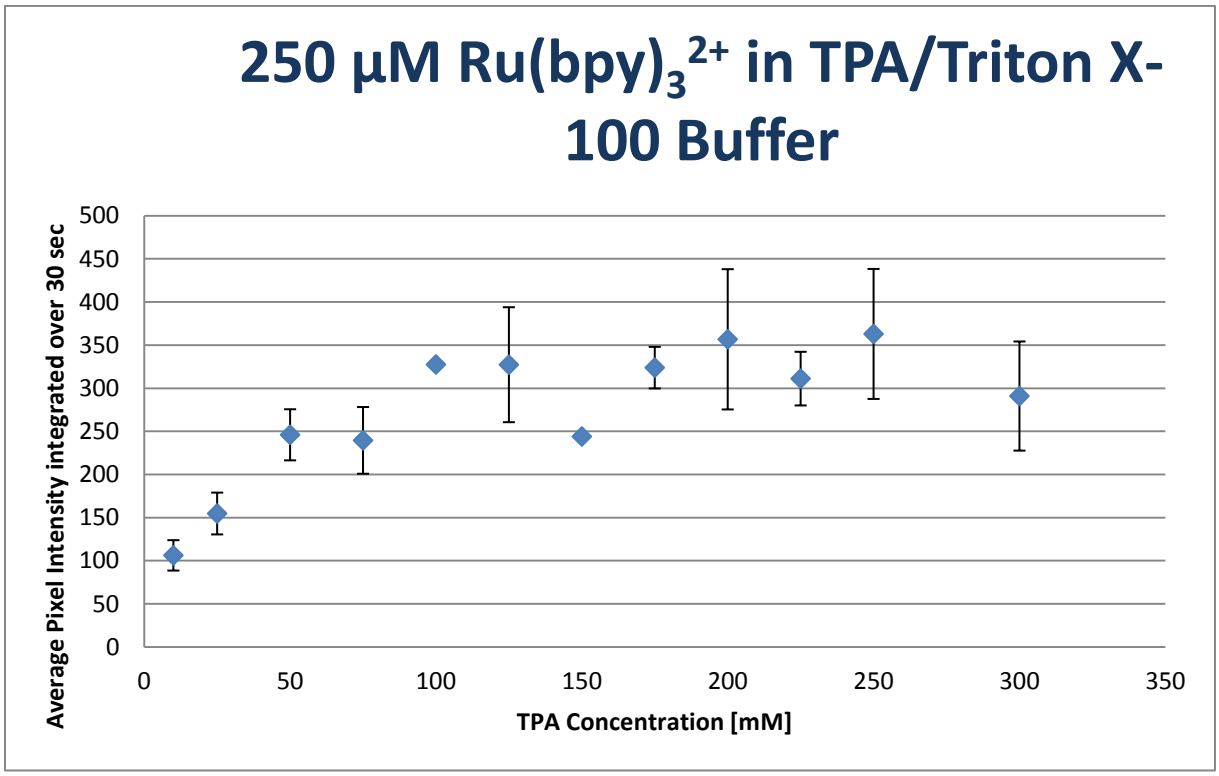

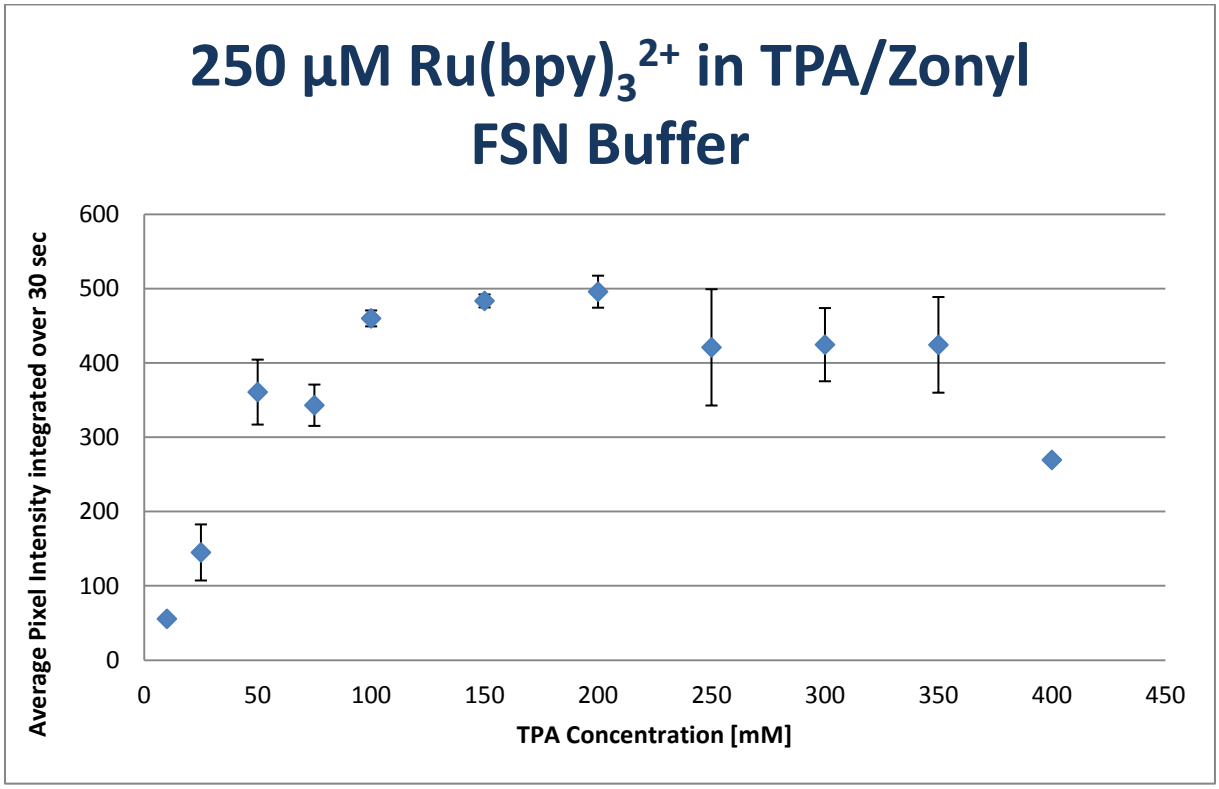

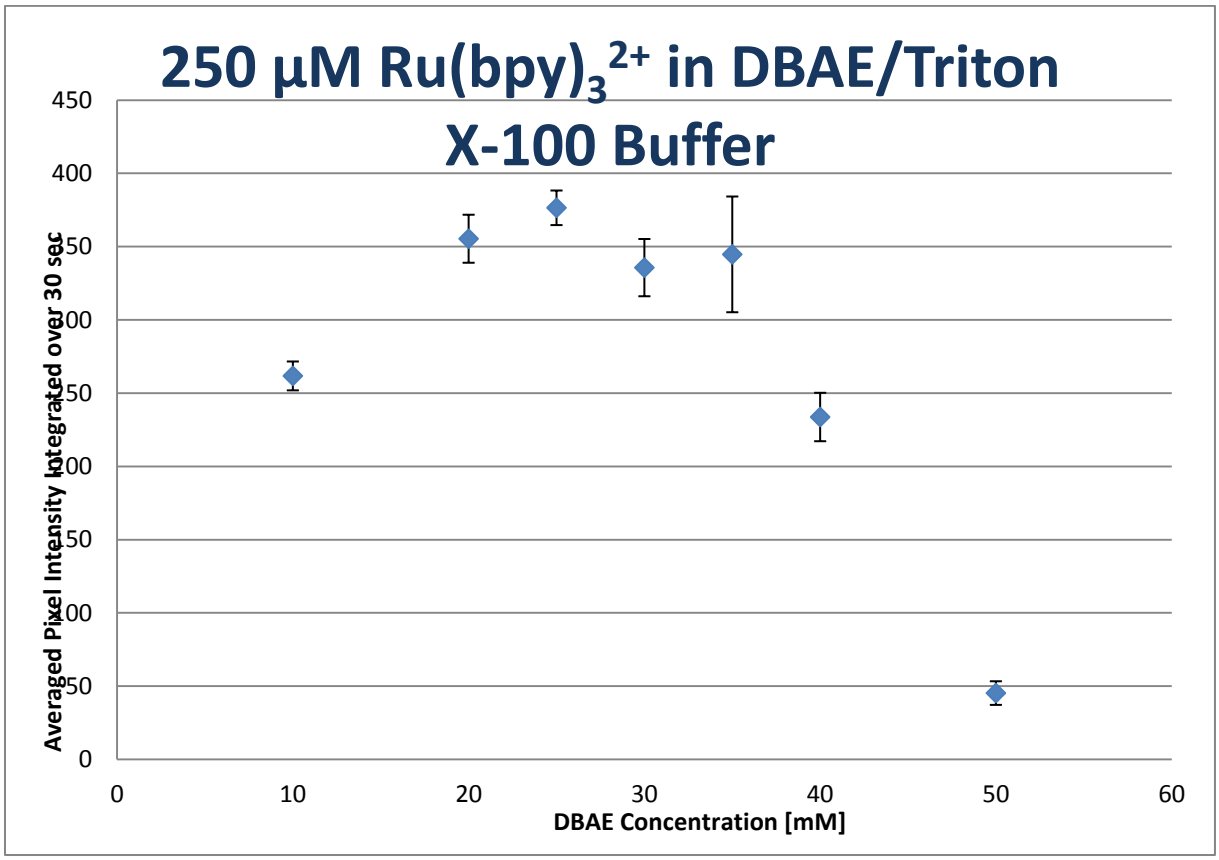
250 µM Ru(bpy)3 2+ in DBAE/Triton X-100 Buffer
Averaged Pixel Intensity Integrated over 30 sec
DBAE Concentration [mM]
0
10
20
30
40
50
60

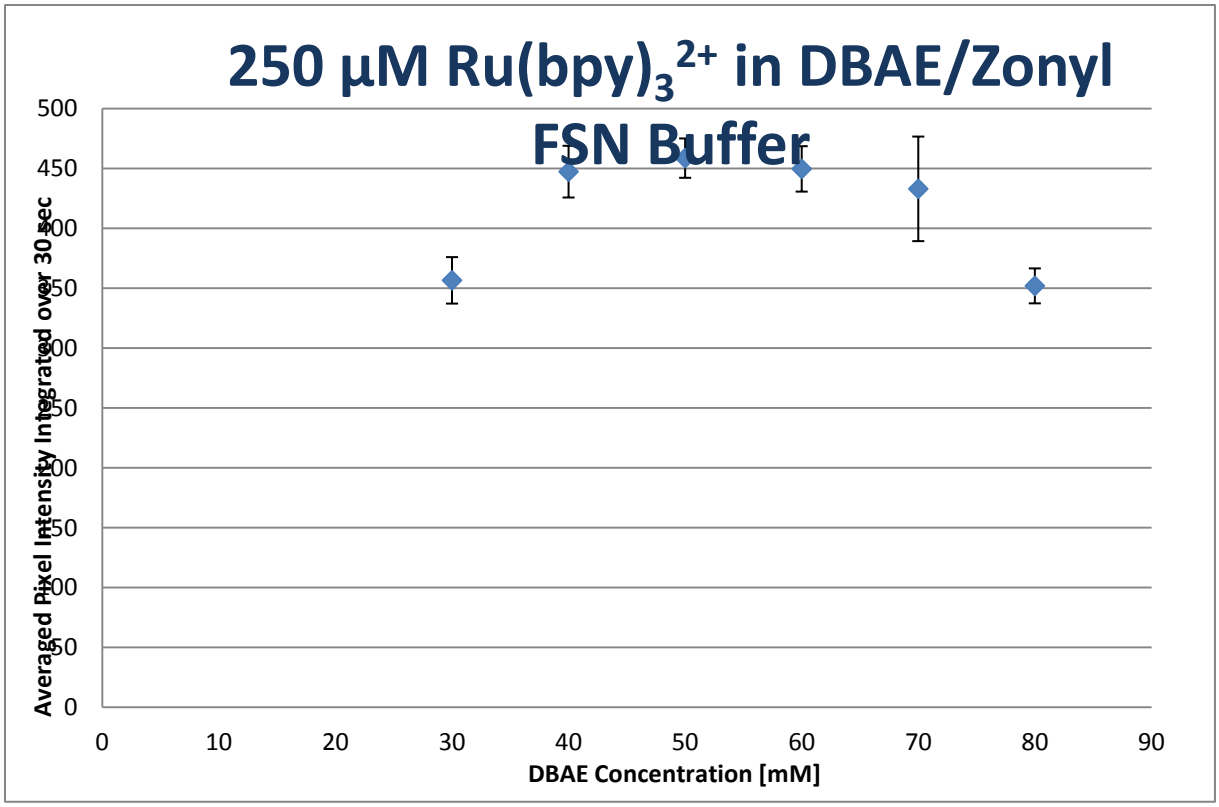
250 µM Ru(bpy)3 2+ in DBAE/Zonyl FSN Buffer
Averaged Pixel Intensity Integrated over 30 sec
DBAE Concentration [mM]
0
10
20
30
40
50
60
70
80
90

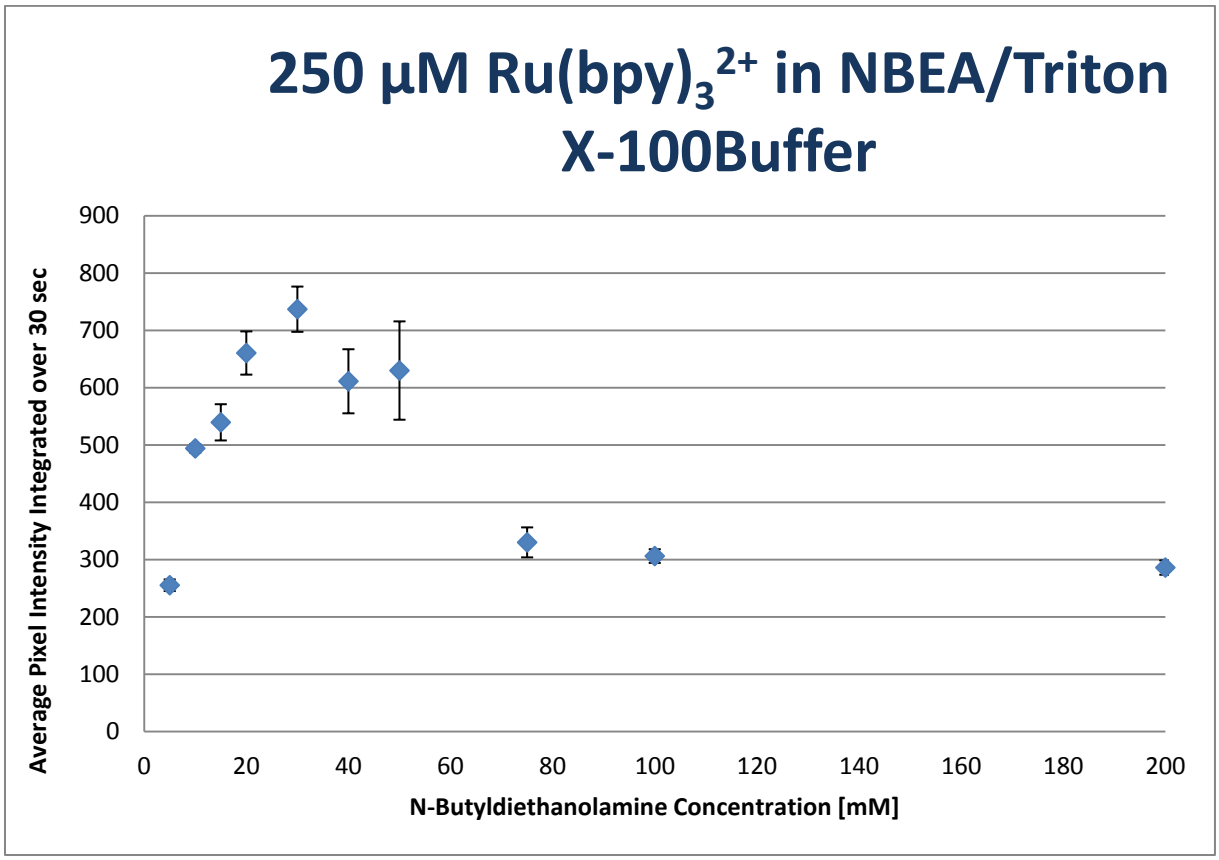
250 µM Ru(bpy)3 2+ in NBEA/Triton X-100Buffer
Average Pixel Intensity Integrated over 30 sec
900
800
700
600
500
400
300
200
100
0
0
20
40
60
80
100
120
140
160
180
200
N-Butyldiethanolamine Concentration [mM]

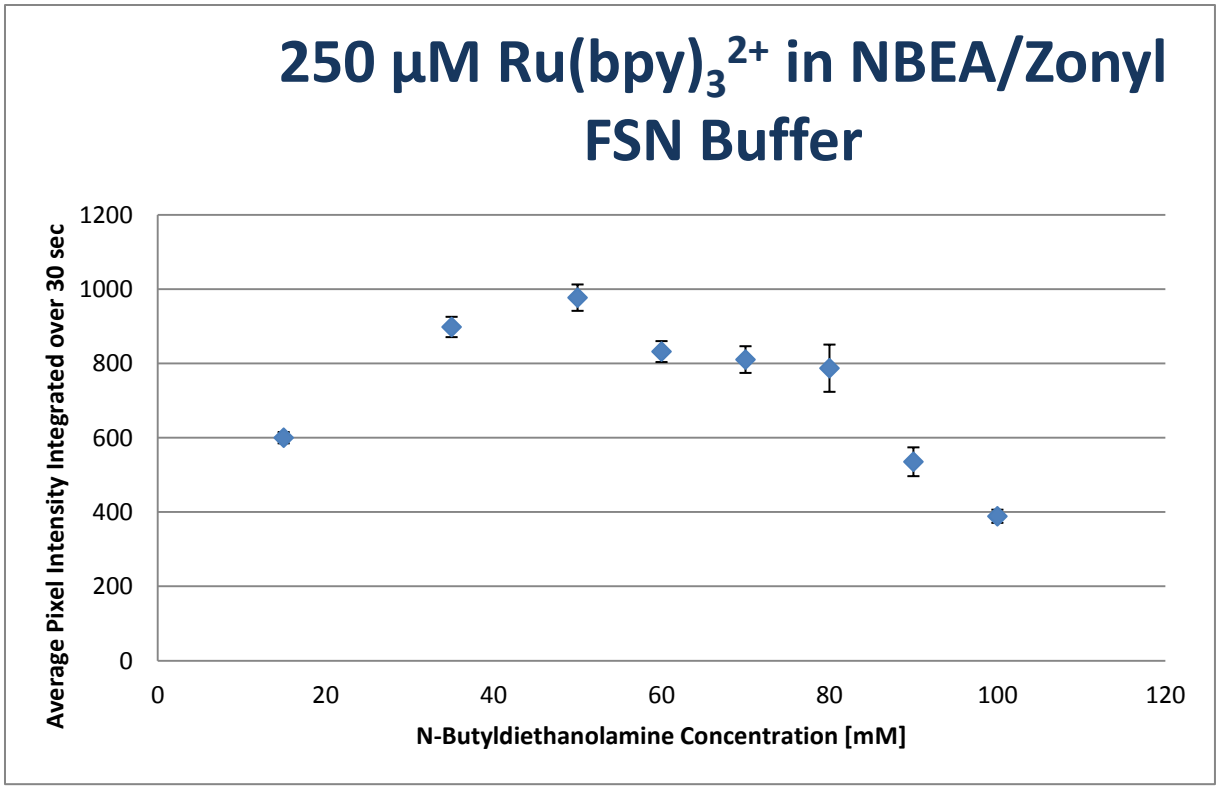
250 µM Ru(bpy)3 2+ in NBEA/Zonyl FSN Buffer
Average Pixel Intensity Integrated over 30 sec
1200
1000
800
600
400
200
0
0
20
40
60
80
100
120
N-Butyldiethanolamine Concentration [mM]

Acknowledgements

I would like to thank the following people for helping me with my work and composing this thesis:

- Professor Dr. Joachim Spatz, for giving me the wonderful opportunity of this thesis.
- Professor Dr. Antje Baeumner, for her great support and guidance.
- Dr. Olivier Bolduc, for being wonderful to work with, for his ideas about the projects, the channel and electrode designs and his insight in all questions related to chemistry.
- Dr. Nongnoot Wongkaew, for showing me how to do EC measurements and providing me with the first test chips and designs. And for being so pleasant to be around.
- Matthew DiSalvo, Angela Zhang and Judith Moench-Tegeder, for working on parts of the project and coming up with new ideas.
- Professor Dr. Michael Hausmann for being a referee of this thesis and his time.
- My family for their never-ending support.